Investigating Small Molecule Behavior in Living Bacterial Membranes with Second Harmonic Scattering

A Dissertation Presented for the

Doctor of Philosophy

Degree

The University of Tennessee, Knoxville

Marea J. Blake

May 2024

© by Marea J. Blake, 2024
All Rights Reserved.

To Mom.

Acknowledgments

I would first like to thank my advisor of the past 5 years, Professor Tessa Calhoun. Your guidance, patience and honesty have taught me more than solely how to be a great scientist, but also what it means to be a great mentor. Thank you most of all for pushing me to my limits and encouraging me to go past those too.

Thank you to my committee members (and Professor Sharani Roy) for advising me and offering unique perspectives I otherwise wouldn't have considered on my own.

I would also like to thank the members of the Calhoun group, both past and present, for being listening ears when things went wrong and supporters when things went right. Thanks especially for proof-reading so many of my emails. Specifically, I would like to thank both Dr. Lindsey Miller and Eleanor Page for your friendship. I have made many friends in graduate school but I wouldn't have been able to survive it without "the trio" - thank you Kristen Kennison-Cook and Aleksandra Antevska for being the best silly geese a girl could ask for.

Thank you to the strong women in my family that have shown me over and over again that we can do hard things. Mom - thank you for everything. Thank you to my siblings, Maddie and Jaxon, for being the reason for everything. I love you both to the moon and back times infinity. Last, but certainly not least, thank you to my best friend and husband, Tyler. Thank you for being the calm in the storm that is graduate school and making me laugh when I wanted to scream. And for killing all the bugs in our house.

Abstract

A molecule's entry into a cell is impeded primarily at the surface of Gram-positive bacteria. This interface serves as the boundary separating cellular contents from the external environment and is composed of a thick layer of peptidoglycan and a lipid bilayer equipped with protein and lipid species with various roles including that of small-molecule transport. As such, understanding these molecule-membrane interactions is imperative to examine in order to design novel drugs or adjuvants to combat the global antibiotic resistance predicament. Knowledge regarding passive diffusion and overall organization of small molecules in the lipid bilayer of living Gram-positive cells is limited as the complexity of this system is not as commonly studied as Gram-negative and eukaryotic species. This dissertation broadly aims to quantify interactions of small amphiphilic molecules with the membrane of living *Staphylococcus aureus* and *Bacillus subtilis* cells by using second harmonic scattering (SHS) techniques. SHS is uniquely qualified to study these phenomena due to being inherently sensitive to surface-bound molecule orientations. First, SHS is employed in a systematic study of how the structure of both the molecule-of-interest and the membrane influence the initial adsorption to and time-resolved dynamics of amphiphilic probe molecules within living bacterial membranes. To better understand the origin of SHS signals from this study, angular distribution of these molecules are extracted by leveraging polarization resolved SHS. Lastly, these techniques are employed to study a small molecule drug system in order to understand its perturbation of membrane properties and transport.

Table of Contents

1 Introduction **1**

1.1 Motivation . . . 2

1.2 Gram-Positive Bacterial Membrane Landscape . . . 2

1.2.1 Membrane Architecture . . . 2

1.2.2 Passive Diffusion of Small Molecules . . . 4

1.2.3 Species Under Investigation . . . 7

1.3 Probing Small Molecule-Membrane Interactions . . . 8

2 Experimental Techniques **10**

2.1 Light-Matter Interactions . . . 11

2.1.1 Linear versus Nonlinear Optical Phenomena . . . 11

2.2 Second Harmonic Generation (Scattering) . . . 15

2.2.1 Second Harmonic Generation versus Second Harmonic Scattering . . . 17

2.2.2 Instrumentation . . . 17

2.3 Fluorescence Techniques . . . 27

2.3.1 Two-Photon Fluorescence . . . 27

2.3.2 Steady State Techniques . . . 28

3 Facilitating Flip-Flop: Structural Tuning of Molecule-Membrane Interactions in Living Bacteria **31**

3.1 Abstract . . . 32

3.2 Statement of Significance . . . 33

3.3 Introduction . . . 33
3.4 Materials and Methods . . . 42
3.4.1 Bacterial Strains and Dye Solutions . . . 42
3.4.2 SHG Instrument and Flow Cell Passivation . . . 43
3.4.3 Adsorption Isotherms . . . 44
3.4.4 Time-dependent Experiments . . . 45
3.5 Results and Discussion . . . 45
3.5.1 Impacts of Molecule Structure . . . 45
3.5.2 Impacts of Membrane Composition . . . 54
3.6 Conclusions . . . 58
3.7 Author Contributions . . . 59
3.8 Acknowledgements . . . 59

4 Probing Bacterial Membranes with Polarization-Resolved Second Harmonic Scattering 60
4.1 Abstract . . . 61
4.2 Introduction . . . 61
4.3 Experimental . . . 65
4.3.1 Instrumentation . . . 65
4.3.2 Sample Preparation . . . 65
4.4 Results and Discussion . . . 66
4.5 Conclusions . . . 70

5 Miltefosine Impacts Small Molecule Transport in Gram-Positive Bacteria 71
5.1 Abstract . . . 72
5.2 Introduction . . . 73
5.3 Materials and Methods . . . 75
5.3.1 Chemicals and Cell Treatment . . . 75
5.3.2 Time-Resolved Second Harmonic Scattering . . . 76
5.3.3 Generalized Polarization Measurements . . . 77
5.3.4 Steady State Fluorescence Anisotropy . . . 77

5.4 Results and Discussion 78
5.4.1 MLT Impact on Global Membrane Fluidity 78
5.4.2 Small Molecule Organization and Transport 80
5.5 Conclusions 90

6 Conclusions and Future Directions **91**
6.1 Conclusions 92
6.2 Future Directions 93
6.2.1 Exploring the Rise 93
6.2.2 Transport Mechanisms 97
6.2.3 More Mesh, More Problems 99
6.2.4 Disrupting Domains 99
6.2.5 Expanding the Toolbox 100

Bibliography **101**

Vita **137**

List of Tables

3.1 Dissociation constants (K_d) and cLogP values[a] for each membrane probe for *S. aureus* and *B. subtilis* extracted from SHG adsorption isotherms fit to the Langmuir adsorption model.[b] 46

List of Figures

1.1 Cartoon schematic of Gram-positive (left) versus Gram-negative (right) bacterial membranes. 3

1.2 Structure of phospholipids. (A) General architecture of a single phospholipid of a cytoplasmic membrane highlighting the headgroup, glycerol backbone, and acyl tails. (B) Structures and shapes of four of the most common phospholipids present in Gram-positive bacterial membranes: Phosphatidylglycerol (PG, -1), Cardiolipin (CL, -2), phosphatidylethanolamine (PE, neutral), and lysylphosphatidylglycerol (LPG, +1). (C) Lipid phases resulting from fatty acid tails that are branched/unsaturated (fluid) versus saturated (rigid). . . 6

2.1 Jablonski diagrams for one-photon fluorescence (OPF), two-photon fluorescence (TPF), and second harmonic generation (SHG). OPF results from a single photon (ω_0) promoting a molecule from the ground state (G) to the electronic excited state (E). After vibrational relaxation, a photon of lower energy (ω_2) is produced. TPF arises after two photons of equal energy (ω_1) excite a molecule from the G state to the E state through the use of an intermediate virtual (V) state. After vibrational relaxation, a photon (ω_2) is emitted. SHG occurs after two photons (ω_1) are promoted to two V states. A photon ($\omega_2 = 2\omega_1$) of twice the energy is simultaneously produced. 12

2.2 Cartoon schematic illustrating how molecule orientation impacts generation of SHS. (Top) When two asymmetric molecules are randomly oriented (i.e. media, cytoplasm, etc) the individual second harmonic signals are incoherent, resulting in HRS. (Middle) Once the molecules are confined to a surface in a parallel arrangement to one another, the two second harmonic signals constructively interfere to produce SHS. (Bottom) When two molecules become anti-parallel, a center of inversion is introduced resulting in deconstructive interference of the two second harmonic signals, and thus, no SHS. 14

2.3 Second harmonic scattering direction depends on the diameter size of the scatterers. (A) Particles with diameters less than $\sim 1\mu m$ will produce SHS at a 90°angle. (B) Particles with diameters greater than $\sim 1\mu m$ will produce SHS in the transmitted geometry. 16

2.4 Schematic of the second harmonic scattering instrument used for trSHS and adsorption isotherm experiments. PL = prism line, $\lambda/2$ = half-waveplate, PBSC = polarizing beam splitting cube, F = filter, FL = focusing lens, CL = collecting lenses, DCM = dichroic mirror, PMT = photomultiplier tube. . 18

2.5 Malachite green/Polystyrene bead power law studies. (Left) Cartoon showing positively charged malachite green (MG, green triangles) adsorbed to sulfonated polystyrene beads (PSBs, orange). The alignment of the molecules onto the surface makes MG/PSBs a model SHS system. (Right) An example power study experiment showing that as the power of the incident light increases, the SHS instensity scales quadratically. Red points are data points, the black line is the fit to the data. 20

2.6 Cartoon schematic showing how the orientation of molecules in a membrane alter the trSHS and TPF signals. The SHS signal for panel (I) shows a decrease in signal (magenta) due to the introduction of symmetry across the bilayer. Alternatively, as the molecules become more aligned with one another (II), the SHS signal (teal) increases over time. For either panel (I) or (II), the TPF signal (orange) is expected to remain stagnant over time. 22

2.7 A schematic representation of the "chemical equation" for adsorption of small amphiphilic dyes to a membrane. The population of molecules in solution ($[M_{Free}]$) interact with the available binding sites along the membrane ($[S_{Empty}]$) to produce a population of membrane sites occupied by the small molecules ($[SM_{Bound}]$). The rates of equilibria between the binding and unbinding of the molecules to and from the membrane are quantified by k_{on} and k_{off}, respectively. 24

2.8 Laboratory frame notation and prSHS instrumentation. A) defines the angles used in the laboratory frame for use in prSHS experiments. B) Instrument used to perform prSHS experiments. P = polarizer, WP = waveplate. 26

3.1 Cartoon schematic of styryl dye molecules interacting with a lipid bilayer and the resulting SHG signals (E_{SHG}). After adsorption to the membrane, (I) dye molecules produce an initial SHG signal. The molecules can then either (II) flip-flop to produce destructive SHG signals, or (III) migrate to a more rigid environment that enhances the overall orientationally averaged hyperpolarizability, producing a greater intensity SHG response. 39

3.2 Structures of membrane probes FM 2-10, FM 1-43, 4-Di-2-ASP, and FM 4-64. Chemical structures of the probe molecules with colored shaded background regions indicating the charged headgroup (blue), conjugated region (purple) and the branched tail (orange). 41

3.3 SHG adsorption isotherms of 4-Di-2-ASP (top) and FM 1-43 (bottom) with *S. aureus* living cells. For each probe, $n = 3$. Circles ($\circ$) represent the averages of the individual trials while the solid lines (—) are the fits from the Langmuir model. Error bars are representative of standard deviations. K_d values are shown in Table 3.1 48

3.4 16 μM membrane probe time-dependent SHG trials with *S. aureus* cells. (A) compares FM 2-10 and FM 4-64 to show differences arising from conjugation length, (B) portrays similar lipophilic lengths of FM 4-64 and FM 1-43 having comparable SHG responses, and (C) shows how headgroup identity impacts membrane dynamics (4-Di-2-ASP versus FM 2-10). For each membrane probe, $n = 3$ and shaded regions represent the standard deviation between the individual trials. 50

3.5 Two-photon fluorescence time-dependent trials of (A) FM 1-43 interacting with *S. aureus* cells, (B) FM 2-10 interacting with *B. subtilis* cells, and 4-Di-2-ASP interacting with (C) *S. aureus* and (D) and *B. subtilis*. 53

3.6 SHG adsorption isotherms of 4-Di-2-ASP (top) and FM 2-10 (bottom) with *B. subtilis* living cells. For each probe, $n = 3$. Circles ($\circ$) represent the averages of the individual trials while the solid lines (—) are the fits from the Langmuir model. Error bars are representative of standard deviations. K_d values are shown in Table 3.1 55

3.7 16 μM 4-Di-2-ASP and FM 2-10 time-dependent normalized SHG trials with *B. subtilis* cells. For each membrane probe, $n = 3$ and shaded regions represent the standard deviation between the individual trials. 57

4.1 Laboratory frame defining angle notation used in this study for γ, Π, and θ. 64

4.2 PrSHS for 16 μM FM 2-10 with *S. aureus*. The squares and circles are experimental data points, the black dotted lines are for ease of visuals. . . . 67

4.3 PySHS output for dipoles normally distributed along the surface of 1 μm diameter particles. (Top) The simulated microscopic orientation of the dipoles (blue arrows) oriented along the surface of the particles. (Bottom) Computed SHS intensity at H_{out} and V_{out}. Parameters for the simulation include: N = 100, $\theta = 180 \pm 5°$, and n = 1.33. 68

4.4 (A) Polarization dependence of 25 μM MG with $\sim$1μm PSBs as a function of SHS polarizer angle with constant P-polarized incident light. (B) prSHS for the same sample as (A) as a function of incident polarization angle. The squares and circles are experimental data points, the black dotted lines are for ease of visuals. 69

5.1 Steady state fluorescence measurements of fluidity with (A) laurdan and (B) DPH. (A) Average GP values of laurdan for *S. aureus* with 0 μM MLT (blue) and 10 μM MLT (purple). (B) Average anisotropy ($\langle r \rangle$) of DPH with *S. aureus* is shown as a function of MLT concentration. For each concentration of MLT, n = 3. 79

5.2 Normalized trSHS trials of *S. aureus* with 25 μM MG with 0 μM MLT (green) and 12 μM MLT (purple). The structure of MG is shown in the plot. For each condition, $n = 3$. Averaged data is shown as circles and the shaded error bars represent the standard deviation between the individual normalized trials. 81

5.3 Normalized trSHS trials of 16 μM FM 2-10 with *S. aureus* with increasing concentrations of MLT. The structure of FM 2-10 is shown in the plot. For each concentration of MLT, $n = 3$. Averaged data is shown as circles and the shaded error bars represent the standard deviation between the individual normalized trials. 83

5.4 Normalized trSHS trials of *S. aureus* with 16 μM 4-Di-2-ASP with 0 μM MLT (orange) and 10 μM MLT (purple). The structure of 4-Di-2-ASP is shown in the plot. For 0 μM MLT, n = 3 and the shaded error bars represent the standard deviation between the individual normalized trials; for 10 μM MLT, n=1. 84

5.5 Initial intensities of trSHS (circles, left axis) and TPF (squares, right axis) signals of *S. aureus* with 16 μM FM 2-10. 85

5.6 Normalized trSHS trials of *B. subtilis* with 16 μM FM 2-10 with 0 μM MLT (blue) and 20 μM MLT (purple). The structure of FM 2-10 is shown in the plot. For each condition, $n = 3$. Averaged data is shown as circles and the shaded error bars represent the standard deviation between the individual normalized trials. 87

5.7 Normalized trSHS trials of *S. aureus* with 16 μM FM 1-43 with 0 μM MLT (yellow) and 12 μM MLT (purple). The structure of FM 1-43 is shown in the plot. For each condition, $n = 3$. Averaged data is shown as circles and the shaded error bars represent the standard deviation between the individual normalized trials. 89

6.1 Cartoon schematic showing hypotheses for the sources of rising SHS signal. Panel A shows the potential origin of an increase in SHS based on N_s (Eq. 6.1) where (i) there could be an increase in binding sites in the cells present or (ii) an increase in the number of cells, and therefore, possible binding sites. Panel B illustrates three different hypotheses for an increase originating from $\langle\beta\rangle$ (Eq. 6.1) where (i) results from a change in orientation ($\langle\rangle$) and (ii) and (iii) results from a change in β itself. 94

6.2 Concentration-dependent trSHS experiments of FM 2-10 and 4-Di-2-ASP with *S. aureus*. A) Normalized trSHS experiments of FM 2-10 at 16 (purple) and 8 (blue) μM. B) Normalized trSHS experiments of 4-Di-2-ASP at 16 (purple) and 8 (blue) μM concentrations. Circles represent the average normalized SHS intensity and shaded error bar regions represent the standard deviation between individual experiments. 96

6.3 Impact of SADH on trSHS dynamics of 16 μM FM 2-10 with *S. aureus*. . . 98

Chapter 1

Introduction

1.1 Motivation

The first physical barrier a drug must overcome to reach its target in a living Gram-positive bacterial cell is the wall encasing the lipid bilayer separating the cell's contents from the environment. The fate of the molecule is then mediated by this structure. In fact, the membrane is often the intended objective for drug design. [77, 93] Further, the membranes of living bacteria are dynamic and can alter their organization and composition at short time and length scales, owing to the emergence of some antimicrobial resistance mechanisms [114, 149, 170]. Therefore, understanding how the membrane dictates the penetration of these molecules is of paramount interest in countering antibiotic resistance mechanisms imparted by bacteria. In the United States alone, over 2.8 million cases of antibiotic-resistance are expected to occur annually [36]. Globally, antibiotic resistance is expected to contribute to approximately 5 million deaths [160]. The overall goal of this research is to investigate small-molecule transport dynamics within Gram-positive bacterial membranes and monitor how these dynamics are impacted by parameters such as 1) the molecule's structure, 2) the identity of the cell species, and 3) perturbations to the membrane through the introduction of other small molecule species.

1.2 Gram-Positive Bacterial Membrane Landscape

1.2.1 Membrane Architecture

Membranes - structures composed of a lipid bilayer with a hydrophilic interior and hydrophobic exterior teemed with proteins throughout - are defining characteristics of living biological matter. For instance, prokaryotic systems, such as bacteria, are distinct from eukaryotic systems in that they do not possess any membrane-bound sub-cellular structures. Bacteria can be further classified based on the membrane that protects their internal components from their environment. For instance, bacteria that possess two lipid bilayers separated by a thin peptidoglycan layer is referred to as Gram-negative while bacteria that possess only a single lipid bilayer surrounded by a thick peptidoglycan layer are Gram-positive, as illustrated in Figure 1.1.

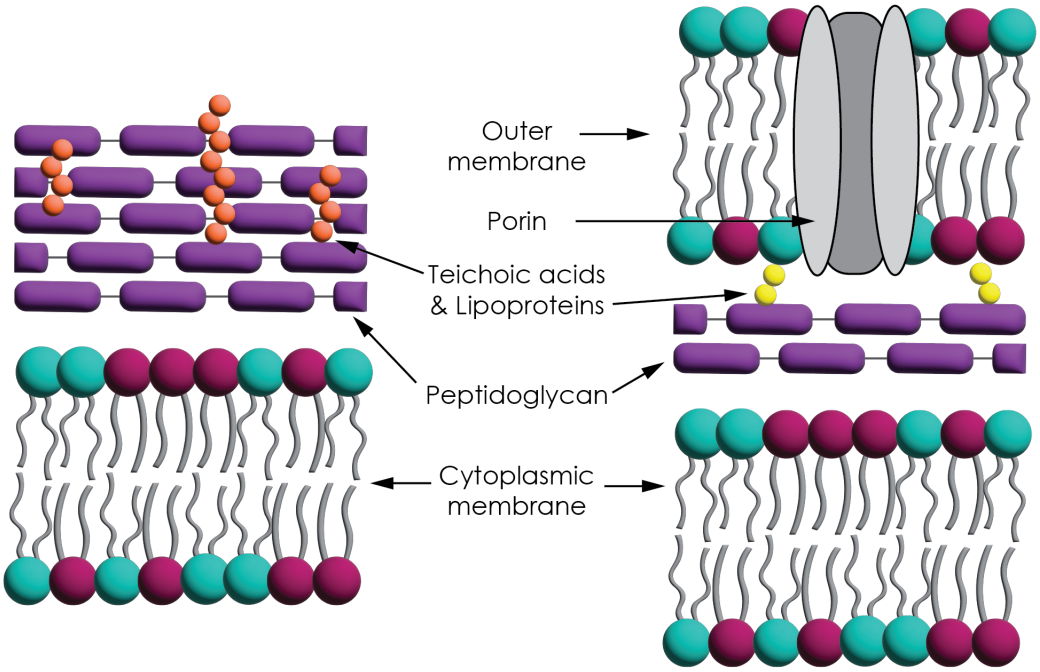


Figure 1.1: Cartoon schematic of Gram-positive (left) versus Gram-negative (right) bacterial membranes.

While the same general macro-structure of the membrane exists for all Gram-positive bacteria, the individual components, and how they are arranged, vary between species and even between strains of the same species. Some basic principles are preserved, however. For instance, many bacteria are known to have the same lipid species, although the distribution differs, which is known to induce local and large-scale changes in membrane shape, curvature, and fluidity. These biophysical properties then result in disparate functions along the membrane such as signal transduction and small molecule transport. [200, 217] The latter objective can broadly be accomplished in either an "active" or "passive" manner. Whereas active passport relies on the use of energy sources to power transport through proteins, passive transport is largely reliant on how the small molecules interact with the lipids that make up the membrane.[220] As such, the focus of this dissertation aims to understand the mechanisms at play for the passive diffusion of small molecules.

1.2.2 Passive Diffusion of Small Molecules

As stated above, the predominant mechanism mediating passive diffusion is based on small-molecule interactions with the phospholipids that comprise the bilayer. A phospholipid is composed of a hydrophilic phosphate head group bound to hydrophobic fatty acid chains (i.e. tails) through a glycerol backbone, as depicted in Figure 1.2(A). As such, the interplay between headgroup and tail pairings elicit different biophysical properties of the membrane, such as fluidity and permeability, depending on their identifies and arrangement.

The headgroup of phospholipids plays a large role in the local curvature and packing, and therefore the overall cell shape and fluidity of the cell membrane.[196] The general shape of a single phospholipid is dependent on the ratio of the size of the headgroup to the width of the fatty acid tails. For instance, headgroups harboring fatty acid tails that exceed the lateral space of the headgroup itself, or vice versa, are expected to portray conical shapes. Lipids can also possess headgroups and tails that inhabit similar lateral space leading to cylindrical shapes. Examples can be seen in Figure 1.2(B) where the most common lipids found in the species studied here, *Staphylococcus aureus* and *Bacillus subtilis*, are shown. Specifically, lipids with cardiolipin (CL), phosphatidylethanolamine (PE), and lysylphosphatidylglycerol

(LPG) headgroups take on cone-like shapes while phosphatidylglycerol (PG) is cylindrically shaped.

In addition to the comparison between the size of the headgroup to the tails influencing shape, the charges of the headgroups, listed for CL, PE, LPG, and PG in Figure 1.2(B), also play a significant role in the organization of the membrane.[119] Bacteria generally have highly negatively charged membranes due to the high concentration of anionic lipids present. As a consequence of these variances in shapes and charges, lipids are recruited to specific regions of the cell membrane - both laterally and across the bilayer. For instance, CL for rod-shaped bacteria, such as *B. subtilis*, is known to localize on the poles of the cells rather than on the sides with minimal curvature [103] but has a more homogeneous distribution for spherical cells such as *S. aureus*. [144] It has also been shown that certain conditions, such as growth stage and shape, result in differences in inner and outer cytoplasmic membrane distributions of PE and CL lipids in rod-shaped Gram-negative *Escherichia coli*[23, 71, 169] and Gram-positive *Bacillus megaterium*[167, 195]. It should be noted that the charge and shape of these headgroups have been found to play a large role in membrane protein recruitment as well. [145, 167, 193, 194, 217, 219] However, as the primary focus of this dissertation is that of passive transport, the discussion here will solely focus on the lipid-lipid interactions.

Aside from the headgroups comprising the polar regions of the lipid bilayer, the non-polar tails attached to these headgroups significantly influence the fluidity of the membrane. Three main classifications exist for phospholipid tails: straight-chain fatty acids (SCFAs), unsaturated fatty acids (USFAs), and branched-chain fatty acids (BCFAs). Most phosphate headgroups present in bacteria harbor two fatty acids, with the exception of CL which carries four fatty acids, illustrated in Figure 1.2(B). Membrane fluidity is largely mediated by the percentage of SCFAs, USFAs, and BCFAs composition in the membrane. [61] SCFAs are saturated acyl chains in which the carbon-carbon single bonds are able to tightly pack through van der Waals interactions. As a result, regions with an increased SCFA composition are generally rigid, as shown in Figure 1.2(C). In contrast, BCFAs, although also comprised of only carbon-carbon single bonds, have branched portions along the tail that result in a fatty acid that requires more lateral space, and therefore is unable to tightly pack. This

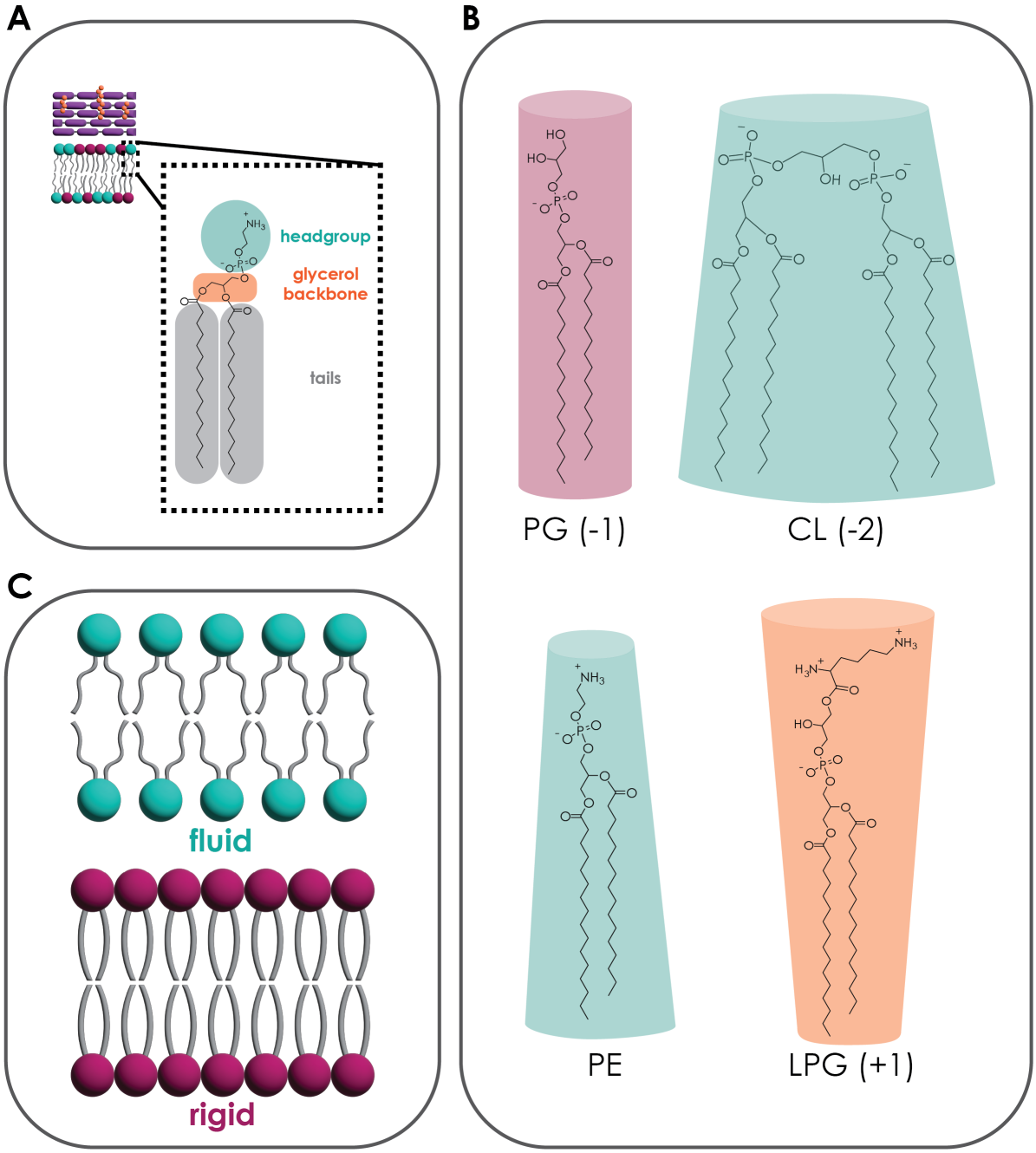


Figure 1.2: Structure of phospholipids. (A) General architecture of a single phospholipid of a cytoplasmic membrane highlighting the headgroup, glycerol backbone, and acyl tails. (B) Structures and shapes of four of the most common phospholipids present in Gram-positive bacterial membranes: Phosphatidylglycerol (PG, -1), Cardiolipin (CL, -2), phosphatidylethanolamine (PE, neutral), and lysylphosphatidylglycerol (LPG, +1). (C) Lipid phases resulting from fatty acid tails that are branched/unsaturated (fluid) versus saturated (rigid).

is similar to the packing ability of USFAs which have one or more carbon-carbon double bonds along the tail resulting in "kinks." Due to the branching and kinks of BCFAs and USFAs, respectively, these are known to be the primary components of fluid regions of the membrane, shown schematically in Figure 1.2(C).

The modulation of membrane fluidity via lipids of bacterial membranes, as surveyed above, has lead to an emergence of studies attempting to understand the organization of these membrane components. For *S. aureus* and *B. subtilis*, this has resulted in the ideas of functional membrane microdomains (FMMs) and regions of increased fluidity (RIFs), respectively. [98, 124, 129, 200, 216] These domains have been implicated in functions ranging from cell division to signal transduction. Further, it has been shown that when these regions are perturbed, some species become more susceptible to antibiotics.[162] These results indicate that these properties of the membrane may play larger roles in small-molecule transport via passive diffusion.

1.2.3 Species Under Investigation

The two Gram-positive bacterial species studied here are *S aureus* and *B. subtilis*. However, most of the work presented here will focus primarily on *S. aureus*. *S. aureus* was chosen for these experiments for several reasons. First, it is a common pathogen that has grown resistance over time to numerous antibiotics. As such, understanding how small molecules interact with the *S. aureus* membrane has direct clinical importance. Second, the spherical shape and single membrane of *S. aureus* is reminiscent of model systems. This is important because many studies attempting to understand molecule-membrane interactions rely on model systems; therefore, direct comparisons can be made to extract how these systems may differ. In alignment with this second reason, *B. subtilis* was also subjected to experiments in this dissertation. *B. subtilis* was chosen as another system to investigate due to also having a single membrane but with differences in membrane composition and expected heterogeneity due to its rod shape compared to *S. aureus*. By implementing both systems, importance of the membrane identity can be inferred in respect to how small molecules interact with living cells.

1.3 Probing Small Molecule-Membrane Interactions

Experimentally probing passive diffusion through bacterial bilayers is a nontrivial endeavor but a necessary one to understand how drugs and drug-like molecules permeate this space. Some of the most widely applied concepts to predict how well a molecule can accomplish this task rely on simple theoretical diffusion models such as Overton's rule [106, 150] and the "rule of 5" [120, 121]. As such, computational studies[15, 16, 75, 76, 109, 232] and work with model lipid systems[17, 178, 202, 221, 259] have expanded our knowledge in this arena. Experimentally, there has been an emergence of techniques to attempt to understand these phenomena in living cells. [204] For instance, fluorescence-based techniques have been able to monitor the permeation kinetics of drug-like molecules either by inducing fluorescence under specific environmental conditions or tagging the molecules of interest. [63, 97, 104, 110, 118, 211, 226, 250] Surface plasmon resonance is a label free alternative that has successfully quantified passive membrane transport largely in model systems. [11, 28, 29, 46] Additionally, techniques reliant on radio labelling [53, 159, 176] and nuclear magnetic resonance [3, 39, 40, 250] have also been shown to be capable of probing molecule permeation across lipid bilayers. While each of these experimental techniques has their own share of advantages, the challenges of specificity, resolution, and non-native conditions persist.

As a way to navigate around these obstacles, approaches based on second-ordered nonlinear optical events, such as second harmonic generation (SHG)/second harmonic scattering (SHS), have been developed for studying translocation of small molecules in many systems, including bacteria. SHG and SHS are often used interchangeably throughout this work but the important distinction between the two is explained in Chapter 2 along with the theoretical basis of the technique. Briefly, SHG is the simultaneous conversion of two photons of equal energy to a single photon of twice the energy. This phenomenon is uniquely sensitive to interfaces as a prerequisite to producing the second harmonic signal is a lack of centrosymmetry. This allows SHG to be a measure of molecule orientation along a surface, such as that of living bacteria, with high specificity. Therefore, this dissertation work will illustrate how SHG/SHS is employed to extract information regarding the individual steps of membrane penetration. Chapter 3 will describe how the structure of the molecule and

the identity of the membrane facilitates initial adsorption and translocation properties. These results are pertinent to rational drug design for living bacterial systems. Then, the orientational arrangement after initial adsorption is explored with an extension of this technique, polarization-resolved SHS, in Chapter 4. Lastly, the membrane organization is explored by monitoring how small molecules interact with *S. aureus* after disrupting FMMs with the drug, miltefosine in Chapter 5. Chapter 6 of this work will conclude with final remarks and an outlook on possible future directions.

Chapter 2

Experimental Techniques

2.1 Light-Matter Interactions

2.1.1 Linear versus Nonlinear Optical Phenomena

To understand how small molecules interact with the membranes of living bacteria, a plethora of optical techniques are employed in this work necessitating an overview of the principles governing them all: light-matter interactions. Light, once incident upon a source of matter (e.g. a molecule), can elicit responses from said matter in many ways - in either the linear or nonlinear optical regimes. [26] This can be depicted by the equation:

$$P = \epsilon[\chi^{(1)}E_{\omega_1} + \chi^{(2)}E_{\omega_1}E_{\omega_2} + \chi^{(3)}E_{\omega_1}E_{\omega_2}E_{\omega_3}...] \tag{2.1}$$

where P is the polarization, or induced dipole per unit volume, after interacting with the incident electric field, E, ϵ is the electric permittivity of the molecule, and $\chi^{(n)}$ is the susceptibility for first-, second-, third-, etc. ordered events. The susceptibility terms can be thought of as the property of the molecules that dictates how the light induces a response. The first term in Equation 2.1, $\chi^{(1)}E$, represents all linear, or first-ordered, optical events. As can be seen from this term, these processes scale linearly with the incident light as opposed to the subsequent terms in the nonlinear regime which scale nonlinearly with the incident light due to the number of electric fields interacting with the material. For example, linear processes rely on the interactions from a single electric field while nonlinear processes depend on two or more electric fields, shown by the Jablonski diagram comparing one-photon fluorescence (OPF), two-photon fluorescence (TPF), and second harmonic generation (SHG) in Figure 2.1. [26]

Examples of linear optical phenomena include one-photon absorption and fluorescence. In this work, the latter is implemented in several ways, specifically in Chapter 5, and will be further explored in Section 2.3, however the basic principles of OPF will be discussed here to compare to the two-photon processes of TPF and SHG. As seen in Figure 2.1, OPF is produced when light of frequency ω_0 promotes an electron from a ground state to a vibrational state in an excited electronic state. Thereafter, the photon relaxes to a lower vibrational state and then back to the electronic ground state. The return of the electron to

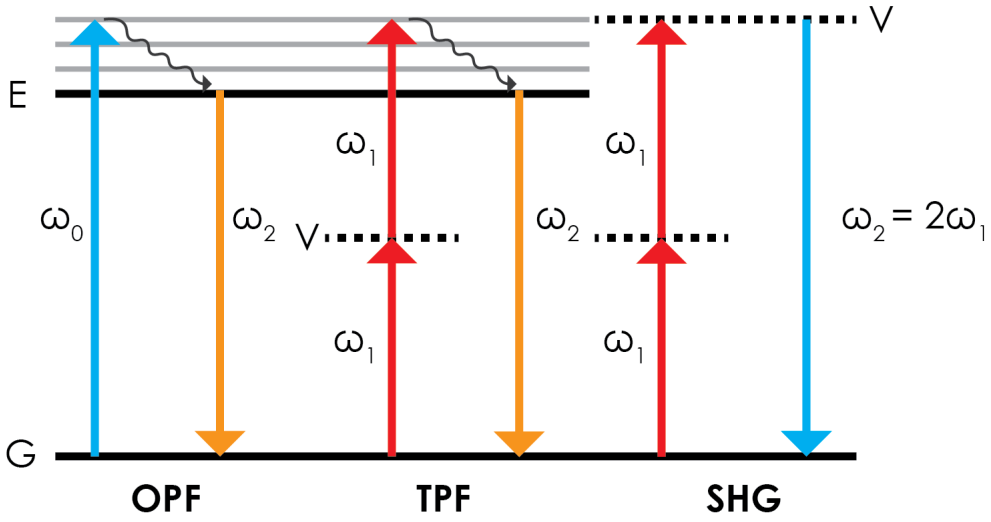


Figure 2.1: Jablonski diagrams for one-photon fluorescence (OPF), two-photon fluorescence (TPF), and second harmonic generation (SHG). OPF results from a single photon (ω_0) promoting a molecule from the ground state (G) to the electronic excited state (E). After vibrational relaxation, a photon of lower energy (ω_2) is produced. TPF arises after two photons of equal energy (ω_1) excite a molecule from the G state to the E state through the use of an intermediate virtual (V) state. After vibrational relaxation, a photon (ω_2) is emitted. SHG occurs after two photons (ω_1) are promoted to two V states. A photon ($\omega_2 = 2\omega_1$) of twice the energy is simultaneously produced.

the ground state results in the emission of light at frequency ω_2. The two-photon equivalence of this transition can be seen in the second panel of Figure 2.1 where instead of a single light field, two photons, each of frequency ω_1, simultaneously promote the electrons from the ground state to the excited state. This transition is mediated by a virtual state. A virtual state is not a real excited state of the molecule but a temporary intermediate state with no lifetime. Once excited, the electrons' path back to the ground state is similar to that of OPF to produce ω_2. It is worth noting, however, that the wavelengths required for TPF are longer for the same transition that could be facilitated with OPF owing to deeper penetration depth and reduced photodamage. [30, 37, 49] The narrower focal volume incited by nonlinear processes additionally results in better resolution and less background signal from outside of the focal volume. [30, 22] The last case shown in Figure 2.1 is that of SHG. SHG differs from the previous two techniques in that the final state before emission relies on the transition to a virtual excited state rather than a real electronic excited state. Another difference between OPF/TPF and SHG is the timescale in which the phenomenon occurs. Where OPF and TPF transpire on a measurable timescale, SHG is a simultaneous event with no relaxation period. Therefore, once the two photons of frequency ω_1 interact with the molecule, a new photon that is twice the frequency ($\omega_2 = 2\omega_1$) of the incident electric field is generated. Perhaps the largest dissimilarity between these three techniques is their reliance on the susceptibility terms in Equation 2.1 owing to differences in their physical origins and dependence on the system under investigation. This is most stark when comparing TPF to SHG as TPF originates from $\chi^{(3)}$ and SHG from $\chi^{(2)}$ causing the latter to be highly sensitive to the overall symmetry of the system as SHG is forbidden in centrosymmetric systems, which will be expanded on in the following sections. As all three mechanisms shown in Figure 2.1 are implemented in this work, the discussion will begin with SHG as this is the predominate technique employed, and then will be followed by TPF and complementary OPF techniques.

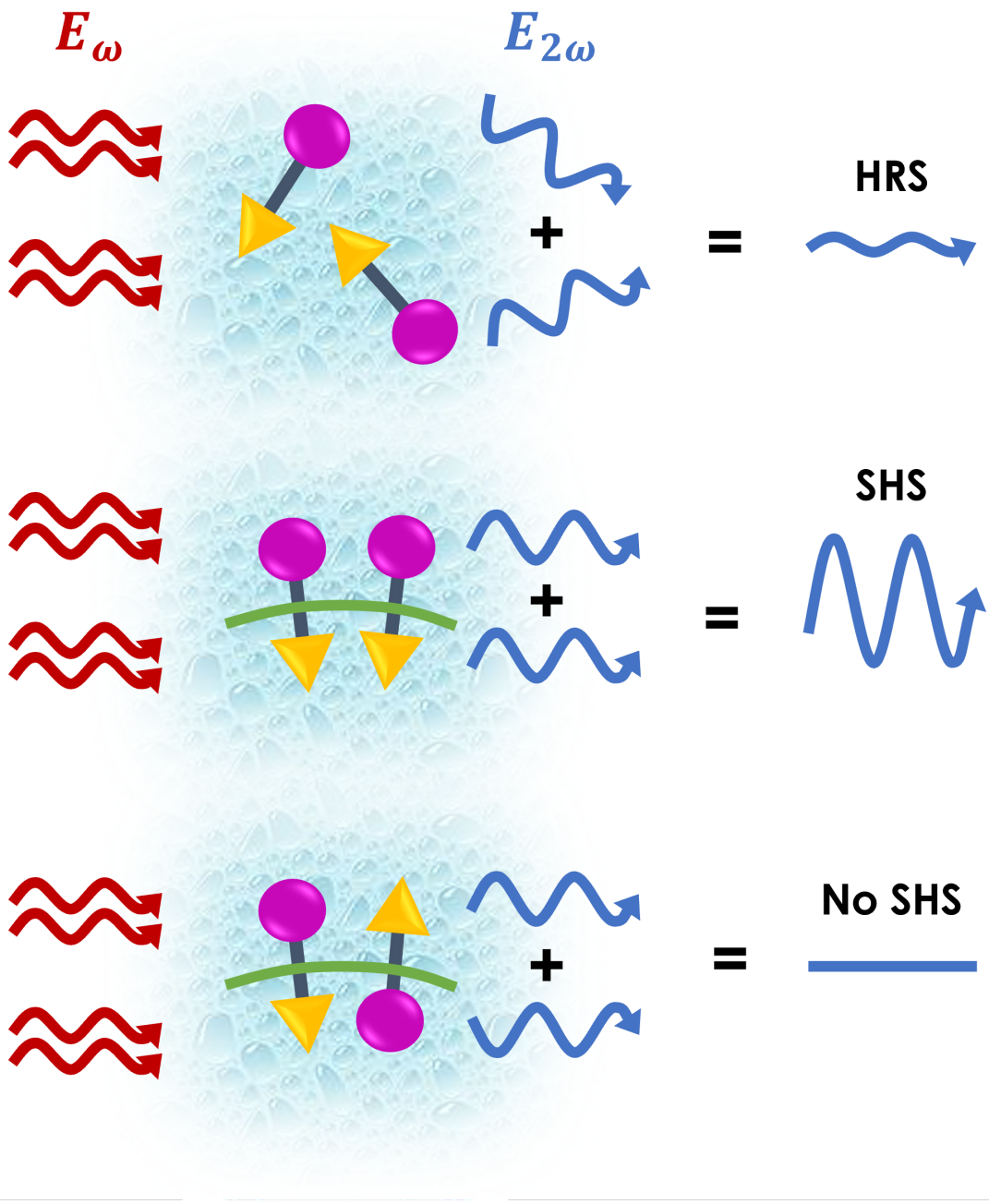


Figure 2.2: Cartoon schematic illustrating how molecule orientation impacts generation of SHS. (Top) When two asymmetric molecules are randomly oriented (i.e. media, cytoplasm, etc) the individual second harmonic signals are incoherent, resulting in HRS. (Middle) Once the molecules are confined to a surface in a parallel arrangement to one another, the two second harmonic signals constructively interfere to produce SHS. (Bottom) When two molecules become anti-parallel, a center of inversion is introduced resulting in deconstructive interference of the two second harmonic signals, and thus, no SHS.

2.2 Second Harmonic Generation (Scattering)

SHG was first theorized in 1931 by Maria Göppert-Mayer in her doctoral dissertation [83] but was not experimentally demonstrated until 1961 by Franken et al. with SHG originating from a quartz crystal. [70] This 30 year delay is due to the conditions necessary to produce two-photon processes - high intensities only afforded by high-peak-powered lasers which were not invented until 1960. [132] Since then, SHG has been used as an invaluable tool for characterizing crystal and material systems [67, 47, 212], studying phenomena at surfaces and interfaces [209, 210, 44, 60], and imaging endogenous biological structures. [153, 32, 2] While these works rely on the bulk noncentrosymmetry of the systems studied, a prerequisite to produce SHG, the pioneering work of Eisenthal et al. extended this technique to centrosymmetric particles in bulk solutions in 1996 [235], paving the way for studies on the surface of model and living membranous systems in solution.

As mentioned in Section 2.1.1, SHG is a nonlinear optical phenomena in which two photons of frequency ω_1 interact with a noncentrosymmetric system to produce a single photon twice the frequency ($\omega_2 = 2\omega_1$) of the incident photons (Fig. 2.1). SHG is a coherent process and is therefore reliant on the second harmonic signal produced from a group of molecules lacking a center of inversion symmetry. When the second harmonic signal is generated from a single molecule or a group of randomly oriented molecules, this phenomenon is referred to as hyper-Rayleigh scattering (HRS) which is an incoherent process, as seen in Figure 2.2 (top). However, once these individual noncentrosymmetric molecules align in a parallel fashion along a surface, as shown in the middle panel of Figure 2.2, the HRS contributions from each molecule constructively interfere to produce an SHG signal that scales quadratically with the number of molecules confined to the surface. In contrast, when molecules are aligned in an anti-parallel geometry, the individual HRS contributions destructively interfere to produce no appreciable SHG, illustrated in Figure 2.2 (bottom).

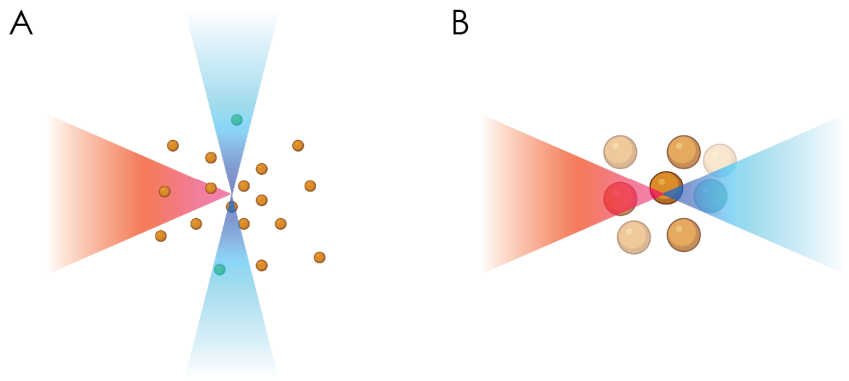


Figure 2.3: Second harmonic scattering direction depends on the diameter size of the scatterers. (A) Particles with diameters less than $\sim 1\mu m$ will produce SHS at a 90°angle. (B) Particles with diameters greater than $\sim 1\mu m$ will produce SHS in the transmitted geometry.

2.2.1 Second Harmonic Generation versus Second Harmonic Scattering

SHG is sensitive to not only to the alignment of the molecules along the interface of a colloidal system but also the size of the particles themselves. Particles with diameters averaging greater than or equal to 1 μm generate SHG in the transmitted geometry with an angular distribution of $\sim 30^{\circ}$. However, particles less than 1 μm radiate the second harmonic in increasingly larger angles with particles on the size range of 50 nm radiating SHG at 90°, as illustrated in Figure 2.3. [96] Due to this directional sensitivity of SHG, the term second harmonic scattering (SHS) has been implemented when discussing the second harmonic signals that are produced from colloidal systems.[80, 189] Since scattering experiments collect SHG from a wide range of angles, it is nearly impossible to successfully tease apart HRS and strictly SHG signals - therefore SHS is commonly used though it is not uncommon to find SHS and SHG used interchangeably. In fact, Chapter 3 uses purely "SHG" terminology while Chapters 4 and 5 use the "SHS" nomenclature although all three are referring to generally the same sources of second harmonic signals.

There are many ways one could leverage the SHG signals generated from the surface of suspended particles, such as that of living bacteria. In this work, there are specifically three ways in which SHG signals are generated to extract useful information pertaining to how small molecules interact with living membranes of *S. aureus* and *B. subtilis*: time resolved SHS (trSHS), adsorption isotherms, and polarization-resolved SHS (prSHS). All three consider the generation of SHS signal as a function of different independent variables to extract distinct information. The base home-built instrument used in these experiments is illustrated in Figure 2.4.

2.2.2 Instrumentation

Following the 80 MHz output of the fundamental 800 nm light from a Ti:Sapphire oscillator compressed to $\sim$ 100 fs, the power and polarization of the light is controlled with a half-waveplate ($\lambda/2$) and polarizing beam splitting cube (PBSC) combination. Then, any SHG from previous optics is filtered out with a 450 longpass filter and focused onto the sample

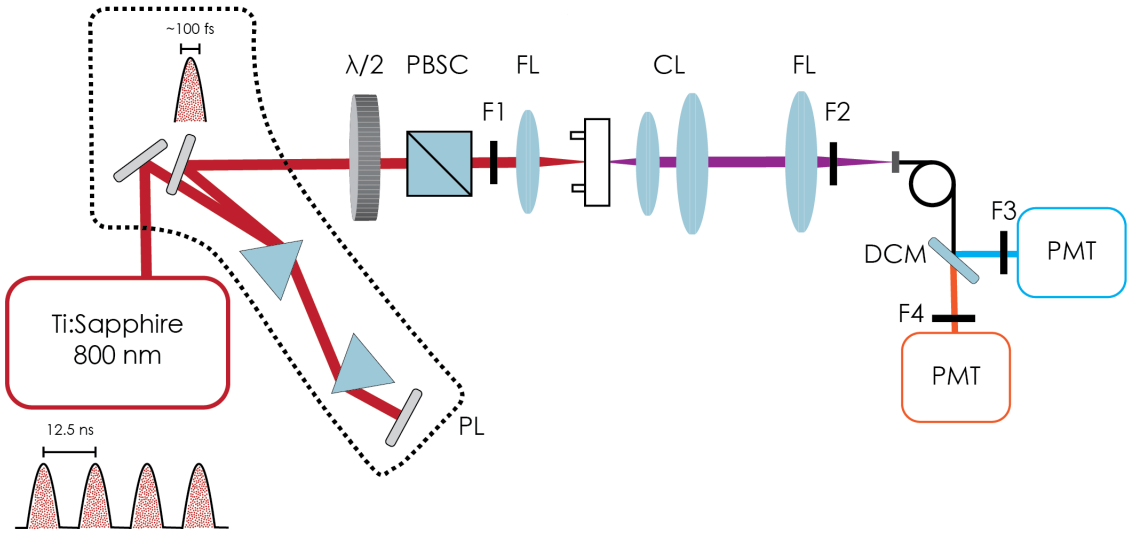


Figure 2.4: Schematic of the second harmonic scattering instrument used for trSHS and adsorption isotherm experiments. PL = prism line, $\lambda/2$ = half-waveplate, PBSC = polarizing beam splitting cube, F = filter, FL = focusing lens, CL = collecting lenses, DCM = dichroic mirror, PMT = photomultiplier tube.

housed in a quartz flow cell. The SHG/SHS generated from the sample is then sent to a series of lenses that collects, collimates, and then focuses the 400 nm light, filtered with a 725 nm shortpass filter to omit the fundamental 800 nm light, onto a fiber that directs the signal to a 450 longpass dichroic mirror that separates TPF and SHS signals and directs them to their respective final filters and photomultiplier tubes (PMTs) for detection, controlled through in-house LabVIEW codes. A 400/10 bandpass filter was used for all SHS experiments while a 625/50 and 695/55 bandpass filters were used for TPF of the fluorescent probes used in these experiments. Prior to using this instrument for data collection, it should be noted that optimization and calibration are performed by monitoring SHS intensity of malachite green (MG) on polystyrene beads (PSBs) as a function of incident power, as shown in Figure 2.5. As explained above, if a proficient laser source is being implemented, the SHS produced should scale quadratically with the incident electric fields. Therefore, experiments are only performed if the MG/PSB power-studies produce an exponent of 2 ± 0.10. Additionally, the intensity of these power studies are optimized by making alterations to collection alignment to ensure maximum signal collection.

Time-Resolved Second Harmonic Scattering

The primary aim of this dissertation work is to deduce how structure - of the membrane itself or the molecule of interest - facilitates a molecule's ability to translocate from one leaflet to the other of living bacterial membranes. In order to accomplish this goal, we utilize SHS in a time-dependent manner through trSHS by monitoring how the SHS intensity evolves over time. As mentioned above, the overall SHS intensity will depend on how the molecules are arranged along a surface and is represented by the second term in Equation 2.1:

$$E_{2\omega} \propto \chi^{(2)}_{eff} E_{\omega_1} E_{\omega_2} \tag{2.2}$$

Equation 2.2 shows the SHS signal, $E_{2\omega}$, is proportional to the electric field intensity of the fundamental light, where $\omega_1 = \omega_2$, and the effective second order susceptibility. The susceptibility term can be further defined by:

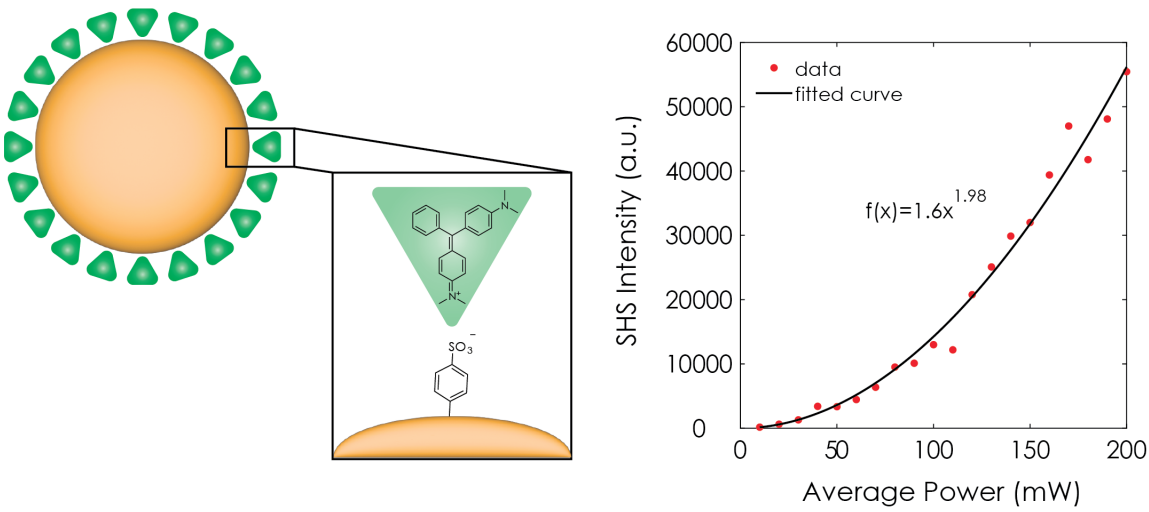


Figure 2.5: Malachite green/Polystyrene bead power law studies. (Left) Cartoon showing positively charged malachite green (MG, green triangles) adsorbed to sulfonated polystyrene beads (PSBs, orange). The alignment of the molecules onto the surface makes MG/PSBs a model SHS system. (Right) An example power study experiment showing that as the power of the incident light increases, the SHS instensity scales quadratically. Red points are data points, the black line is the fit to the data.

$$\chi^{(2)}_{eff} \propto N_s \langle \beta \rangle \tag{2.3}$$

where N_s is the population of molecules confined to the surface and $\langle \beta \rangle$ is the orientational average of the first hyperpolarizability which describes the overall arrangement of the individual dipoles of the membrane-bound molecules. Therefore, any change in SHS intensity can be correlated to the orientation of the molecule in the membrane space, which is described in more detail in Chapter 3. Figure 2.6 shows how the trSHS signals are interpreted in relation to the alignment of molecules along the bacterial membranes. Briefly, the first SHS peak arises from the molecules initial interaction with the membrane space. Afterward, the intensity can either increase or decrease in correlation with one of two hypothesized events. A subsequent decay in SHS intensity is indicative of the molecules translocating from the outer leaflet to the inner leaflet, a process referred to in Chapter 3 as "flip-flop" although this term is most commonly in reference to phospholipids flipping between the inner and outer leaflets of cell membranes. Conversely, a second rise following the initial increase in signal is indicative of further organizational forces at play, such as 1) the molecules are witnessing a change in solvation, 2) molecules are aggregating along the surface, and/or 3) molecules are becoming more aligned with one another through organization of the membrane.

TrSHS experiments are performed with the instrument shown in Figure 2.4, however in addition, a peristaltic pump and gravity flow system is used to move the samples through the focal length of the flow cell. Briefly, a liquid culture of cells are housed in a 10 mL media bottle, referred to here as the bulk reservoir, equipped with a 3-port screw cap. Autoclave-sterilized C-flex tubing is used throughout the setup to flow cells from the bulk reservoir to a smaller reservoir that is located at a greater height above the quartz flow cell. Cells then flow from the smaller reservoir from one side of the quartz flow to the other end and then is funneled back into the bulk reservoir. The flow rate is calculated to be ~7 mL/min at the point directly before entering the flow chamber. For comparison to the SHS implementations listed below, the power used for trSHS experiments is 35 mW to limit photodamage to the cells since they are continuously subjected to the focal volume over the duration of the experiment.

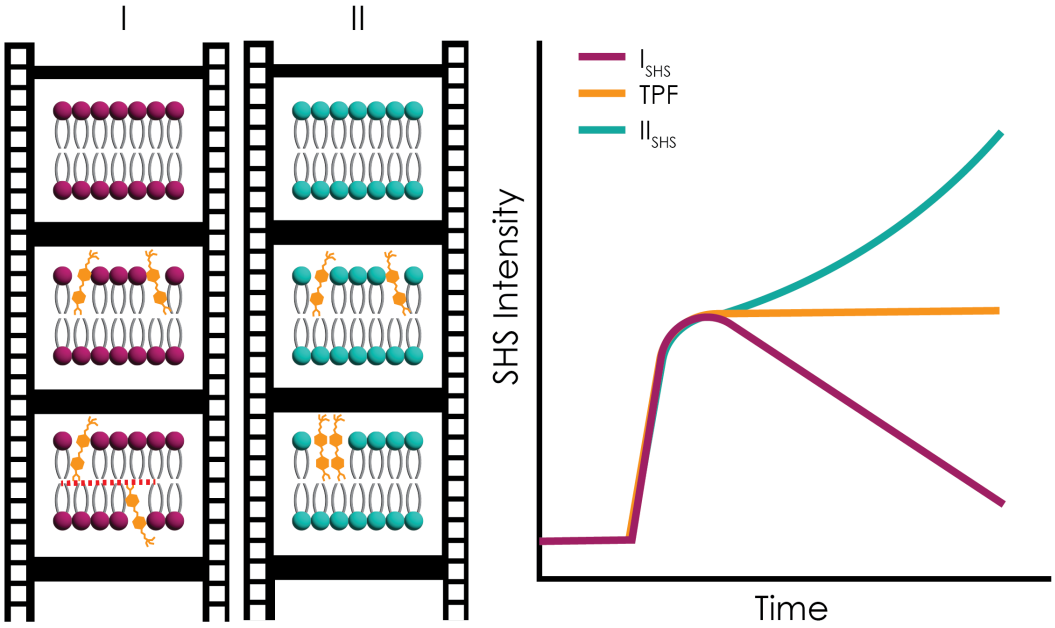


Figure 2.6: Cartoon schematic showing how the orientation of molecules in a membrane alter the trSHS and TPF signals. The SHS signal for panel (I) shows a decrease in signal (magenta) due to the introduction of symmetry across the bilayer. Alternatively, as the molecules become more aligned with one another (II), the SHS signal (teal) increases over time. For either panel (I) or (II), the TPF signal (orange) is expected to remain stagnant over time.

Adsorption Isotherms

Another important parameter to consider when assessing how molecules interact with living cells is the molecule's affinity for the membrane. This can be experimentally determined with SHS by performing adsorption isotherm measurements.[234] Essentially, this is done by recording the SHS intensities as a function of molecule concentration rather than time. The following equations can be used to extract the dissociation constant from this measurement where θ is the number of surface sites being occupied and further defined by the Langmuir adsorption model.

$$I_{SHS} \propto \theta = \frac{\frac{[c]}{K_d}}{1 + \frac{[c]}{K_d}} \tag{2.4}$$

In Equation 2.4, [c] is the total concentration of molecules, both bound and in solution, and K_d represents the dissociation constant which can also be expressed as:

$$K_d = \frac{k_{off}}{k_{on}} \tag{2.5}$$

where k_{off} is the rate molecules are dissipating from the membrane and k_{on} is the rate molecules are binding to available surface sites, as shown by the "chemical equation" in Figure 2.7. Therefore, the K_d value can be thought of as the concentration required to fill half of the available binding sites and provides the affinity the molecules have for the membrane space. As such, a low K_d value indicates strong binding. While K_d is the terminology used in this work as it is most common in biological studies, it is frequently written in terms of the association constant, $K_a = \frac{1}{K_d}$, for the Langmuir model. A physical representation of this equilibrium is shown in Figure 2.7.

The workflow of this implementation is as follows. Briefly, a bulk cell sample is prepared and then aliquoted for a fresh cell sample per data point. The dye molecules at increasing concentrations are then introduced to these aliquots and immediately transferred to the quartz flow cell for data collection via C-flex tubing connected with an elbow fitting. Since this data is only collected over the course of one second, a power of 350 mW of incident light is used. The samples are then discarded before continuing to the next concentration.

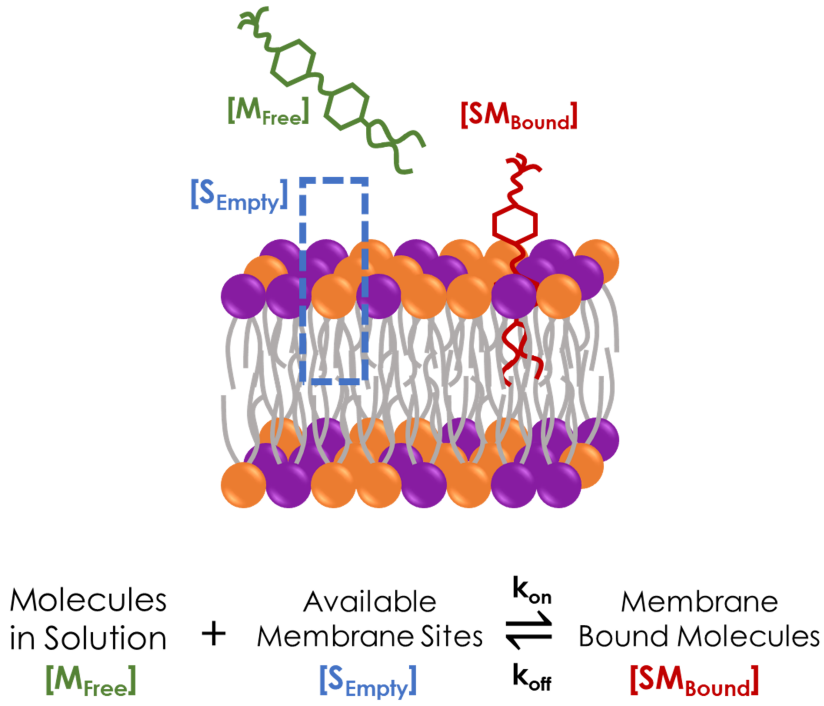


Figure 2.7: A schematic representation of the "chemical equation" for adsorption of small amphiphilic dyes to a membrane. The population of molecules in solution ($[M_{Free}]$) interact with the available binding sites along the membrane ($[S_{Empty}]$) to produce a population of membrane sites occupied by the small molecules ($[SM_{Bound}]$). The rates of equilibria between the binding and unbinding of the molecules to and from the membrane are quantified by k_{on} and k_{off}, respectively.

Polarization-Resolved Second Harmonic Scattering

While trSHS is a valuable measure of translocation and hints towards organization of molecules in the membrane, as shown in Chapter 3, it fails to determine more precise orientational information beyond whether molecules are broadly parallel or anti-parallel to one another. PrSHS is an extension of SHS that is capable of determining the angular distribution of molecules confined to a surface. This could provide valuable insight into changes induced by membrane organization, such as molecules encountering rigid and fluid regions along the membrane. As such, the work shown in Chapter 4 is the first implementation of this technique to living bacteria. In order to do so, slight modifications are made to the instrument shown above in Figure 2.4. The differences include the addition of a motorized half-waveplate to manipulate the angle of incident polarization and a polarizer after the second collection lens to analyze the vertical (V) and horizontal (H) contributions of the total SHS signal. Another modification made to the instrument is the addition of right angle detection. In order to collect signals at 90°, a different 3 mm path length flow cell with three polished sides is used. Calibration of this instrument was performed with molecules aligned along 50 nm PSBs, which radiates the second harmonic frequency at a 90°angle as discussed previously. These instrument alterations are illustrated in Figure 2.8 along with the definitions used in respect to the laboratory macroscopic frame.

In order to determine the angular distribution, prSHS responses are gathered as a function of incident polarization angle (γ) while collecting the SHS intensities produced at the V and H polarization states where V_{out} is defined when $\Pi = 0°$. Conversely, H_{out} is defined as $\Pi = 90°$. The theoretical framework is based on the work by Boudjema et al. which made this endeavor accessible by providing an open source software, PySHS, to simulate the prSHS responses based on molecular orientations along the surface of spherical and spheroid colloidal systems.[24] Briefly, the prSHS signal produced from molecules adsorbed to spherical colloidal particles can be explained by the equation:

$$I_{SHS}(\gamma, \Pi) = K^{\Pi}_{SHS}(1 + I^{\Pi}_{2,SHS}cos(2\gamma) + I^{\Pi}_{4,SHS}cos(4\gamma)) \tag{2.6}$$

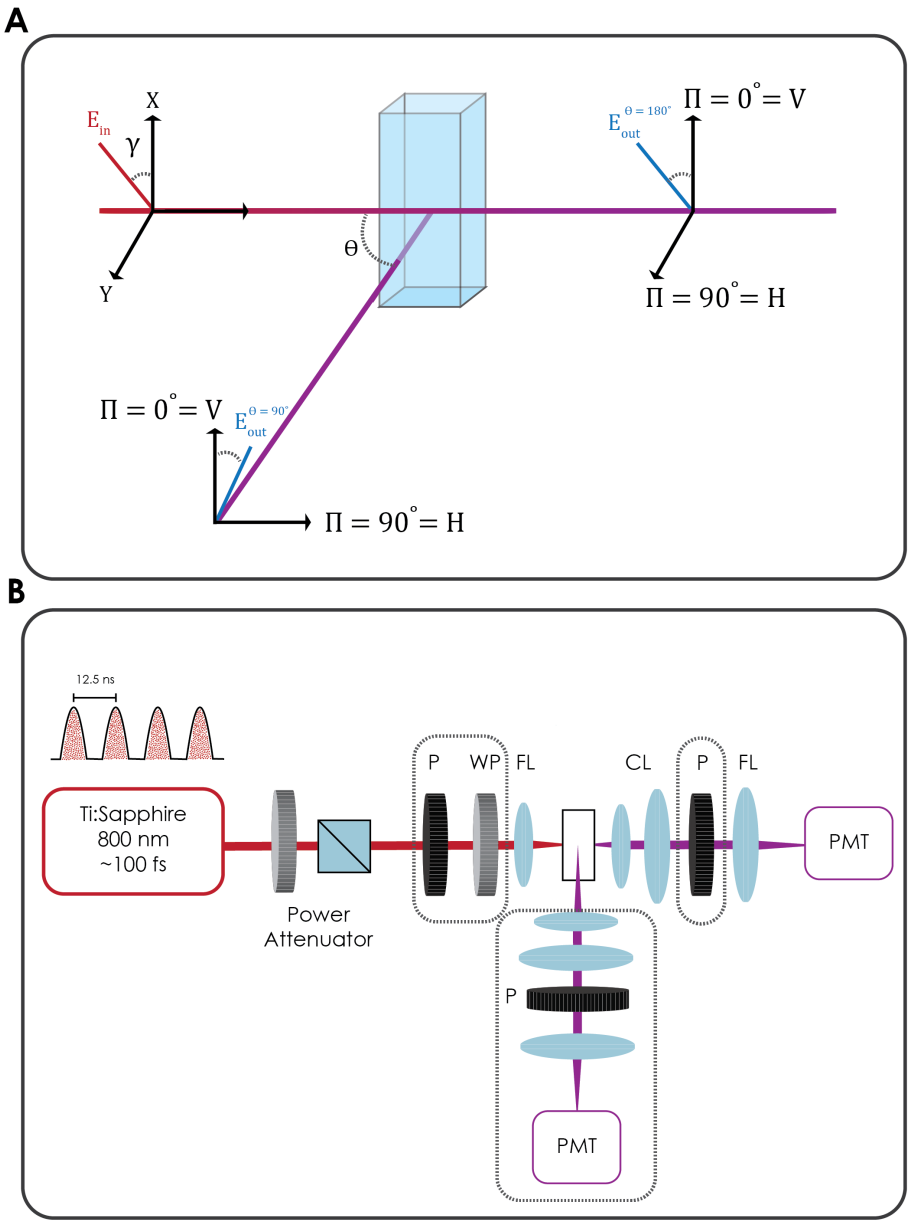


Figure 2.8: Laboratory frame notation and prSHS instrumentation. A) defines the angles used in the laboratory frame for use in prSHS experiments. B) Instrument used to perform prSHS experiments. P = polarizer, WP = waveplate.

where K^{Π}_{SHS} is a constant and $I^{\Pi}_{2,SHS}$ and $I^{\Pi}_{4,SHS}$ are coefficients that describe the local uncorrelated and correlated structures of the adsorbates. For instance, $I^{V}_{2,SHS}$ is related to the first hyperpolarizability (see Section 2.2.2) of the molecules whereas $I^{H}_{2,SHS}$ and $I^{V}_{4,SHS}$ describe the long-range order of the molecules along the surface. In cases where molecules are uncorrelated, or not confined to a surface with any organization, the I^{Π}_{4} terms approach 0 leaving only I^{Π}_{2} contributions.[138, 24] This equation is used to simulate how molecules will orient along colloidal samples, and as such, will be compared to the experimental data shown in Chapter 4.

2.3 Fluorescence Techniques

Although the primary techniques used to understand how small molecules are interacting with the membranes of living *S. aureus* and *B. subtilis* in this work are based on SHS, many fluorescence techniques are implemented here to provide complementary information about these systems. For instance, TPF is used as a probe of photobleaching and general molecule population in Chapter 3 and steady-state techniques, such as laurdan Generalized Polarization and 1,6-diphenyl-1,3,5-hexatriene (DPH) anisotropy, are used as a measure of overall membrane fluidity in Chapter 5.

2.3.1 Two-Photon Fluorescence

TPF is a third-order nonlinear optical technique in which two photons promote an electron from the ground state to an electronically excited state to produce a photon at a higher energy than the incident light source, in contrast with OPF where the generated fluorescence is typically of lower energy than the original photon, as shown in the Jablonski diagram in Section 2.1.1 (Fig. 2.1). TPF differs from SHS in that it is not reliant on the symmetry of the system because it is an incoherent technique that relies on the $\chi^{(3)}$ term in Equation 2.1 as a third-ordered technique. For instance, while SHS requires noncentrosymmetry, TPF can be produced similarly in all instances of Figure 2.2 in Section 2.2.2. The fluorescent probes used in this dissertation are fluorophores that only fluoresce when they are in a lipid environment. Therefore, the TPF signal produced is a direct reflection of the probe molecule

population in the membrane of the living cells and can consequently be used to measure a change in this population due to photodamage.

To implement TPF, like SHS, high-peak powered lasers are required. However, because TPF can be produced from the fluorophores presented in Chapter 3 with the same wavelengths used to produce SHS, but emits at a wavelength sufficiently longer than that of SHS, both TPF and SHS can be collected simultaneously from the same sample. Therefore, the same instrument proposed in Section 2.2.2 can be used for this purpose by implementing a second PMT. Consequently, the TPF signal over time can be interpreted as the probe population over time. The cartoon schematic in Figure 2.6 shows a static TPF response after the initial rise meaning that any change in the SHS signal can be assumed to result from $\langle\beta\rangle$ and not N_s which becomes a significant observation for Chapters 3 and 5.

2.3.2 Steady State Techniques

Due to the high probabilistic nature of one-photon fluorescence techniques, no specialized equipment is generally needed. Therefore, the linear, steady state methods discussed here are performed with commercial fluorometer instruments. Steady state fluorescence techniques are valuable tools to gain information pertaining to bulk properties of the systems under investigation such as overall fluidity of the membranes of living species studied here. Two techniques employed the generalized polarization of laurdan and anisotropy of DPH.

Generalized Polarization

Laurdan Generalized polarization (GP) has been extensively used to characterize lipid phase transitions of model and living membrane systems both in "bulk" geometries with fluorometry and microscopically. First synthesized and characterized in 1979 by Weber et al., laurdan is a fluorescent probe with a lauric acid fatty acid tail that is known to align with the lipid tails comprising biological bilayers while the fluorophore, a naphthalene derivative, associates with the glycerol backbone. [236] Additionally, depending on the fluidity of the bilayer, laurdan exhibits differential emission properties due to the solvent environment of the fluorophore. Specifically, laurdan is sensitive to polarity with variances in water

content. As such, it is thought that with rigid membrane regions, the laurdan molecules are less likely to be exposed to a high water content whereas when laurdan occupies fluid regions, the fluorophore is surrounded by more water molecules. This difference in hydration between rigid and fluid phases of the membrane results in a blue shift and red shift in the emission spectrum, respectively.[172, 173] Consequently, a GP value can be calculated from the fluorescence intensity at a "blue" (I_B) and "red" (I_R) wavelength, as shown by Equation 2.7.

$$GP = \frac{I_B - I_R}{I_B + I_R} \tag{2.7}$$

By calculating the GP value, the relative fluidity of the membrane can be quantitatively assessed. As such, the higher the GP value, the greater contribution of the blue shift, and therefore the membrane is expected to be more rigid. Conversely, a lower GP value signifies a more fluid membrane. [172, 173] This experiment is performed in Chapter 5 through the use of a commercial fluorometer. An excitation of 350 nm is used to observe the intensity at 440 nm and 490 nm as the blue and red wavelengths to calculate the GP values, as these are the most common in the literature.

Anisotropy

Like laurdan, DPH is a fluorophore that preferentially resides in lipid environments. However, DPH has been hypothesized to reside deeper in the hydrophobic region between the phospholipid tails, which is thought to provide a more accurate measure of membrane fluidity. To report on the lipid order, steady state anisotropy measurements of DPH are obtained. This measurement is fundamentally different from laurdan GP experiments although they provide complementary information to inform on membrane fluidity. While laurdan infers fluidity based on solvent polarity, DPH anisotropy probes the depolarization due to rotational diffusion of DPH to surmise fluidity based on changes in DPH orientation. [115]

Anisotropy of fluorophores is a measure of variances in the emission intensities at different excitation and emission polarization schemes. [1] For instance, the DPH molecule has one primary dipole moment along the long axis of the molecule that produces fluorescence when

the incident light is polarized parallel to this dipole arrangement. This photo-selection causes molecules that are oriented perpendicular to the incident light polarization to not be excited. Subsequent depolarization of the photo-selected molecules gives rise to information about the molecule's ability to rotate which is proportional to the fluidity of the membrane. The overall emitted fluorescence is then measured and analyzed based on the output polarization in respect to the excitation polarization state. This ratio of parallel and perpendicular polarized emissions is used to calculate the anisotropy using Equation 2.8:

$$r = \frac{I_{VV} - I_{VH}G}{I_{VV} + 2I_{VH}G} \tag{2.8}$$

where I_{VV} and I_{VH} are fluorescence intensities with excitation/emission polarizer combinations set to vertical/vertical and vertical/horizontal, respectively, and G is a correction factor to account for detection sensitivity and is calculated by Equation 5.3. For the G factor, excitation/emission polarizers are set to horizontal/vertical (I_{HV}) and horizontal/horizontal (I_{HH}).

$$G = \frac{I_{HV}}{I_{HH}} \tag{2.9}$$

The possible anisotropy values are limited by the photo-selection probability being proportional to $cos^2\theta$ where θ is the angle between the vertical axis of the incident polarized light and the transition moment. [1] Because of this, the theoretical limits of fluorescence anisotropy values can be derived to show:

$$r = 0.6(cos^2\beta - 1/3) \tag{2.10}$$

where β is the angle between the absorption and emission transition moments. As a consequence, the theoretical anisotropy values can range from a minimum of -0.2 to a maximum of 0.4. [1] The calculated anisotropy is telling of the membrane environment that DPH is sensing. [115] As such, a high anisotropy is indicative of a more rigid membrane whereas a low anisotropy value is representative of a more fluid membrane.

Chapter 3

Facilitating Flip-Flop: Structural Tuning of Molecule-Membrane Interactions in Living Bacteria

A version of this chapter was originally published as listed below and is reproduced with permission from Biophysical Journal.

Blake, M.J., Castillo, H.B., Curtis, A.E., Calhoun, T.R. "Facilitating flip-flop: Structural tuning of molecule-membrane interactions in living bacteria" *Biophysical Journal* **2023**, 122,10, 1735-1747.

This chapter describes experiments designed by myself and Tessa R. Calhoun. Data analysis and preparation of the manuscript was performed by myself and Tessa R. Calhoun. Experiments were performed by myself, Hannah B. Castillo and Anna E. Curtis.

3.1 Abstract

The first barrier a small molecule must overcome before trespassing into a living cell is the lipid bilayer surrounding the intracellular content. It is imperative, therefore, to understand how the structure of a small molecule influences its fate in this region. Through the use of second harmonic generation (SHG), we show how the differing degrees of ionic headgroups, conjugated system, and branched hydrocarbon tail disparities of a series of four styryl dye molecules influence the propensity to 'flip-flop' or to be further organized in the outer leaflet by the membrane. We show here that initial adsorption experiments match previous studies on model systems, however, more complex dynamics are observed over time. Aside from probe molecule structure, these dynamics also vary between cell species and can deviate from trends reported based on model membranes. Specifically, we show here that the membrane composition is an important factor to consider for headgroup-mediated small molecule dynamics. Overall, the findings presented here on how structural variability of small molecules impacts their initial adsorption and eventual destinations within membranes in the context of living cells could have practical applications in antibiotic and drug adjuvant design.

3.2 Statement of Significance

Remediation of bacterial infections is a global predicament that is challenged by the prevalence of antibiotic resistant species and the limited progress in novel drug design and discovery. It is well known that the success of antibiotics relies on an initial interaction with the plasma membrane of the target bacteria regardless of the drug's mode of action. However, few robust empirical methods currently exist for tracking and quantifying the progression of the individual steps of permeation in living bacterial membranes. These steps are, broadly, 1) initial adsorption, 2) flipping of the molecule into the inner bilayer leaflet and 3) subsequent desorption tactics. Each event leading to plasma membrane penetration is imperative to isolate in order to understand their individual contribution to the overall infiltration process. More specifically, how the structure of the exogenous small molecules, and the membrane composition they are exposed to, impact these processes is a necessary direction to explore as slight modifications of chemical structure can pose differences in membrane interactions and further pharmacokinetic properties. To address this, the interface specificity of second harmonic generation, a nonlinear optical technique, is employed to reveal how structural variances among small molecules influence their affinity to and dynamics within living bacterial lipid bilayers.

3.3 Introduction

One of the most important natural interfaces is the cellular plasma membrane. This boundary between the cytoplasm and extracellular space is responsible for maintaining structural integrity, protecting the cell from environmental stressors, and mediating small molecule transport and signaling. [217, 246] This last role is especially important for efforts to combat antibiotic resistance as penetration into the cell has limited rational drug design. [116] The typical biological membrane is often portrayed as a heterogeneous, multidimensional unit composed primarily of a phospholipid bilayer - equipped with a hydrophobic core and hydrophilic exterior - with proteins and cytoskeletal components interspersed throughout. Moreover, lipid membrane architecture is one of the characteristics that defines a living

system. For instance, the presence of membrane-bound organelles differentiates a eukaryotic cell from a bacterium, and having a single or double membrane present discerns between Gram-positive and Gram-negative bacteria classifications. Although cell types can be generally classified by their membrane design, the membranes between individual species, and even among strains of the same species, differ drastically in composition and organization. For instance, although *Staphylococcus aureus* and *Bacillus subtilis* are both Gram-positive bacteria, their carotenoid content and phospholipid headgroup/tail compositions vary drastically, imposing significant differences in membrane organization.[10, 217, 73, 237] This compositional difference between bacterial species can consequently result in contrasting interactions with small molecules, including antibiotics.[89, 225, 147]

Further, the lipid bilayer is an ever-changing landscape in which the components can alter their arrangement and composition in response to environmental cues such as changes in pH, temperature, and the presence of ions, fatty acids, and small molecules in the cells' surroundings [217, 48, 13, 258]. In some cases, this characteristic imparts drug-resistant capabilities[163, 114, 149], further necessitating the ability to examine interactions between small molecules (*i.e.* drug molecules) and living cells. As such, how small molecules adsorb and subsequently traverse this complex boundary is a facet of the scientific community that offers insight into drug development and understanding antibiotic mechanisms of actions.[213, 203, 227, 82, 186, 66, 31, 84]

Thus far, a majority of experiments capturing these phenomena are conducted on model systems although the compositions of the most commonly studied mimetic membranes differ drastically from that of infectious Gram-positive bacteria. For instance, fluidity in model systems is mostly mediated by various degrees of saturation in the fatty acid tails and cholesterol content, while for bacteria, fluidity is primarily determined by the abundance of branched-chain fatty acids instead.[5, 102] The highly negatively charged bacterial membrane is an additional factor that makes mimicking this environment a difficult task. Although there has been progress in addressing these discrepancies, model systems are still overall limited, particularly for Gram-positive bacteria. [166, 41, 52, 253, 34, 125] Due to the prevalence of Gram-positive bacteria in life-threatening infections[142, 247], it is of paramount importance to understand how small molecules navigate the living cell membrane

terrain. LogP values, a measure of a molecule's partitioning ability between hydrophobic and hydrophilic environments, is one of the primary considerations for predicting membrane permeation in current methods of drug design and alteration. Specifically, molecules with more positive computed LogP (cLogP) values are more lipophilic and thus more prone to membrane penetration up to the threshold of 5 after which reduced penetration is expected. [121] However, this approach is not always reliable as there are numerous ways to calculate this value for a molecule with a wide range of successes and failures[135], and new rules governing this behavior are needed. [116] Here, we examine how tunable parameters of small molecules, such as charge and lipophilicity, alter their adsorption and movement within the living membranes of Gram-positive bacteria, *S. aureus* and *B. subtilis* by leveraging the surface specificity of second harmonic generation (SHG).

The membrane space of living bacteria is historically difficult to probe due to, for example, a typical *S. aureus* cell spanning $\sim$1 μm in diameter and the lipid bilayer averaging $\sim$5 nm in thickness [81, 140]. Exploring intrinsic dynamics in real-time at this spatial scale is difficult due to traditional techniques being either destructive to the living specimens or lacking resolution and specificity. While electron microscopies have capabilities to resolve structures on these spatial length scales, sample preparation requires cells suspended in time [231, 50, 45, 87, 238, 255]. Additionally, separation and subsequent mass spectrometry techniques are also limited by their destructive nature [8, 79, 25, 62, 108, 113]. While not generally detrimental to biological samples, traditional light-based microscopies, such as one-photon fluorescence modalities, are limited by the diffraction limit of light. [10, 78, 143, 182, 22].

Aside from the technical limitations experimental techniques pose, living cells are impressively complex, and thus, oftentimes computational methods and, as mentioned above, mimetic membranes, such as planar or vesicular lipid bilayers, are employed to explore fundamental properties such as transport through the membrane.[34] Model membranes serve as a simplistic view of an otherwise complicated space and have offered an abundance of fundamental insight into small molecule passive diffusion. Of special interest is a membrane's ability to migrate cargo from one leaflet of the lipid bilayer to the other (*i.e.*, flip-flop) as this movement is responsible for the diffusion of small molecules, incorporating newly synthesized phospholipids from the intracellular environment to the outer leaflet, and maintaining lipid

asymmetry.[4] This is also often seen as the rate-limiting step in permeation making it a crucial parameter in assessing antibiotic penetration.[190] As such, much attention has been devoted to understanding which small molecule structural parameters impact the molecule's ability to flip-flop. There is a large body of literature proposing that contributions from the polar/charged headgroup and the hydrophobic tail regions of the penetrating molecules have significant impacts on the rate at which flip-flop occurs. For instance, many have shown that the charged nature of fatty acids and phospholipid headgroups predominantly impact the rate of flip-flop [141, 90], while others have shown that their hydrophobic tail portion may play a larger role than initially thought.[105, 157] Others have shown that both should be regarded as having considerable impacts on their translocation capabilities.[122, 7] Among this debate, other differences between classes of molecules have also been linked to dictating translocation rate. For instance, Regev, *et al.* have shown with a series of drug molecules that there is no correlation between their lipophilicity and their flip-flop kinetics;[185] Rog, *et al.* and Parisio, *et al.* attributed changes in sterol polarities to their flip-flop discrepancies;[198, 174] and lastly, Rokiskaya, *et al.* describe conflicting results owing to a small ions ability to flip-flop in correlation with their size and hydrophobicity.[192, 191] However, this large range of results suggests that the impact of these molecular parameters are highly influenced by the composition of the membrane under investigation.[100, 9, 157]

While there has been tremendous progress toward understanding how small-molecule structure influences permeation and flip-flop, there remains a necessity to employ techniques that are able to directly monitor the impacts of these parameters on living cells as their membranes are expected to be far more complex in structure and function than that of model systems. Gram-positive bacteria, such as *S. aureus*, serve as ideal bridges between studies on living and model systems. As living cells, they have a complex membrane composition as well as direct relevance for human health, but they also contain only a single plasma membrane with a size and uniform curvature reminiscent of model vesicles. The composition of Gram-positive bacterial membranes, however, varies significantly from many of the model systems typically employed. Specifically, model membrane systems often incorporate phosphatidylcholine lipid headgroups and cholesterol which are significant components of mammalian cell membranes but not membranes of Gram-positive bacteria. In

contrast, Gram-positive bacterial membranes often contain a significant amount of branched fatty acid lipid tails which aren't included in model membrane systems.[131] Therefore, here, we use SHG, a surface-specific nonlinear optical technique, to examine differences between structural variants of small molecules and their interactions with living cells.

SHG relies on the interaction of two photons of the same energy with a noncentrosymmetric medium to generate a single photon of twice the incident photon energy. [80, 210] Because of the symmetry requirement for this process, interfaces and surfaces make ideal candidates to study with SHG as symmetry is inherently broken. SHG has previously been employed in many experiments to quantify the adsorption and transport kinetics of small molecules across the membranes of model systems[155, 164, 111, 51, 85, 254, 214, 86, 197, 38, 91], living eukaryotic cells [117, 33, 208, 256, 152], and live bacteria [146, 147, 257, 248, 243, 240, 242, 206, 205, 241, 245, 244]. As such, we have previously illustrated the membrane adsorption characteristics and subsequent behavior of the styryl dye molecules FM 2-10 and FM 4-64, within *Enterococcus faecalis* and *S. aureus* membranes with SHG and two-photon fluorescence [147]. In regards to *S. aureus*, Miller *et al.* determined that the smaller, less lipophilic FM 2-10 molecule had a significantly weaker affinity for the membrane environment,[147] thus following predictions posed by Overton's Rule.[106, 150] However, the more surprising result was how the conjugation length altered their dynamics within the membrane over time. It was observed that the more highly conjugated FM 4-64 molecule had a greater propensity to experience flip-flop while FM 2-10 had a more complex behavior associated with either aggregation or movement into more rigidly organized membrane domains. [147] This study further demonstrated the feasibility of using SHG to evaluate molecule dynamics in living Gram-positive membranes. As drug molecules exhibit drastically different effects on their target cells from minuscule alterations in their structure[42, 180], it is imperative to understand how the individual moieties, aside from conjugation length, impact the independent steps of permeation, including flip-flop. There exists multiple styryl dye molecules, beyond these two, that differ in their charged headgroups, conjugation length, and branching in their tail region. By expanding our studies to include a wider range of these molecules and other cell types, we can begin to tease apart the factors with the most significant influence on the interplay between the molecules and membranes.

Here we utilize styryl dye molecules in order to examine the individual contributions to overall structure that may impact a molecule's translocation abilities without imposing detrimental effects on living cells.[147] Styryl dyes are popular membrane probes as they exhibit distinctive fluorescence signatures when bound in lipophilic environments as opposed to free molecules in solution[252, 72]. Additionally, their non-symmetric induced dipoles make them 'SHG-active' in that they can produce prominent second harmonic signals dependent on how their individual dipoles are arranged along the membrane surface. Unlike more commonly studied SHG probes, styryl dyes also remain within the membrane instead of just transporting through. This offers two unique advantages: 1) it allows a longer viewing time of the membrane environment and 2) it provides insight for more amphiphilic antibiotics including those specifically targeted to the membrane, which continues to receive attention as an attractive drug target.[93, 77, 148] The second harmonic signal produced is sensitive to how the molecules are arranged relative to one another and in response to their immediate environment, as explained schematically and mathematically below in Figure 3.1 and Equations 3.1 and 3.2, respectively.

The SHG signal (I_{SHG}) resulting from the alignment of molecules at an interface is directly proportional to the product of the two incoming electric fields (E_ω) and the effective second-order nonlinear susceptibility term ($\chi^{(2)}_{eff}$) as depicted in Equation (3.1).

$$I_{SHG} = \mid E_{SHG} \mid^2 = \mid \chi^{(2)}_{eff} E_\omega E_\omega \mid^2 \tag{3.1}$$

$\chi^{(2)}_{eff}$ is a tensor element that describes the symmetry dependence of the resulting signal. Assuming the electric field of the incoming light being applied to a sample stays constant for the duration of an experiment, it can also provide insight into the source of change in the intensity of an SHG signal over time by considering its two constituent terms:

$$\chi^{(2)}_{eff} \propto N_s \langle \beta \rangle \tag{3.2}$$

As seen in Equation (3.2), the value of $\chi^{(2)}_{eff}$, and therefore the resulting SHG intensity, can be described by 1) the relative population of the probe molecules in the membrane (N_s) and 2) the orientational average of the hyperpolarizability ($\langle \beta \rangle$). N_s is simply determined

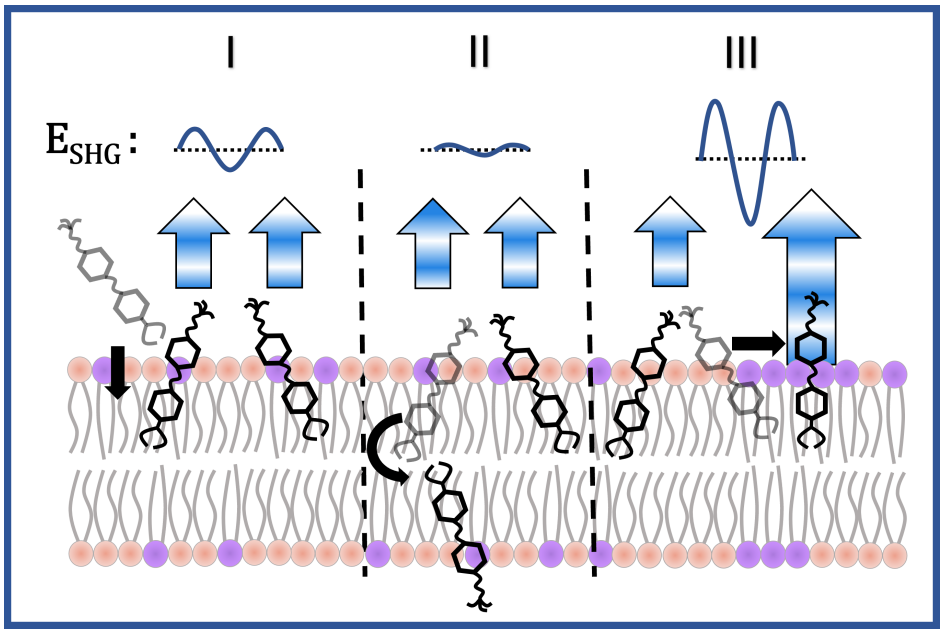


Figure 3.1: Cartoon schematic of styryl dye molecules interacting with a lipid bilayer and the resulting SHG signals (E_{SHG}). After adsorption to the membrane, (I) dye molecules produce an initial SHG signal. The molecules can then either (II) flip-flop to produce destructive SHG signals, or (III) migrate to a more rigid environment that enhances the overall orientationally averaged hyperpolarizability, producing a greater intensity SHG response.

by how many molecules are being illuminated in the noncentrosymmetric space of the bacterial surface and can vary depending on the number of surface sites available and the probe molecule concentration. In the second term, the hyperpolarizability alone (β) refers to the oscillatory strength of the light-induced dipole in response to the molecule's chemical environment (i.e. presence of ions and/or solvent identity), whereas $\langle\beta\rangle$ describes the orientational average of the overall arrangement of these dipoles. Figure 3.1 illustrates how the latter term can alter the ensuing signal. In each case displayed, the number of probe molecules stays constant, but the orientation of them varies. In panel I, two molecules are inserted into the outer leaflet of the example lipid bilayer. Assuming the location of these probe molecules is in a fluid-like region of the membrane, the probes will insert with a large degree of variability in their angular orientation with respect to each other, and thus a less-than-perfect constructive interference of their second harmonic signals. After initial adsorption into the outer leaflet, possible fates of the molecules are shown in the successive panels. In panel II, it is illustrated how when one of the molecules present in the outer leaflet flip-flops into the inner leaflet, the orientation of each molecule arranges in an anti-parallel fashion producing opposite phases, and thus, destructive interference lowering the SHG intensity. Lastly, as illustrated in panel III, the probe molecules could instead migrate to a more rigid environment in the membrane space. The rigidified lipids surrounding the membrane probe reduce the variability in the molecules' angular orientation promoting a higher degree of alignment with one another. This phenomenon significantly increases the $\langle\beta\rangle$ term and the resulting SHG intensity. This contribution to $\langle\beta\rangle$ is what we propose herein, however other possible factors resulting in a change to β itself could also be at play. These factors include the probe molecules aggregating or experiencing a change in solvent identity. [218, 199, 215]

Herein, we perform a series of experiments to answer the following posed questions: 1) How do the size and shape of the hydrophobic moieties impact the molecules' behavior in the membrane of a living cell? 2) Does the headgroup identity of the styryl probes have a significant role in these dynamics? and, 3) does the cell membrane composition between cell types impose differences in small molecule translocation? Answers to these questions will identify those structural properties that control membrane permeation and discrepancies

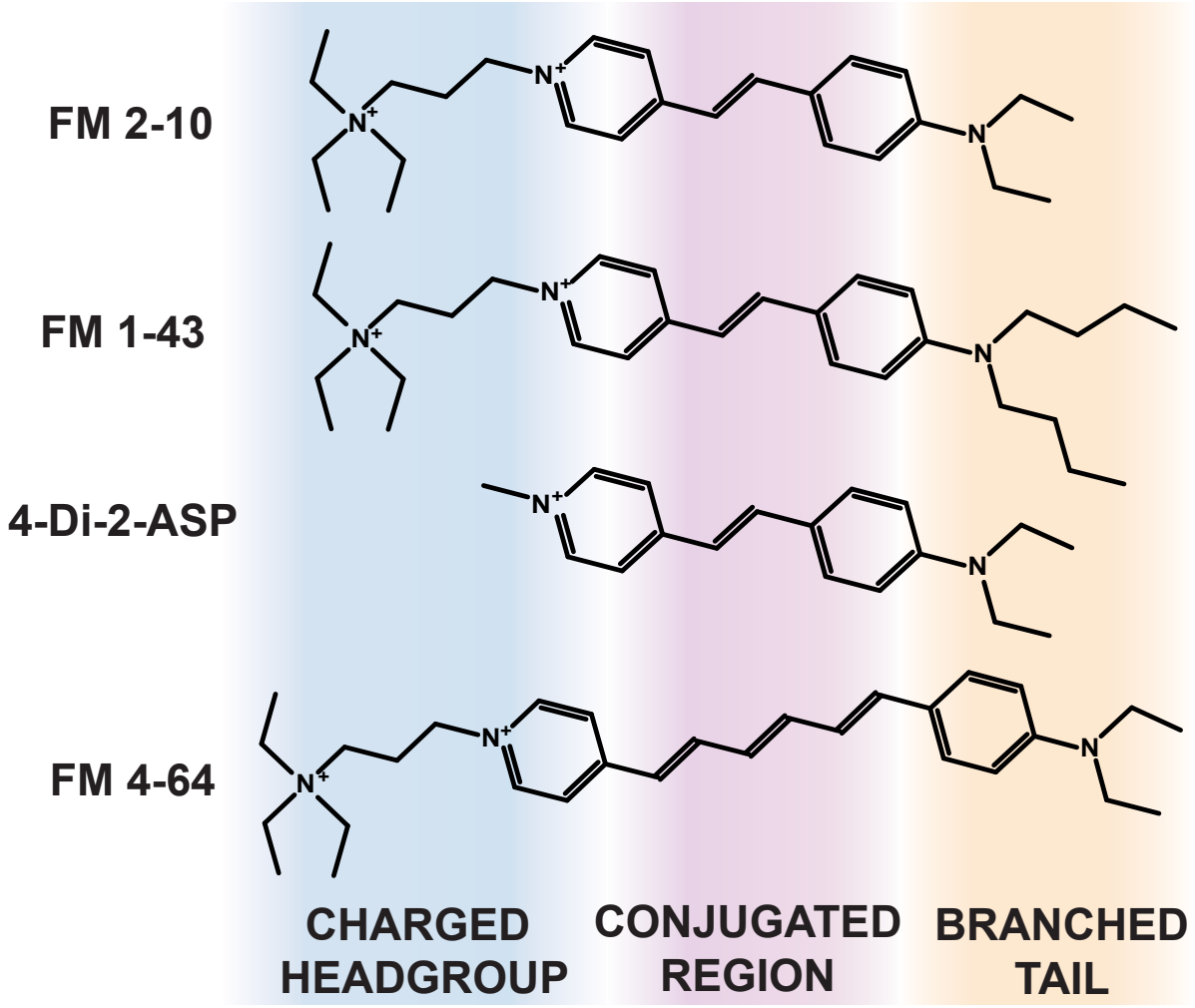


Figure 3.2: Structures of membrane probes FM 2-10, FM 1-43, 4-Di-2-ASP, and FM 4-64. Chemical structures of the probe molecules with colored shaded background regions indicating the charged headgroup (blue), conjugated region (purple) and the branched tail (orange).

between behavior on living cells relative to those published for model systems. As such, we examine the structural parameters of headgroup identity, length of the conjugated region, and the length of the branched tails on molecules FM 2-10, FM 4-64, FM 1-43 and 4-Di-2-ASP (Figure 3.2). The latter two parameters allow us to differentiate between the impacts of overall hydrophobicity versus the shape of the hydrophobic region. Additionally, we examine the impact of the membrane composition by showing differences in molecule dynamics in the membranes of *S. aureus* and *B. subtilis*.

We employ SHG in two ways: first to quantify the adsorption of the aforementioned molecules onto living bacterial cell membranes with adsorption isotherm experiments, and second, to monitor the movement of the molecules with time-resolved SHG measurements. In the first set of experiments, SHG is measured as a function of probe molecule concentration ranging from 0 to 800 μM in order to extract adsorption affinities to the membrane surface. In the second set of experiments, SHG is measured as a function of time to reveal time-dependent dynamics of the styryl dye molecules within the membrane space. For all time-resolved SHG experiments, the probe dye concentrations were fixed at 16 μM. We determine that branching in the tail of the probe molecules has minimal impact on the initial interactions but drastically impacts flip-flop once inserted into the membrane compared to a molecule with its hydrophobic tendencies localized in a straight conjugated chain. Conversely, we show that the probe's headgroup identity plays a small role in membrane affinity and, for *S. aureus*, little difference in dynamics over time, in direct opposition to model systems. However, by performing similar experiments with *B. subtilis*, we determine that the membrane composition is a crucial determinant in the dynamics imparted by the headgroup identity of styryl molecules.

3.4 Materials and Methods

3.4.1 Bacterial Strains and Dye Solutions

S. aureus (ATCC 27217) and *B. subtilis* 168 were the bacteria used in the experiments outlined above. Cells were prepared similarly to what we have done previously.[147] *S. aureus*

and *B. subtilis* cells were incubated overnight on brain-heart infusion (BHI)(Sigma-Aldrich, St. Louis, MO) and Luria-Bertani Broth (LB)(Sigma-Aldrich, St. Louis, MO) agar plates , respectively. Single colonies were then inoculated into liquid BHI or LB with a 1:5 media-to-head space ratio. Flasks of *S. aureus* and *B. subtilis* were grown anaerobically and aerobically at 250 RPM, respectively, overnight at 37°C until cells reached stationary phase and then transferred to fresh media to an optical density at 600 nm (OD_{600}) of ∼0.01 and grown until the OD_{600} reached ∼0.2. OD's were measured using an ultraviolet-visible spectrophotometer (SHIMADZU UV-2600; Shimadzu, Columbia, MD). Once the appropriate OD was reached, the cells were filtered using a 0.22-micron cellulose nitrate vacuum filter with phosphate buffered saline solution and subsequently resuspended into BHI or LB supplemented with 2% EC-OxyRase to an OD_{600} of ∼0.2. All cell samples were prepared immediately before beginning each trial.

For each dye, 0.4, 0.8 and 1.6 mM stock solutions were prepared in 0.2 micron filter-sterilized 80:20 MilliQ water (Sigma-Aldrich, Burlington, MA; 18.2 MΩ · cm) to dimethyl sulfoxide (DMSO) (Thermo Fisher Scientific, Suwanee, GA). FM 2-10 (SynaptoGreen C2), FM 1-43 (SynaptoGreen C4), and FM 4-64 (SynaptoRed C2) were purchased from Biotium (Fremont, CA). 4-Di-2-ASP (4-di-2-asp) was purchased from Sigma-Aldrich. All probe molecules were used as received.

3.4.2 SHG Instrument and Flow Cell Passivation

A home-built SHG spectroscopy instrument was used in the adsorption isotherms and time-dependent experiments, details of which have been previously described elsewhere [147, 146]. Briefly, laser pulses from an 80 MHz MaiTai Ti:Sapphire oscillator (Spectra Physics, Santa Clara, CA) compressed to approximately 95 fs were directed through a power attenuator comprised of a half-wave plate and polarizing beam splitting cube and then sent towards the sample housed in a 2 mm path length quartz flow cell (Starna Cells, Atascadero, CA). After traversing through the sample, the forward propagating signal was collected through a series of lenses followed by a fiber and sent to a photomultiplier tube (Hamamatsu, Bridgewater, NJ) and filters to collect SHG responses. A 450 nm long pass filter (Edmund Optics, Barrington, NJ) was placed before the sample to ensure the second harmonic frequency

being detected was produced from the sample itself and not any previous optics. A 725 nm short pass filter (Edmund Optics) was placed directly before the optical fiber to omit the fundamental wavelength. For all cases, a 400/10 nm bandpass filter (Edmund Optics) was used directly before the respective PMT to obtain the SHG response. Additionally, malachite green/polystyrene beads power studies were carried out both before and after data collection to ensure instrument stability.[235] All data was collected using LabView and analyzed with MATLAB using in-house codes.

To ensure no cell or protein adsorption onto the sample housing, the quartz flow cell was passivated 30 minutes before each individual isotherm and time-dependent trial using a bovine serum albumin (BSA)(Sigma-Aldrich)/1% glutaraldehyde (Thermo Fisher Scientific) cross-linking procedure [175]. Briefly, 1 M hydrochloric acid was introduced to the flow cell for ∼30 minutes and then flushed with 50 mL of sterile MilliQ deionized water. Cold (∼ 4°C) 10 mM Tris buffer (pH adjusted to ∼7.4) (Sigma-Aldrich) was then rinsed through to prepare for the BSA solution. BSA was prepared immediately before introduction to the flow cell with Tris buffer to a final concentration of 50 mM and then filter sterilized with a 0.22 micron PES filter. BSA was incubated in the flow cell for 10 minutes and then followed with a 10 minute incubation period of a 1% glutaraldehyde solution prepared with Tris. Lastly, Tris was flushed through once more. Air was pushed through the flow cell followed by a 1 mL aliquot of prepared cells that was then discarded.

3.4.3 Adsorption Isotherms

For the SHG adsorption isotherm experiments, 990 μL of cells suspended in BHI and 2% OxyRase were aliquoted into sterile micro-centrifuge tubes. Stock solutions of each dye were made in a filter-sterilized solution of 80:20 MilliQ water:DMSO. A serial dilution of the dye solutions were prepared into separate sterile micro-centrifuge tubes. To prepare the sample, the dye was introduced into the aliquot of cells for a final DMSO concentration of 0.2% and then transferred to the quartz flow chamber. Data were acquired immediately after sample preparation. Cells were exposed to 350 mW of light for a total of 1 s with the signals being recorded every 25 ms. A Langmuir adsorption isotherm model was then fitted to the average of 3 trials to obtain the dissociation constant (K_d) of each dye:

$$\theta = \frac{\frac{[c]}{K_d}}{1 + \frac{[c]}{K_d}} \tag{3.3}$$

where θ is the number of available surface adsorption sites and [c] is the concentration of available probe molecules.[147, 146, 55, 165]

3.4.4 Time-dependent Experiments

A home-built gravity flow apparatus with autoclave-sterilized tubing was used in the time-dependent experiments. In a sterile media bottle, 7 mL of cells in BHI/OxyRase were flowed cyclically through the apparatus at a rate of ∼7 mL/min. Signal was recorded every 25 ms for a total of 8000 s with 70 μL of dye solution being introduced to the initial reservoir of cells at 600 s for a final DMSO concentration of 0.2%. Power was reduced to 35 mW for these experiments due to the extended period of data collection.

3.5 Results and Discussion

3.5.1 Impacts of Molecule Structure

Tail Branching and Conjugation Length

We start our analyses by considering the hydrophobic moieties of the probe molecules, namely the conjugated regions and branched tails highlighted by the purple and orange regions in Figure 3.2. First, we will examine how this region influences the affinity of the probe molecules to the membrane environment. This is quantified by fitting the SHG responses to increasing probe molecule concentration to a Langmuir adsorption model as the SHG intensity is directly proportional to the dye coverage along the cell surface (*i.e.*, θ in Equation 3.3 in Materials and Methods). In doing so, the dissociation constant (K_d), equivalent to the inverse of the association constant (K_a), for each molecule can be extracted.The K_d values are indicative of the fraction of the rate molecules are dissipating (k_{off}) from to the rate they are adsorbing to the lipid bilayer (k_{on}), which are metrics that have been used previously to

Table 3.1: Dissociation constants (K_d) and cLogP values[a] for each membrane probe for *S. aureus* and *B. subtilis* extracted from SHG adsorption isotherms fit to the Langmuir adsorption model.[b]

Membrane Probe	***S. aureus*** $\mathbf{K}_d(\mu\mathbf{M})$	***B. subtilis*** $\mathbf{K}_d(\mu\mathbf{M})$	**cLogP**
FM 4-64	14.5 ± 5[c]	-	-1.6
FM 1-43	9.0 ± 1.6	-	-0.29
FM 2-10	280 ± 33[c]	72.1 ± 21	-2.4
4-Di-2-ASP	152 ± 40	56.7 ± 13	-0.28

[a] Values were obtained from ChemDraw software.
[b]Error is displayed as standard error to the fit of the model, $n = 3$ for each probe.
[c]K_d values reported in [10]

describe adsorption of FM probe molecules to model systems.[252] This ratio is representative of the concentration of molecules required to inhabit 50% of the available surface adsorption sites on the membrane.[60] As such, the lower the K_d value is, the higher affinity the probe molecule has for the membrane. We have previously assessed the adsorption behavior of the probes FM 4-64 and FM 2-10 (K_d values shown in Table 3.1). [147] As such, we have shown that the increased lipophilic nature of FM 4-64 resulted in an increased affinity for the membrane environment. Here, we extend our studies to consider how the shape of the branched portion may impact initial adsorption. Specifically, between FM 4-64 and FM 1-43 (Fig. 3.3b), there is no significant difference between their affinities to the membrane, despite a relatively large difference in their cLogP values, -1.6 vs. -0.29, as determined by ChemDraw software and listed in Table 3.1. These two molecules are expected to reside in the same depth as their hydrophobic moieties are similar in length. However, their hydrophobic moieties are distributed differently where FM 4-64 has a longer straight conjugated chain and FM 1-43 has longer saturated carbon chains extended from the tail. We expect this structural difference between FM 4-64 and FM 1-43 will allow for differing lateral occupation, or the area of space in which a molecule resides when incorporated into a membrane leaflet. It can be noted, however, that this difference in lateral occupation does not lead to any difference in anchoring within the membrane as the k_{off} values between these molecules are presumably comparable given the similarities in their K_d values. As such, the width of the molecule seems to have minimal effects on the overall adsorption to the membrane space of *S. aureus*. Therefore, the more notable feature giving rise to a strong affinity to the membrane is the overall hydrophobic moiety lengths of the exogenous molecule regardless of whether this property lies in the branched tail or the conjugated chain.

While increasing both the length of the branched tail and the conjugated region resulted in similarly increased affinities for the membranes, the individual contributions to the molecule's architecture show significant time dynamic discrepancies. First, we will discuss the impact of increasing the length of the conjugated region, while the rest of the molecule remains the same. To do so, we will directly compare the behavior observed in the time-dependent trials of FM 2-10 and FM 4-64, as shown in Figure 3.4A. We have previously reported how increasing only the conjugation length changes the dynamics of the small

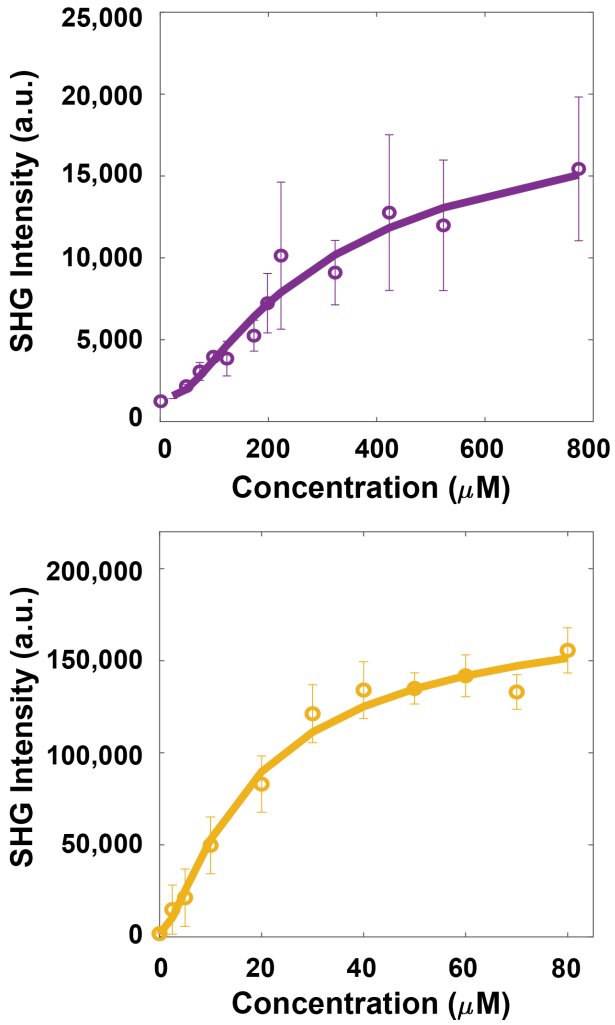


Figure 3.3: SHG adsorption isotherms of 4-Di-2-ASP (top) and FM 1-43 (bottom) with *S. aureus* living cells. For each probe, $n = 3$. Circles ($\circ$) represent the averages of the individual trials while the solid lines (—) are the fits from the Langmuir model. Error bars are representative of standard deviations. K_d values are shown in Table 3.1

molecules within the membrane over time [147]. Briefly, both dyes initially adsorb to the membranes seen as the first rise in SHG signal (Figure 3.1(I)). Thereafter, the less lipophilic molecule, FM 2-10 (see cLogP values in Table 3.1), shows an increase in SHG signal as is also shown in this report. In contrast, the FM 4-64 probe experiences a decrease in SHG signal over time indicative of flip-flop (Figure 3.1(II)). We consequently concluded that increased conjugation, and thus increased lipophilicity, results in flip-flop.

While comparing FM 2-10 and FM 4-64 above considers the impact of the length of the small molecule's hydrophobic portion, we can also assess the impact of the shape of the hydrophobic region by comparing FM 4-64 and FM 1-43 (Figure 3.2). Here there is a divergence between the increased dye molecules' hydrophobicity arising from either the length of the conjugation (FM 4-64) vs. the branched tail (FM 1-43) leading to overall similar molecular lengths but different widths in the hydrophobic region. This structural difference results in disparate behaviors between these probe molecules in the membrane space over time despite them experiencing comparable adsorption affinities for the *S. aureus* membrane. Both molecules experience flip-flop indicated by a relative decrease in SHG signal over time but, as seen in Figure 3.4B, while FM 4-64 slowly decreases until it reaches approximately 50% of its maximum intensity after the two-hour duration, the FM 1-43 molecules flip-flop more rapidly, reaching it's lowest intensity within 30 minutes but then slowly rises in signal for the remainder of the experiment which may indicate aggregates forming in one or both bilayer leaflets or the eventual migration of molecules to more rigid environments, as depicted in Figure 3.1. These discrepancies can be explained by the increased length of the *branched region* in the tail of the FM 1-43 probe in comparison to the two-carbon chains of FM 4-64. As alluded to above, FM 1-43 occupies a larger lateral site than would be expected for the straighter FM 4-64 molecules when adsorbed to the membrane due to the increased width in the tail region of the FM 1-43 molecules. By requiring more lateral space in the membrane, the FM 1-43 molecules can be expected to create an immediate area of increased fluidity which may provide the space to facilitate flip-flop. Alternatively, this difference in lateral occupation may vary the probe molecule's affinity for certain portions of the membrane in which FM 1-43 is attracted to more fluid-like regions that were already present in the membrane. While the studies monitoring impacts from the hydrophobic tails mentioned

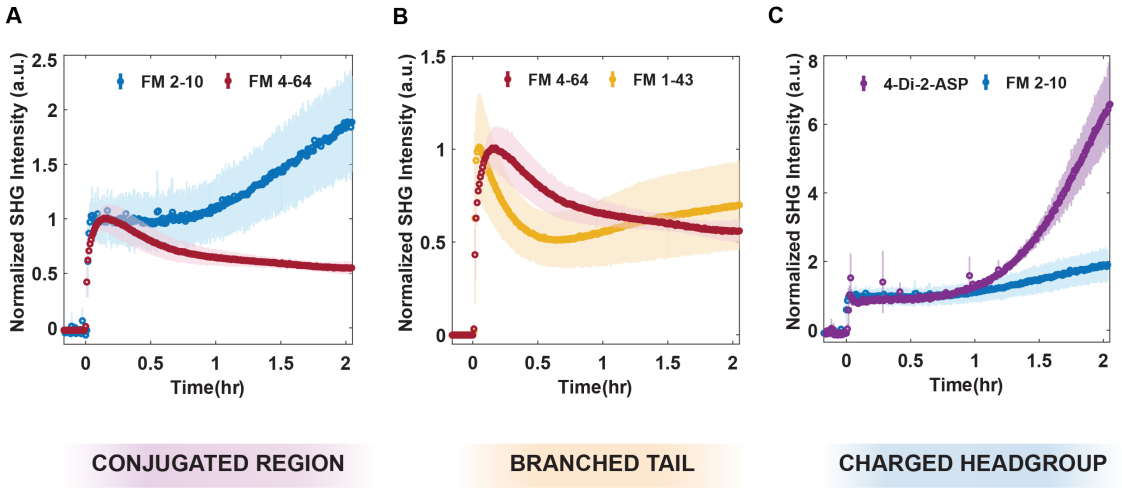


Figure 3.4: 16 μM membrane probe time-dependent SHG trials with *S. aureus* cells. (A) compares FM 2-10 and FM 4-64 to show differences arising from conjugation length, (B) portrays similar lipophilic lengths of FM 4-64 and FM 1-43 having comparable SHG responses, and (C) shows how headgroup identity impacts membrane dynamics (4-Di-2-ASP versus FM 2-10). For each membrane probe, $n = 3$ and shaded regions represent the standard deviation between the individual trials.

above increase the length, here, we are examining a modification to the lateral structure in addition to the length of the exogenous molecules.

It is interesting to acknowledge that while FM 1-43 molecules primarily flip-flop in the membrane space of *S. aureus*, alternate mechanisms begin to arise soon thereafter - a transpiration not previously considered a possibility as it is not commonly reported in model systems. This implies that the dynamic landscape of the bacterial membrane is mediating additional organizational forces. Further, it seems that this phenomenon is highly dependent on the probe molecule's structure as a rise is not seen during the same time period for FM 4-64. The results from this experiment further demonstrate the necessity to monitor flip-flop and potential events occurring afterward in living cell membranes.

Impact of Probe Headgroup Charge/Size

The headgroup of membrane-residing small molecules has been hypothesized to be a crucial ingredient when attempting to promote flip-flop dynamics.[141, 90, 198, 174] By comparing molecules FM 2-10 and 4-Di-2-ASP (Fig. 3.2), we can directly assess how the contributions arising from the headgroup region impacts initial adsorption and subsequent membrane dynamics. The K_d values observed for probes FM 2-10 and 4-Di-2-ASP are both significantly greater than those witnessed for molecules FM 4-64 and FM 1-43, discussed above. Moreover, it can be seen that the reduced headgroup charge from +2 on FM 2-10 to that of +1 on 4-Di-2-ASP results in a smaller K_d value signifying the singly-charged molecule has a greater affinity for the membrane. Aside from differences in charge, FM 2-10 has a bulkier substituent in the headgroup so sterics may also be involved in the differences seen between FM 2-10 and 4-Di-2-ASP adsorption. Further, the adsorption discrepancies between FM 2-10 and FM 1-43/FM 4-64 are expected as FM 2-10 is significantly less lipophilic than both FM 1-43 and FM 4-64. However, 4-Di-2-ASP is the most lipophilic molecule of the four examined here, as determined by their cLogP values (Table 3.1). These results show that the cLogP values are not always reliable indicators of membrane adsorption.

The time-dependent experiments performed with FM 2-10 and 4-Di-2-ASP interacting with *S. aureus* show that these two molecules exhibit the same overall dynamics, although to different extents. As can be seen in Figure 3.4C, both show a relatively static initial

signal with an overall increase in SHG over the two-hour time period. We have previously considered both cell growth and increased probe population (*i.e.* components responsible for changes in N_s, Eq. 3.2) in the membrane space as contributing factors to this rise in signal.[147] However, we have shown that the cells are restricted in their growth by the temperature at which these experiments are conducted and the two-photon fluorescence signal remained fairly static throughout the course of the experiments (Figure 3.5).[147] As such, as seen by Equation 3.2, this leaves the only contribution to an increase in SHG to be due to a change in the $\langle\beta\rangle$ term. As discussed above, we propose that the increase in this term could arise from the probe molecules associating with a change in solvent identity or neighboring lipids, aggregating in the membrane space, or moving to more rigid environments.

While both rise in signal, 4-Di-2-ASP appears to have a more significant rise in comparison to FM 2-10. In fact, while the overall SHG intensity increases by the two-hour mark for both membrane probes, the final SHG intensities rise more than a factor of 7 and 2 for 4-Di-2-ASP and FM 2-10, respectively. As discussed above, the charge, steric characteristics, or a combination of both, may be the cause of this behavior. We hypothesize that the quicker rate and larger signal may be due to the reduced charge and size of 4-Di-2-ASP causing less repulsive forces between one another while embedded in the membrane resulting in more favorable lateral migration throughout the membrane. The decrease in size may enable a tighter packing of probe molecules in the membrane which could cause a large rise in SHG signal, as observed here. [199, 215] More importantly, while others have seen that decreasing the sterics and altering the charge of the headgroup may lead to an increased rate of flip-flop[190, 191], this phenomenon is not observed here. In fact, it appears that 4-Di-2-ASP has a greater aversion to flip-flop than FM 2-10 which is in opposition to what is commonly reported for model systems. Additionally, as for 4-Di-2-ASP, in the presence of one particular type of model vesicles, it was shown that the molecules readily flip from one leaflet into the other, with no indications of aggregation or organization. [38] The disparities described here between our experiments and those performed on model systems further illustrate the necessity for future experiments to supplement the repertoire of small molecules with varying headgroup charge and/or size in the context of living cells.

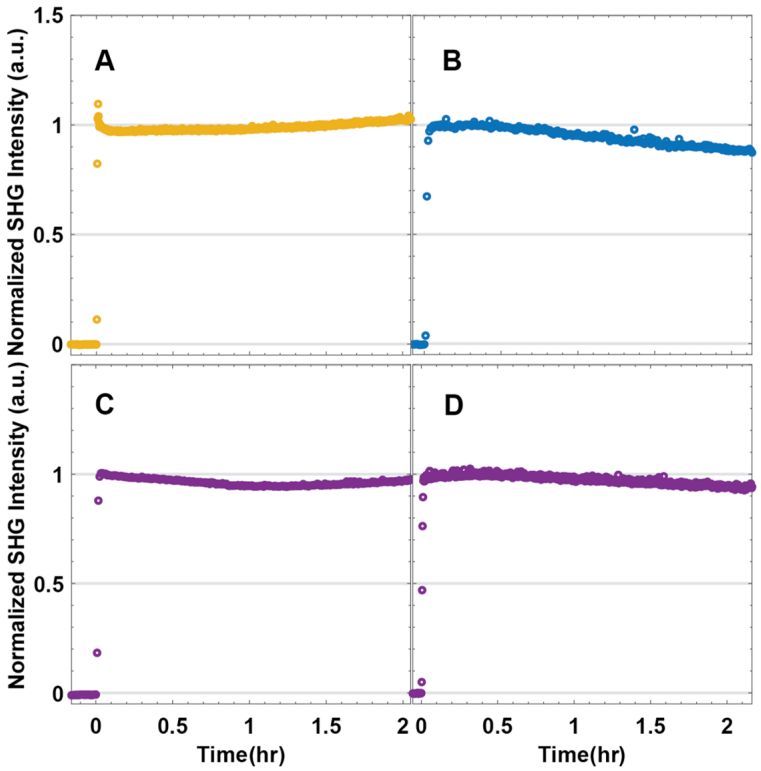


Figure 3.5: Two-photon fluorescence time-dependent trials of (A) FM 1-43 interacting with *S. aureus* cells, (B) FM 2-10 interacting with *B. subtilis* cells, and 4-Di-2-ASP interacting with (C) *S. aureus* and (D) and *B. subtilis*.

3.5.2 Impacts of Membrane Composition

It is ubiquitously agreed upon that the bilayer lipid composition influences molecule-membrane dynamics among the mimetic membrane community.[100, 9, 157] However, the extent of this factor has yet to be fully explored in living bacterial cells. We have shown here that the membrane identity plays a crucial role in the dynamics displayed by a small molecule. As alluded to above, *B. subtilis* is another Gram-positive bacterium that differs from *S. aureus* by its shape, protein population and lipid headgroup and tail identities. Our purpose for studying this cell species was to address the generality of the claims gathered from our experiments with the FM dyes presented here and *S. aureus*. To do so, we focused on revisiting the apparent minimal role of the probe molecule's headgroup identity on adsorption and dynamics over time.

As can be seen in Figure 3.6 and Table 3.1, FM 2-10 and 4-Di-2-ASP have considerable differences in their affinity to *B. subtilis* compared to *S. aureus*. Although the trend remains the same - the smaller, less bulky headgroup substituent results in a greater affinity to the cell species - the magnitude of the molecules' affinity is greater for *B. subtilis*. Specifically, FM 2-10 has an affinity for the *B. subtilis* membrane ∼4 times greater than that for *S. aureus*. Similarly, the K_d of 4-Di-2-ASP is ∼3 times larger for *S. aureus* than *B. subtilis*. However, the results from the time-dependent trials, shown in Figure 3.7, reveal the two probe molecules demonstrate starkly different dynamics in *B. subtilis*. Whereas FM 2-10 had an immediate rise due to adsorption and a subsequent slow increase over the duration of the experiment in *S. aureus*, for *B. subtilis*, the second rise for the probe molecule, associated with membrane organization, is ∼6 times faster. Soon thereafter, the signal in *B. subtilis* decays slightly and remains fairly constant for the duration of the experiment. However, 4-Di-2-ASP did not share this trend at longer times. Despite 4-Di-2-ASP displaying a large propensity to remain in the outer leaflet of *S. aureus*, the exact opposite occurs when this molecule interacts with *B. subtilis*. After the initial interaction, a slight rise is detected similarly to FM 2-10 with *B. subtilis*. Following this increase in signal, instead of a drastic rise over time as seen with *S. aureus*, 4-Di-2-ASP in the *B. subtilis* membrane environment exhibits flip-flop at a rate congruent to FM 1-43 with *S. aureus*.

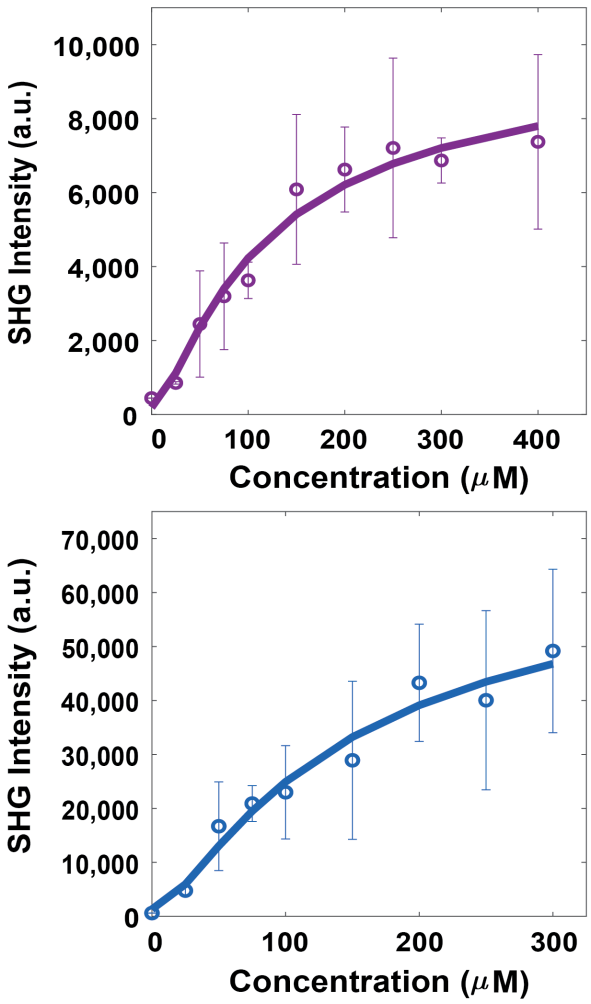


Figure 3.6: SHG adsorption isotherms of 4-Di-2-ASP (top) and FM 2-10 (bottom) with *B. subtilis* living cells. For each probe, $n = 3$. Circles ($\circ$) represent the averages of the individual trials while the solid lines (—) are the fits from the Langmuir model. Error bars are representative of standard deviations. K_d values are shown in Table 3.1

This discrepancy in membrane dynamics most likely arises due to differences in membrane composition and organization between these two bacteria. A recent study on model systems has proposed that membrane thickness is one of the leading parameters controlling small molecule permeation.[68] Based on electron microscopy experiments, the membrane thickness of *S. aureus* is 5.4±0.4 nm[140] while the *B. subtilis* plasma membrane was found to be thicker at 6.6±0.8 nm.[139] Given that more flip-flop is observed in our *B. subtilis* experiment, membrane thickness is not expected to be the dominant contributor. Both *B. subtilis* and *S. aureus* have been shown to possess membrane structural heterogeneity, most commonly referred to as regions of increased fluidity (RIFs) or functional membrane microdomains (FMMs), respectively, which are thought to play roles in passive diffusion of small molecules.[216, 124, 68] These domains are primarily described as localized, distinct ares of increased or decreased fluidity. Overall, fluidity in the membranes of both species is governed by the ratio of branched-chain fatty acids (BCFAs) of the lipids. Domains differing in rigidity/fluidity in the bacterial membrane then arise from spatial heterogeneity in the concentrations of these BCFAs which has been proposed to be mediated by multiple molecular species including carotenoids and specific proteins.[73, 233, 200] The percentage of BCFAs in the membranes of these bacteria is starkly different: ∼50% of the lipids in the *S. aureus* plasma membrane contain BCFAs[201] while in *B. subtilis* this is over 90%.[101, 166] In addition, *S. aureus* membranes contain the carotenoid, staphyloxanthin, which is absent in *B. subtilis*.[64] This disparity in membrane composition between these bacterial species results in differing overall membrane fluidity and organizational forces. The more fluid membrane corroborates what is commonly seen in the literature where a probe molecule with a smaller headgroup results in a quicker flip-flop rate, and thus a greater propensity to do so.[191] However, these results show that this generalized statement cannot be applied to all systems, especially complex and dynamic living bacterial membrane systems.

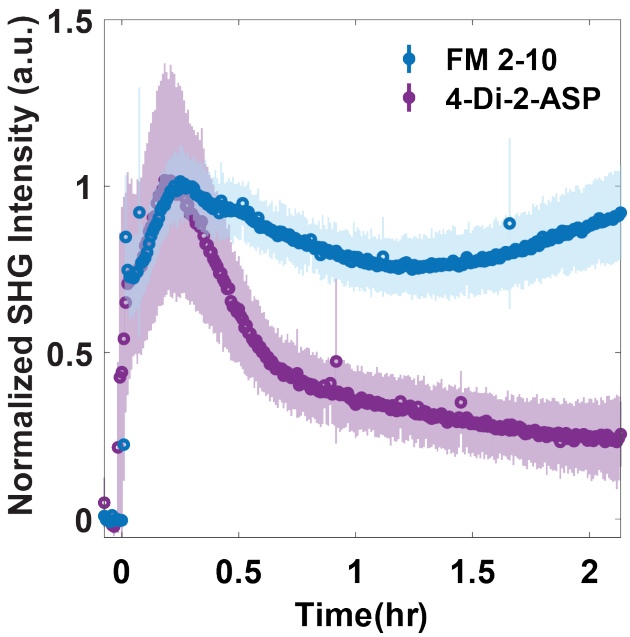


Figure 3.7: 16 μM 4-Di-2-ASP and FM 2-10 time-dependent normalized SHG trials with *B. subtilis* cells. For each membrane probe, $n = 3$ and shaded regions represent the standard deviation between the individual trials.

3.6 Conclusions

In summary, we have shown through the interface specificity of second harmonic generation that the fate of small molecules interacting with the membrane of living *S. aureus* can be tuned through specific structural changes. Moreover, we have shown that the dynamics of these small molecules cannot be generalized for all membrane systems, or even the seemingly similar Gram-positive bacterial membranes, by illustrating that dynamics of small molecules are also dependent on the membrane composition. Through adsorption kinetic studies, we have found that the major factor contributing to initial interactions is reliant on the length of the hydrophobic region of the molecule, no matter whether that length resides in the conjugated chained region or the branched tail of the styryl dyes presented here. However, these results do not always trend along with apparent LogP values. To a smaller degree, we have also shown that a smaller charge and size in the headgroup region of the small molecule interacting with the phospholipid headgroups of the lipid bilayer are associated with stronger adsorption to the outer leaflet for both species investigated. These initial adsorption experiments support what has been shown in the literature regarding how the structure of a small molecule impacts binding to the membrane space of model systems despite models, eukaryotic cells, and bacteria displaying differences in phospholipid headgroup distributions.[131]

The time-dependent experiments presented here provide new insight as to what parameters on small molecules result in flip-flop versus the molecules undergoing predominate organization in the outer leaflet. For *S. aureus*, smaller molecules, FM 2-10 and 4-Di-2-ASP, show a propensity toward the latter while larger, more lipophilic molecules exhibit flip-flop. More specifically, increasing the length of the branched tail, and more so the width of the tail, promotes the most rapid flip-flop observed for the molecules examined. However, as exhibited by FM 1-43, the small molecules may be subjected to additional organization by living cell membranes after flip-flop has occurred. This finding is significant in that we explicitly show lateral contributions should be considered when assessing flip-flop dynamics as well as the events taking place afterward. As for *B. subtilis*, there was a greater impact from the headgroup identity with the singly charged 4-Di-2-ASP molecule exhibiting a large

degree of flip-flop, demonstrating how the membrane composition can alter these dynamics. These results are not only important considerations for designing drugs that will successfully penetrate into bacterial cells but can also be exploited to target specific cell species.

3.7 Author Contributions

M.J.B. and T.R.C. contributed to the design of the experiments, data analysis, and preparation of the manuscript. M.J.B., H.B.C., and A.E.C. performed the experiments.

3.8 Acknowledgements

The authors thank the National Institute of General Medical Sciences of the National Institutes of Health under award number R35GM142928 and the National Science Foundation REU fellowship under award number NSF-CHE-1852160 for support.

Chapter 4

Probing Bacterial Membranes with Polarization-Resolved Second Harmonic Scattering

A version of this chapter is in preparation to be submitted as a proceeding for an SPIE Optical Engineering + Applications conference on Ultrafast Nonlinear Imaging and Spectroscopy XII from August 18-22, 2024 in San Diego, California.

This chapter describes experiments designed by Marea J. Blake and Tessa R. Calhoun. Data analysis and preparation of the manuscript was performed by Marea J. Blake and Tessa R. Calhoun. All experiments were performed by Marea J. Blake.

4.1 Abstract

For antibiotics that target Gram-positive bacterial cell structures, optimizing their interaction with the cytoplasmic membrane is of paramount importance. Recent time-resolved second harmonic scattering (trSHS) experiments with living bacterial cells have shown that some amphiphilic small molecules display signals consistent with organization within the membrane environment. Such organization could arise, for example, from aggregation, solvent interactions and/or environmental rigidity. To expand our study of this system, we turn to polarization-resolved SHS (prSHS). prSHS has previously been used with model membranes to extract information about the angular distribution of integrated small molecules. Here we apply prSHS, for the first time, to cells, specifically living *Staphylococcus aureus*.

4.2 Introduction

A sample of living cells in solution is, in its essence, a complex colloidal system. Specifically, *Staphyloccocus aureus* is a Gram-positive bacterial species spanning approximately 1μm in diameter. The boundary protecting its genetic machinery is composed of a cell envelope consisting of a thick cell wall on the scale of $\sim$ 30-100 nm which encases the cytoplasmic lipid bilayer.[177] The membrane is responsible for mediating the passive transport of small molecules from the environment to the molecule's target within the cell. Ideas and methodologies investigating model systems with similar qualities to those of lipid bilayers,

in the form of liposomes or surfaces baring a high degree of negative charges such as polystyrene beads (PSBs), are essential in addressing questions arising from how a small molecule interacts with biological membranes. The question then is can these ideas and methodologies be extended to living systems to extract information directly as to how small molecules are interacting with bacterial cells?

Second harmonic scattering (SHS) is a technique with promising transferability from understanding small molecule dynamics at interfaces in solution for models to living cells. SHS is a technique based on the principles of second harmonic generation (SHG) in which two photons of frequency ω interact with a noncentrosymmetric medium, in this case molecules confined to a membrane, to produce a single photon of twice the energy, 2ω. This symmetry requirement makes SHG an inherently surface specific technique. However, because of the geometry and therefore, wide scattering angle of generated second harmonic signal, when referring to SHG produced from colloids, the technique is termed as SHS. [80, 189] The generation of SHS can summarized by $I_{2\omega} = |\chi^{(2)} E_\omega E_\omega|^2$ where $\chi^{(2)}$ is the hyperpolarizability further represented as a product of the number of molecules confined to the surface (N_s) and the orientational average of the hyperpolarizability ($\langle\beta\rangle$) in Equation 4.1.

$$\chi^{(2)} = N_s \langle\beta\rangle \tag{4.1}$$

SHS was first demonstrated from colloids with the model system cationic malachite green (MG) and anionic PSBs by Eisenthal et al. [235] Soon thereafter, the technique was extended to liposomes.[155, 164, 111, 51, 85, 254, 214, 86, 197, 38, 91] Subsequently, the Dai group applied this technique to Gram-negative *Escherichia coli* cells and thereafter, SHS has been shown to be capable of quantifying initial adsorption to and transport rates within bacterial cell membranes of multiple species under varying conditions.[146, 147, 257, 248, 243, 240, 242, 206, 205, 241, 245, 244] We have previously extended this technique to the Gram-positive bacterial regime to determine how variances in the structure of styryl probes and the membrane itself impact dynamic properties of their association.[147, 21] An interesting result of these studies was witnessing a rise in the SHS signal of small molecules, FM 2-10 and 4-Di-2-ASP, as this transpiration has not been previously documented for cells.

Subsequently, we determined this rise is due to a change in $\langle\beta\rangle$ due to potential contributions including aggregation of the molecules, a change in the molecules' chemical environment, or a difference in dipole alignment. Recent reports suggests this last source can be extracted using an extension of SHS: polarization-resolved SHS (prSHS).[24]

Specifically, Boudjema et al. have provided an open source software, PySHS, which simulates the polarization dependent SHS intensities for molecules organized on spherical particles as well as particles that deviate from a perfect sphere (e.g. living cells). [24] The SHS intensity (I_{SHS}) polarization dependence can be computed using Equation 4.2,

$$I_{SHS}(\gamma, \Pi, \theta) = i_0^{\theta,\Pi}(1 + I_2^{\theta,\Pi} cos(2\gamma) + I_4^{\theta,\Pi} cos(4\gamma)) \tag{4.2}$$

where angles γ, Π, and θ are defined in Figure 4.1. Figure 4.1 shows the laboratory frame where γ is the polarization angle of the incident fundamental light; Π is the second harmonic output polarization angle defined as either V when $\Pi = 0°$ or H when $\Pi = 90°$; and θ is the direction of scattered SHS which is equal to 90° for right angle SHS detection for signals arising from particles with a diameter $< 1\mu$m and 180° for a transmitted geometry arising from particles $\geq 1\mu$m. Terms $i_0^{\theta,\Pi}$, $I_2^{\theta,\Pi}$, and $I_4^{\theta,\Pi}$ are constants that represent the individual β contributions and therefore, relates the general order and angular distribution of the molecules on the particle surfaces. The complete derivations and relation from the macroscopic laboratory frame to the microscopic molecule orientations can be found in multiple previously published studies.[56, 57, 24]

In this report, we apply prSHS and the PySHS simulation software in order to begin to understand the molecular organization within living bacterial cell membranes for the first time to the best of our knowledge. We begin with measurements of the probe molecule, FM 2-10, as it interacts with *S. aureus* cells. We then illustrate this technique with model system MG with PSBs. Overall, we find that these preliminary experimental results agree with some previously published experimental work but conflict with others and the simulation. Additional studies to better understand the source of these differences are still ongoing.

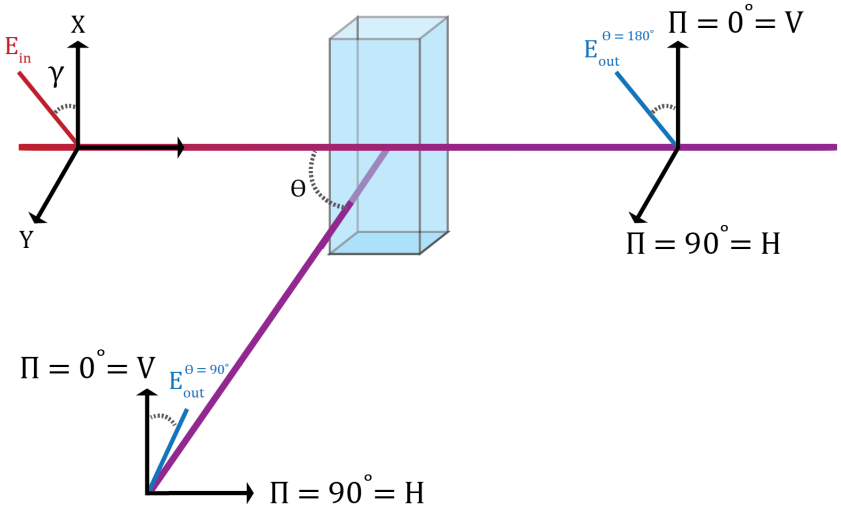


Figure 4.1: Laboratory frame defining angle notation used in this study for γ, Π, and θ.

4.3 Experimental

4.3.1 Instrumentation

The output power of a Ti:sapphire oscillator (800 nm, 80 MHz), compressed to $\sim$ 200 fs, was controlled using a half-waveplate and polarizer combination. The polarization angle of the fundamental 800 nm light was then controlled using a rotating half-waveplate. For prSHS experiments, incident polarization angles were defined based on 0° being the V polarization state. The beam was then filtered to reject any 400 nm light before being focused into a 2-3 mm quartz flow cell chamber. The signals generated either at 90° or 180° were collected and collimated with a series of lenses and then passed through an additional rotating polarizer. The SHS signals were selected using a combination of a 725 nm shortpass filter and a 400/10 bandpass filter before being focused onto a photomultiplier tube for detection.

4.3.2 Sample Preparation

Dye molecules FM 2-10 and 4-Di-2-ASP were prepared in 80:20 Mili-Q water:DMSO solutions while malachite green was prepared in Mili-Q water corrected to a pH of $\sim$4. Sulfonated polystyrene (latex) bead (PSB) suspensions were prepared in pH $\sim$4 Mili-Q water. Final PSBs solutions were made to be $\sim$ 0.01% suspensions.

Staphylococcus aureus (ATCC 27217) cells were grown on brain heart infusion (BHI) agar plates. Single colonies were then inoculated into liquid BHI media and allowed to grow overnight to stationary phase. An aliquot was then taken from the stationary phase cell solution to prepare an optical density at 600 nm (OD_{600}) of $\sim$ 0.01 and then grown until cells reached an OD_{600} of 0.2. Cells were then filtered by centrifugation and rinsed with and resuspended in phosphate buffered saline (PBS) to a final OD_{600} of 0.2.

For both PSBs and cells, the probe molecules were added directly before data collection. Each set of experiments (collecting all data points for both V_{out} and H_{out} took less than 30 minutes.

4.4 Results and Discussion

As mentioned above, when employing time-resolved SHS (trSHS), the probe molecule FM 2-10 generates a rise in SHS intensity when interacting with *S. aureus* membranes.[21, 147] To determine the impact of the molecule's orientation in the membrane, we employed prSHS for the first time to living cells. Figure 4.2 shows the prSHS plot produced when monitoring the SHS intensity at either the V or H polarization states as a function of incident polarization angle. The results shown in Figure 4.2, however, do not match what simulation suggests for a system with parameters consistent with dipoles equally distributed along the surface of 1μm particles, as can be seen in Figure 4.3. Specifically, simulation predicts the V_{out} signals should have four peaks at 45°, 135°, 225°, and 315°, however, results with *S. aureus* show maximums at 90° and 270°. Overall, while the H_{out} data matches theory, the V_{out} data does not.

In order to investigate whether the computations are able to capture the complexities of cell surfaces, we extended this technique to a model system that has been extensively characterized with SHG techniques: malachite green (MG) adsorbed to the surface of polystyrene beads (PSBs). We do this in two ways. First, we used a polarization dependent experiment that has been previously applied to MG/PSBs by the Dai group where the SHS intensity is monitored while changing the polarization angle of detected SHS with a constant incident polarization angle set to the H position, referred to here as H_{in}. [58] As such, 0° on the x-axis of Figure 4.4 A is referring to the SHS detected at H_{out}. As can be seen in Figure 4.4 A, the SHS intensity has two maximums at 90° and 270° which are representative of V_{out} (or *s*-polarization) SHS polarization. This result was also seen by Dai and coworkers.[58] Further, Dai et al. performed similar experiments with additional functionalized PSB surfaces and was successful in determining the relative tilt angle of MG on each surface based on similar polarization dependent trends but differences in their relative amplitudes.[58]

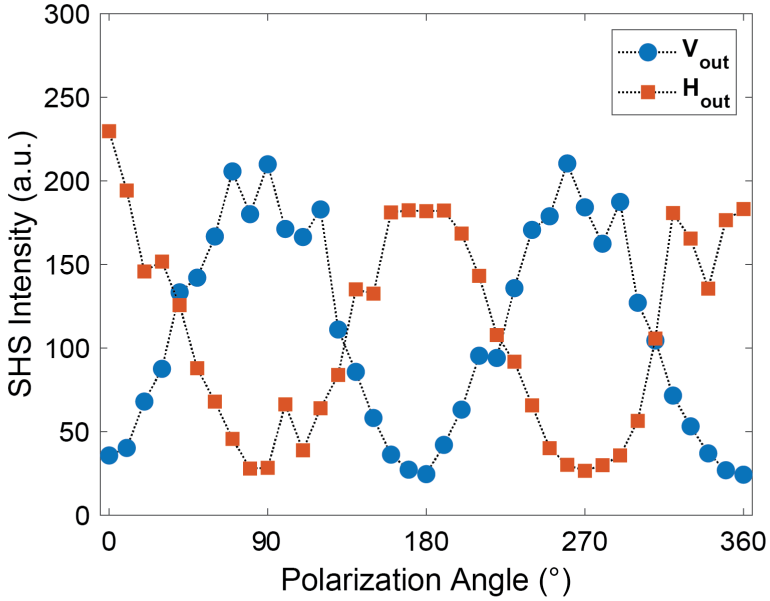


Figure 4.2: PrSHS for 16 μM FM 2-10 with *S. aureus*. The squares and circles are experimental data points, the black dotted lines are for ease of visuals.

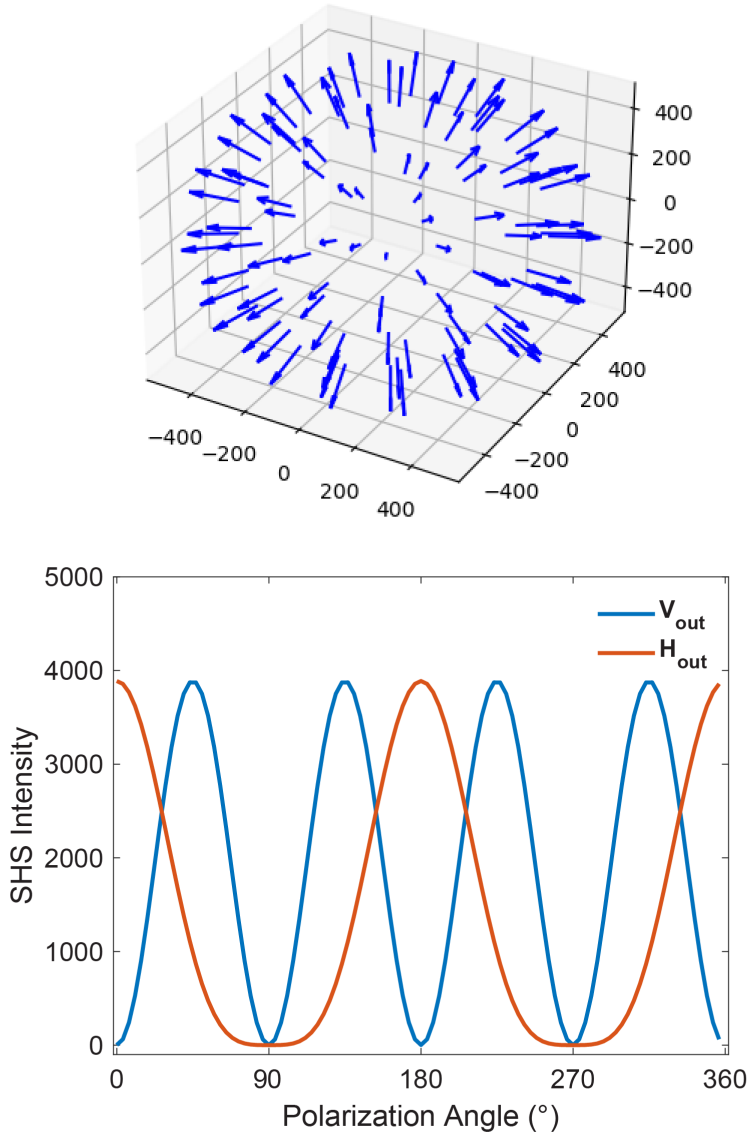


Figure 4.3: PySHS output for dipoles normally distributed along the surface of 1 μm diameter particles. (Top) The simulated microscopic orientation of the dipoles (blue arrows) oriented along the surface of the particles. (Bottom) Computed SHS intensity at H_{out} and V_{out}. Parameters for the simulation include: N = 100, $\theta = 180 \pm 5°$, and n = 1.33.

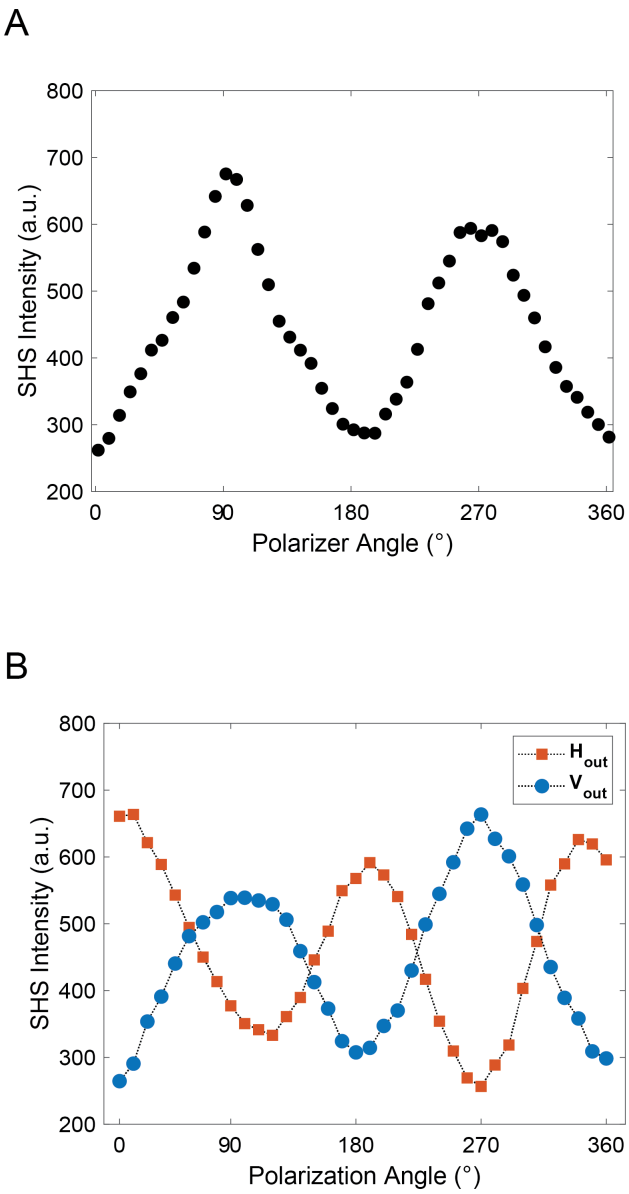


Figure 4.4: (A) Polarization dependence of 25 μM MG with $\sim$1μm PSBs as a function of SHS polarizer angle with constant P-polarized incident light. (B) prSHS for the same sample as (A) as a function of incident polarization angle. The squares and circles are experimental data points, the black dotted lines are for ease of visuals.

Following a successful replication of this result, we then turned back to prSHS in which we monitored the SHS intensity while rotating the polarization of the incident light. As seen in Figure 4.4 B, the prSHS data is reminiscent of the data observed with living cells in Figure 4.2 where the H_{out} seems to replicate the simulated results but V_{out} deviates. It should be noted that the Figures 4.4 A and B are consistent with one another as well. The minimum points of H_{out} at 0°, 180°, and 360° (at H_{in}) in Panel A also are seen as data points in Panel B for H_{out} at incident polarization angles of 90° and 270°. Likewise, the maximum features in panel A representing H_{in}/V_{out} at 90° and 270° can be seen in the V_{out} data in Panel B at incident polarization angles of 90° and 270°. Overall, the data shown in Figure 4.4 A and B are consistent with one another but inconsistent with the computed simulations.

4.5 Conclusions

prSHS has been shown to be capable of extracting angular distribution of molecules aligned along a colloidal surface. In particular, Boudjema et al. have provided a new framework to analyze data of this nature that takes into consideration particles that are not perfectly spherical, such as that of living cells.[24] Here, we show the first application of this technique to living cells, though the results obtained are not consistent with what has been simulated for spherical particles similar in size to that of *S. aureus* cells. We do, however, observe that these results are similar to what is seen with MG and PSBs. Ongoing work seeks to evaluate changes to the prSHS signal as a function of probe incubation time with work to either identify the source of the simulation discrepancies with PySHS [24] or alter our experimental plans to better match the previous work of Eckenrode et al. [58]

Chapter 5

Miltefosine Impacts Small Molecule Transport in Gram-Positive Bacteria

A version of this chapter is in preparation to be submitted.

This chapter describes experiments designed by Marea J. Blake, Eleanor F. Page, and Tessa R. Calhoun. Data analysis and preparation of the manuscript was performed by Marea J. Blake, Eleanor F. Page, and Tessa R. Calhoun. Eleanor F. Page performed FM 1-43 and Malachite Green time-resolved second harmonic scattering experiments; Madeline E. Smith assisted with generalized polarization of laurdan experiments; and Marea J. Blake performed the rest of the experiments.

5.1 Abstract

Miltefosine (MLT) is an alkylphosphocholine with clinical success as an anticancer and antiparasitic drug. Although the mechanism of action of MLT is highly debated, the interaction of MLT with the membrane, specifically lipid rafts of eukaryotes, is well-documented. Recent reports suggest MLT impacts the functional membrane microdomains (FMMs) in bacteria - regions of the membrane structurally and functionally similar to lipid rafts. There have been conflicting reports, however, as to whether MLT impacts the overall fluidity of cellular plasma membranes. Here, we apply steady-state fluorescence techniques, generalized polarization of laurdan and anisotropy of diphenylhexatriene, to discern how MLT impacts the global fluidity of *Staphylococcus aureus* membranes. Additionally, we investigate how the transport of a range of small molecules is impacted by MLT for *S. aureus* and *Bacillus subtilis* by employing time-resolved second harmonic scattering. Overall, we observe MLT does not have an influence on the overall fluidity of *S. aureus* membranes. Additionally, we show that the transport of small molecules across the membrane can be significantly altered by MLT - although this is not the case for all molecules studied. The results presented here illustrate the potential use of MLT as an adjuvant to assist in the delivery of drug molecules in bacteria.

5.2 Introduction

Hexadecylphosphocholine, or Miltefosine (MLT), is a synthetic alkylphospholipid (APL) that was originally developed as an anticancer agent [59] and is currently in clinical use as an antiparastic drug. [54] More recently, the antibacterial and antifungal activity of MLT has received attention.[168, 251, 136, 107, 123] While only modest antibacterial activity has been observed, it has been suggested that MLT, and APLs more generally, could serve as a new framework for developing novel antibiotics or adjuvants.[168] For the latter, it is imperative to investigate how the presence of MLT impacts small molecule transport through the membrane.

Despite decades of research, the mechanism of action of MLT remains a point of debate and discussion. While there is agreement that the plasma membrane is compromised with MLT treatment, it is not clear if this is achieved via lipid or protein targets. It has been shown that MLT specifically targets membranes composed of lipid raft constituents of eukaryotic and fungal species, such as cholesterol and ergosterol, respectively.[126, 251, 260, 134, 35, 88] As such, some have reported that this lipid raft association results in MLT impacting the cell membrane fluidity[6, 65, 181, 156], while others report this is not the case. [35, 134] For instances when membrane fluidity was altered, there is evidence that supports the presence of proteins is required. Specifically, Alonso *et al.* demonstrated that stratum corneum membranes had a significant increase in membrane fluidity due to MLT but vesicles formed from the lipid extract of stratum corneum membranes had no change in fluidity.[6] Additional mechanisms that have been proposed include miltefosine affecting the enzyme, cytochrome *c* oxidase,[261, 127] in eukaryotes and halting the cell's ability to synthesize phosphatidylcholine,[126, 228, 184] both cases leading to cell death. Most MLT research, however, has focused on eukaryotic systems or model membranes containing lipid species that are less common or nonexistent in bacteria.

In bacteria, MLT has been shown to interrupt aggregation of flotillin in *Staphylococcus aureus* cell membranes.[107] Flotillin are scaffold proteins that have been proposed as crucial components for the formation of functional membrane microdomains[129, 107] although inconsistent results remain.[217] It is not clear, however, if such a change in protein

behavior would arise from direct MLT-protein interactions or, if instead, MLT alters the lipid environment preferred by the protein. In a recent paper, molecular dynamics simulations suggest that the lipids themselves are a major determinant in MLT passive transport into the membrane and may play a large role in its mechanism of action.[134] When extending such questions to the potential use of MLT as an adjuvant species, it is necessary to consider how MLT's impact on the membrane alters small molecule transport through this important lipid boundary. In order to monitor transport dynamics, here, we implement time-resolved second harmonic scattering (trSHS).

SHS is a surface-specific spectroscopic technique based on second harmonic generation (SHG) originating from molecules adsorbed to surfaces in colloidal environments, such as that of living cell membranes.[80] SHG occurs when two photons of equal energy interact with a group of asymmetric molecules to produce light at the second harmonic, or at twice the energy of the incident photons. The emitted photons originating from an isotropic distribution of molecules, such as those in an aqueous solution, are incoherent leading to a weak, often insignificant signal. In contrast, once these molecules adsorb to a surface, the individual second harmonic signals originating from these molecules constructively interfere, producing appreciable SHS. The evolution of this signal over time can provide information on transport events of molecules within the membrane space. For instance, a decrease in SHS results from molecules becoming aligned in an anti-parallel fashion which is indicative of translocation from one leaflet into the other.[171, 240] Conversely, a rise in signal can be attributed to an overall greater alignment of the molecules to one another in the membrane,[171, 92] aggregation [215, 137], or a change in the local chemical environment. [218, 12] Previous studies have demonstrated SHS and SHG can be used to quantify molecule-membrane interactions within model systems [155, 164, 111, 51, 86, 85, 254, 214, 197, 38], eukaryotic species [117, 33, 208, 256, 156], and bacterial cells.[146, 147, 21, 171, 257, 248, 241, 243, 245, 242, 240, 244, 206, 205] Specifically, we have implemented this technique to elucidate how structural moieties of small molecules facilitate its transport through the Gram-positive membranes of living *S. aureus* and *Bacillus subtilis*.[21]

After employing the steady-state fluorescent assays, generalized polarization (GP) of laurdan and anisotropy of diphenylhexatriene (DPH), to determine the impact of MLT on global fluidity of *S. aureus* membranes, we monitor the trSHS of small molecules (malachite green,[257, 240, 207, 248, 112, 74] FM 2-10,[147, 21] FM 1-43,[21] and 4-Di-2-ASP[21]) with previously documented transport behavior to assess the impact of MLT. We also consider the role of membrane composition by extending trSHS studies to another Gram-positive bacterial species, *B. subtilis*. Although we do not observe a change in the overall fluidity of *S. aureus* membrane, we do observe significant alterations in the interactions of multiple small molecule species with the lipid bilayer. These results are not universal, however, leading to a discussion of the localized impact of MLT on the membrane and the potential relationship to the small molecule structures that are affected.

5.3 Materials and Methods

5.3.1 Chemicals and Cell Treatment

Stock solutions of dye molecules FM 2-10 (Biotium), 4-Di-2-ASP (Sigma-Aldrich) and FM 1-43 (Biotium) were prepared in filter sterilized 80:20 Milli-Q water to DMSO to maintain a final DMSO concentration of 0.02% when introduced to cell solutions. Malachite green oxalate (Sigma-Aldrich) was prepared in sterile Milli-Q water. Stock solutions of laurdan (ThermoFisher Scientific), 1,6-Diphenyl-1,3,5-hexatriene (diphenylhexatriene, Sigma-Aldrich), and miltefosine (Sigma-Aldrich) were prepared in DMSO.

Single colonies of *Staphylococcus aureus* (ATCC27217) and *Bacillus subtilis* 168 grown on brain heart infusion (BHI) and Luria Bertani (LB) broth agar, respectively, were inoculated into liquid BHI and LB media, respectively. Cultures were grown anaerobically for *S. aureus* and aerobically at 250 RPM for *B. subtilis* overnight at 37°C. Aliquots were then resuspended in fresh liquid media to an optical density at 600 nm (OD_{600}) of 0.01 and allowed to grow to an OD_{600} of 0.2 at the same conditions. Cell samples were then filtered by centrifugation or vacuum filtration and washed twice with phosphate buffered saline (PBS). For trSHS

experiments, cells were resuspended in their respective media supplemented with 0.2% EC-OxyRase. For steady state fluorescence experiments, cells were resuspended in PBS. Final cell suspensions were measured to be at an OD_{600} of 0.2. MLT was incubated with cells at room temperature for a minimum of 10 minutes before experimentally probed.

5.3.2 Time-Resolved Second Harmonic Scattering

TrSHS experiments were performed using home-built instruments previously described in detail elsewhere.[147] Briefly, the output of a Ti:sapphire oscillator (80 MHz) was compressed to <100 fs and focused into a 2 mm quartz flow cell (Starna) that housed the cell samples. The resulting signals were then collected with a series of lenses and directed towards a photomultiplier tube (PMT) for detection. Filters were implemented to block any second harmonic (400 nm) produced by optics before the sample housing and fundamental light (800 nm) after the sample. The second harmonic responses were selected using a 400/10 bandpass filter before the PMT. The power sent to the sample was controlled using a half-waveplate and polarizer. For FM 2-10 and 4-Di-2-ASP, the power was set to 35 mW and for experiments with MG and FM 1-43, the power was set to 100 mW. These experiments were accomplished using a gravity flow peristaltic pump at a rate of <7 mL per minute.

Immediately prior to trSHS experiments, the quartz flow cell was passivated to ensure there was no cell adsorption to the surface during the course of the trials. First, the sample chamber was sterilized with 1 M hydrochloric acid, then rinsed with a copious amount of sterilized Milli-Q water. Then, we used an established bovine serum albumin (BSA)/glutaraldehyde cross-linking procedure, previously described. [94] In short, 50 mM BSA (Sigma-Aldrich) was incubated for 10 minutes, rinsed with 10 mM TRIS buffer(corrected to pH 7.4)(Sigma-Aldrich), and then replaced with another 10 minute incubation of a 1% glutaraldehyde (Thermo-Fisher Scientific) solution. Finally, the flow cell was rinsed with the TRIS buffer. All solutions were sterilized before performing the cross-linking procedure.

5.3.3 Generalized Polarization Measurements

Membrane fluidity was assessed using generalized polarization (GP) measurements of laurdan. Laurdan is a fluorescent molecule that shifts its emission spectra due to the polarity of the surrounding environments. For instance, for environments with low polarity such as that of rigid regions of the membrane, the emission maximum of laurdan is 440 nm. When laurdan is an environment of high polarity (e.g. a fluid membrane), laurdan has an emission maximum shifted to 490 nm. The ratio of the emission intensities at 440 nm and 490 nm, or GP, can be calculated to quantify changes in membrane fluidity according to Equation 5.1,

$$GP = \frac{I_{440} - I_{490}}{I_{440} + I_{490}} \tag{5.1}$$

where I_{440} and I_{490} are the fluorescence intensities at 440 nm and 490 nm, respectively. For GP measurements, after cells were treated with MLT as outlined above, samples were washed by centrifugation, resuspended in PBS, and then incubated with 0.5 μM laurdan at 37°C for ∼30 minutes in the dark. Measurements were then taken with a Perkin Elmer LS 55 fluorometer with 350 nm excitation at room temperature.

5.3.4 Steady State Fluorescence Anisotropy

Another measure of fluidity used here is the steady state fluorescence anisotropy of diphenylhexatriene (DPH). DPH preferentially localizes in the hydrophobic region of the membrane. As such, the orientation and rotational freedom of the DPH molecules in this region directly reflects the fluidity of the environment it is residing in. This can be quantified by calculating the anisotropy, $\langle r \rangle$, of DPH:

$$\langle r \rangle = \frac{I_{VV} - I_{VH}G}{I_{VV} + 2I_{VH}G} \tag{5.2}$$

$$G = \frac{I_{HV}}{I_{HH}} \tag{5.3}$$

where I is the fluorescence intensity at different excitation and emission polarizer combinations, denoted by the subscripts,respectively, where V is vertical and H is horizontal, and G is a correction factor to account for detector sensitivity.

Anisotropy measurements were recorded with an Agilent Cary Eclipse fluorometer. After cells were treated with MLT, cells were resuspended in PBS and incubated with 10 μM DPH for ∼45 minutes at 37°C. Samples were excited at 350 nm and emission was collected at 430 nm. Measurements were taken at room temperature.

5.4 Results and Discussion

5.4.1 MLT Impact on Global Membrane Fluidity

While there has been debate in the literature regarding the impact MLT has on the fluidity of the membranes it interacts with,[6, 65, 181, 156, 35, 134] no such studies have been performed with bacteria. Therefore, we first sought to investigate whether the presence of MLT results in a more fluid membrane environment in *S. aureus*. In order to do so, we employ two steady state fluorescence techniques: GP of laurdan and steady-state anisotropy of DPH. Both laurdan and DPH are fluorescent molecules commonly used as probes to assess membrane fluidity.[95, 161] As the laurdan chromophore is polar, it reports on the presence of water near the junction between the lipid headgroup and tail with a higher GP value associated with a decrease in the membrane fluidity.[95, 230] The nonpolar DPH molecule is expected to embed more deeply within the hydrophobic portion of the membrane and a lower DPH anisotropy value indicates higher membrane fluidity.[128, 230] While many studies find similar trends between these different probe assays,[161] occasional differences are noted.[128]

Figure 5.1A shows the GP values for laurdan in *S. aureus* membranes either with or without a MLT incubation prior to the measurement. For the cells not exposed to MLT, the GP value obtained is 0.381 ± 0.07 which is consistent with values others have reported for exponential phase *S. aureus* at room temperature.[179, 19] In comparison to the cells exposed to MLT, there is no significant difference. This suggests that there is no overall

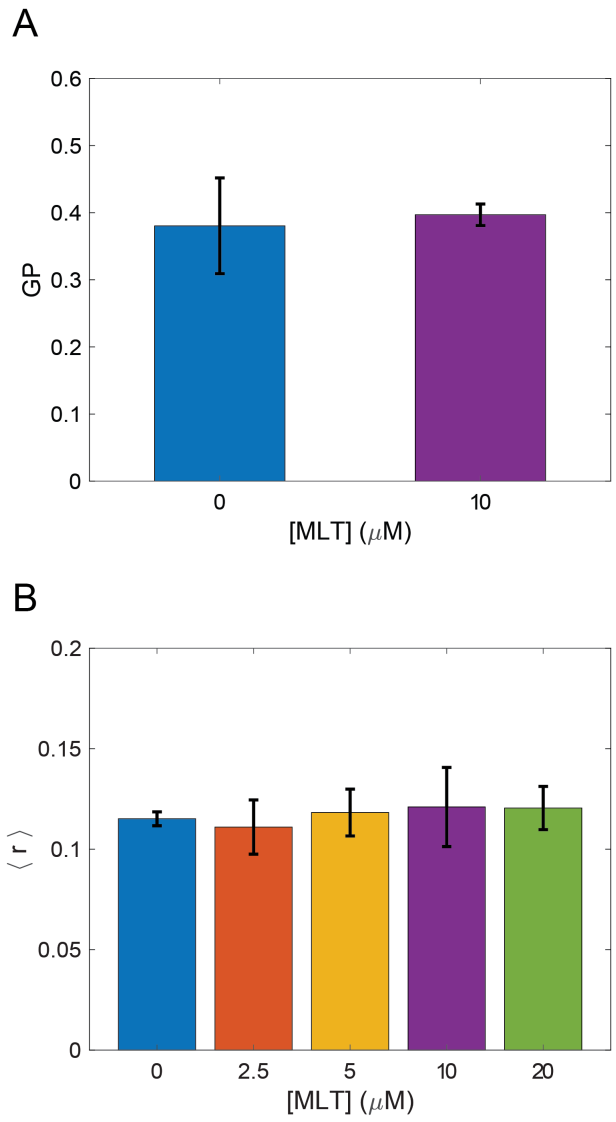


Figure 5.1: Steady state fluorescence measurements of fluidity with (A) laurdan and (B) DPH. (A) Average GP values of laurdan for *S. aureus* with 0 μM MLT (blue) and 10 μM MLT (purple). (B) Average anisotropy ($\langle r \rangle$) of DPH with *S. aureus* is shown as a function of MLT concentration. For each concentration of MLT, n = 3.

increase in the fluidity of the *S. aureus* membrane due to the presence of MLT. The anisotropy of DPH adds further support to this conclusion. As can be see in Fig. 5.1B, the DPH anisotropy values are found to be 0.115 ± 0.003 which is also consistent with previous literature values [20] and remains unchanged over multiple MLT concentrations.

5.4.2 Small Molecule Organization and Transport

For consideration of MLT as an adjuvant to treat bacterial infections, understanding how MLT affects the interaction of small molecules with the membrane, and moreover their transport through it, is crucial. Four dye molecules with different established membrane interactions are studied here: MG, FM 2-10, 4-Di-2-ASP, and FM 1-43. MG is a small, positively charged molecule that has been extensively characterized with model liposomes[214, 254, 111, 249] as well as *Escherichia coli*[257, 74, 240, 112, 207] and eukaryotic cells[208]. In all previous work, MG has exhibited an SHS response consistent with a relatively rapid passive diffusion through lipid bilayers. Further, we have previously reported on the bacterial membrane interactions of the three styryl molecules listed where slight variances in their structures result in differences in their affinity for and translocation within the membranes of *S. aureus*.[147, 21] For instance, we have proposed that for molecules with short hydrophobic tails and small headgroups (FM 2-10 and 4-Di-2-ASP, respectively), the molecules have a greater propensity to remain in the outer leaflet of the membrane. After $\sim$1 hour, however, the molecules produce a rise in SHS signal indicative of further organization within the membrane.[147, 21] Further, we demonstrated that the introduction of molecules with larger branched tails (FM 1-43) result in a rapid decrease in SHS. This response is due to the molecules moving from the outer leaflet to the inner leaflet of the membrane.[21]

Immediate alterations to small molecule transport induced by MLT can be seen by examining the behavior of MG. Figure 5.2 shows that at 0 μM MLT, the molecules rapidly diffuse through the hydrophobic portion of the membrane in agreement with MG SHS studies with both liposomal membranes[214, 254, 111, 249] as well as *E. coli* cells.[257, 74, 240, 112, 207] After *S. aureus* cells are treated with 12 μM MLT (Fig. 5.2), the trSHS decreases more rapidly compared to untreated cells. These results indicate that MG may be experiencing a more fluid membrane environment to mediate quicker passive

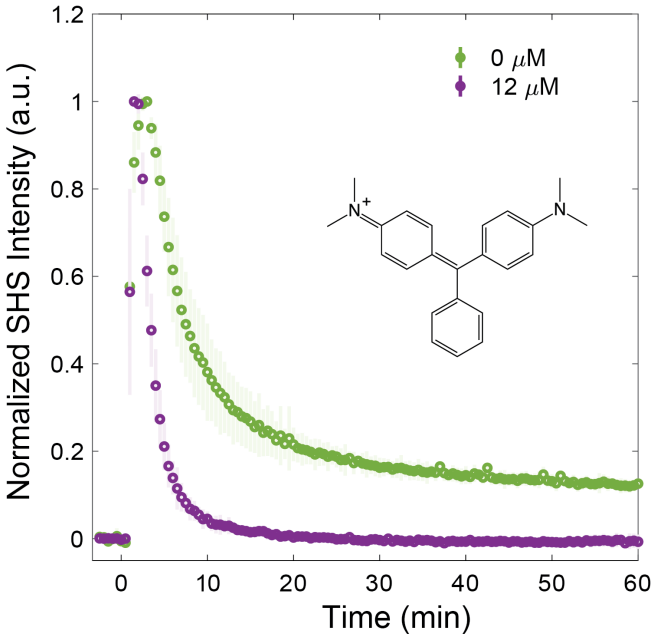


Figure 5.2: Normalized trSHS trials of *S. aureus* with 25 μM MG with 0 μM MLT (green) and 12 μM MLT (purple). The structure of MG is shown in the plot. For each condition, $n = 3$. Averaged data is shown as circles and the shaded error bars represent the standard deviation between the individual normalized trials.

diffusion across the lipid bilayer.[249]

More complex dynamics are observed when moving to the styryl dye molecules which have a stronger association with the membrane environment. Past studies with FM 2-10 and 4-Di-2-ASP hypothesized that the molecule undergoes organization in the membrane of *S. aureus*. This hypothesis arises from the fact that the SHS signal in these samples rises over time and can be understood by examining the factors that contribute to the intensity of the SHS signal (I_{SHS}). Specifically, $I_{SHS} = |\chi^{(2)}_{eff} E_\omega E_\omega|^2$ where E_ω is the incoming electric field and $\chi^{(2)}_{eff}$ is the second order effective susceptibility which can be further decomposed to $\chi^{(2)}_{eff} \propto N_s \langle\beta\rangle$. Here, N_s is the population of probe molecules in the membrane while $\langle\beta\rangle$ is the orientational average of the hyperpolarizability. As we have previously determined, the population of cells throughout the duration of our measurements is static and subsequently there is no increase in membrane probe population [147], therefore the SHS rise is attributed to $\langle\beta\rangle$. This term can increase through a change in the probe molecule's environment either due to differences in solvation or an overall increase in molecular alignment due to environmental rigidity.

Since MLT has been shown to disrupt membrane regions of increased rigidity,[126] the membrane interactions of FM 2-10 and 4-Di-2-ASP were studied here. As can be seen in Figure 5.3, when no MLT is present, the SHS signal is relatively static over the first 40 minutes but then nearly doubles after two hours. This behavior, and especially the rise, are clearly altered by MLT. As the concentration of MLT increases from 0 to 20 μM, the SHS rise is diminished and eventally lost. A reduced SHS rise is also observed for 4-Di-2-ASP after cells are treated with 10 μM MLT (Figure 5.4).

Another change induced by MLT is also observed within the first 20 minutes. Whereas the SHS signal of FM 2-10 with no MLT present displays a static signal, cells treated with MLT exhibit an SHS decay after the initial adsorption of FM 2-10. Such a decrease is most often interpreted as a movement of some population of the probe molecule to the inner leaflet.[257, 240, 171] Alternatively, the same way a more rigid environment would induce a rising SHS signal, a more fluid environment can cause a reduction as the alignment of the molecules is decreased. More support for this argument can be seen by examining the trends in SHS intensity values. While Fig. 5.3 shows the time-resolved SHS signals normalized to the initial absorption peak to better differentiate the dynamic changes, Fig. 5.5 compares

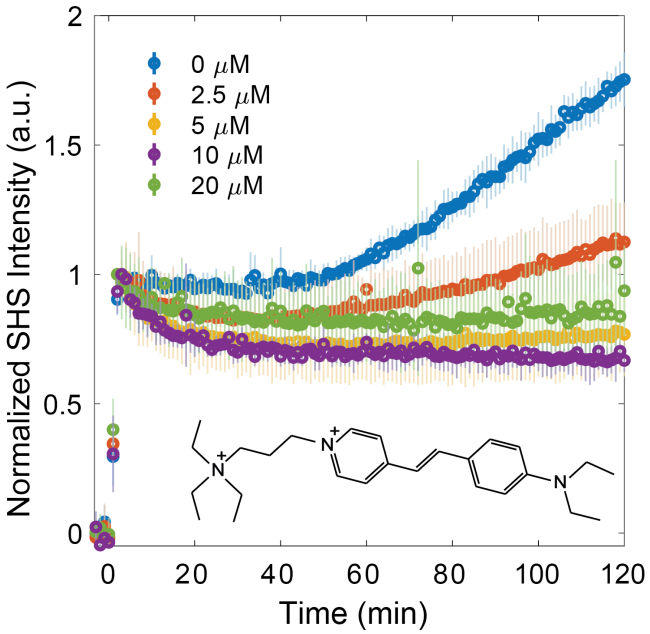


Figure 5.3: Normalized trSHS trials of 16 μM FM 2-10 with *S. aureus* with increasing concentrations of MLT. The structure of FM 2-10 is shown in the plot. For each concentration of MLT, $n = 3$. Averaged data is shown as circles and the shaded error bars represent the standard deviation between the individual normalized trials.

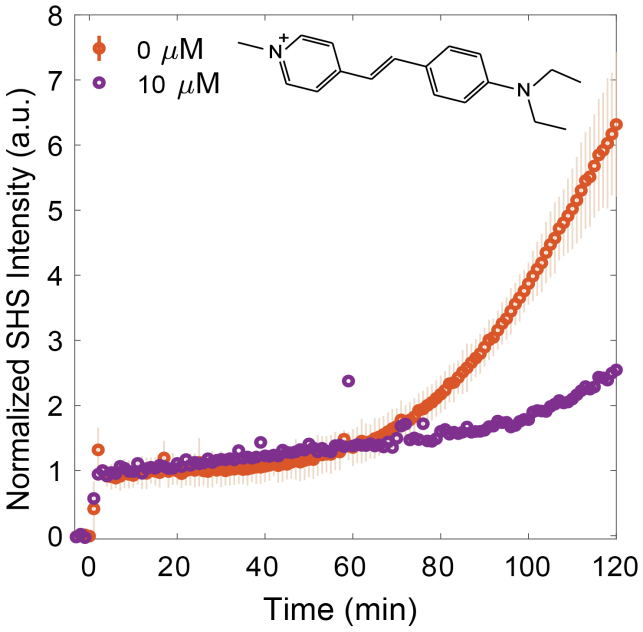


Figure 5.4: Normalized trSHS trials of *S. aureus* with 16 μM 4-Di-2-ASP with 0 μM MLT (orange) and 10 μM MLT (purple). The structure of 4-Di-2-ASP is shown in the plot. For 0 μM MLT, n = 3 and the shaded error bars represent the standard deviation between the individual normalized trials; for 10 μM MLT, n=1.

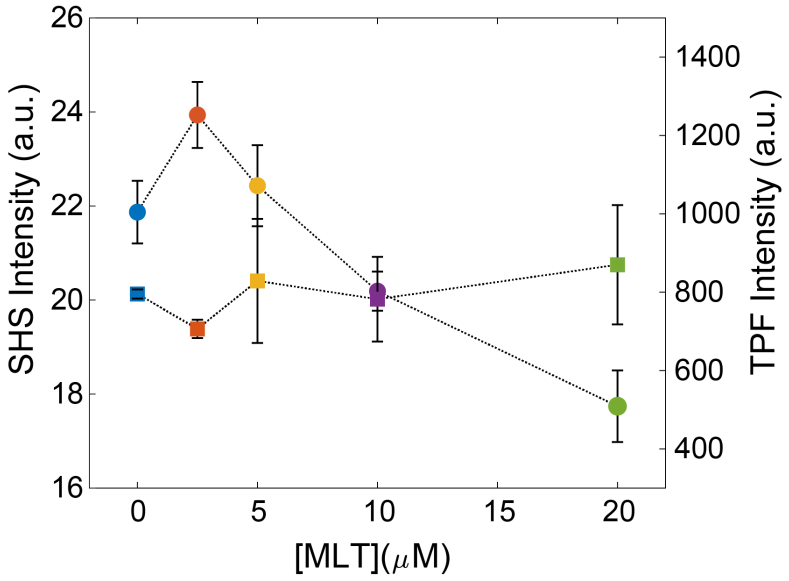


Figure 5.5: Initial intensities of trSHS (circles, left axis) and TPF (squares, right axis) signals of *S. aureus* with 16 μM FM 2-10.

the initial SHS intensity after adsorption to that of the two-photon fluorescence signal taken at the same time. As FM 2-10 only exhibits significant fluorescence when embedded in the membrane environment, monitoring the fluorescence signal allows us to separately monitor the population contribution to the SHS signal. As can be seen in Fig. 5.5, the fluorescence intensity for different MLT concentrations remains unchanged, suggesting that the same number of probe molecules are adsorbed onto the membrane. In contrast, the SHS intensity shows an overall decreasing trend with increasing MLT concentration suggesting that $\langle\beta\rangle$ is decreasing over these conditions. Taken together, these data suggest that FM 2-10 does not experience a more rigid environment over time and that, in fact, it's initial lipid environment may be more fluid, potentially promoting translocation to the inner leaflet.

We have previously shown that the membrane composition itself plays a large role in how small molecules trespass the bacterial surface.[21] Specifically, we observed that for FM 2-10 and 4-Di-2-ASP, where a rise over the two hour time period is seen with *S. aureus*, a slight rise is followed with a decrease in SHS intensity over time for *B. subtilis*. This discrepancy was proposed to be attributed to the generally more fluid membrane of *B. subtilis*, which in turn facilitated translocation events, whereas *S. aureus* mediated molecule organization in the outer leaflet over the same time period.[21] The fact these membranes facilitate starkly different transport properties of FM 2-10 allows an opportunity to determine how translatable MLT's impact is for different species. Figure 5.6 shows that when MLT is introduced to *B. subtilis*, FM 2-10 produces an immediate decrease in SHS intensity after initial adsorption, similar, albeit more rapid, to what was witnessed with *S. aureus* (Fig. 5.3). Following this first translocation event, the SHS intensity displays a slight increase over time and then remains relatively stagnant for the duration of the experiment.

Although the two cell species have different FM 2-10 transport in the absence of MLT, the final result after MLT incubation is very similar. This could be due to MLT having the same mechanism of action for both cell types. While *S. aureus* and *B. subtilis* have differences in their overall phospholipid membrane composition, [133] they do have similarities that could explain the analogous MLT results. For instance, both membranes have been shown to be equipped with flotillin scaffold proteins[129, 107, 124] - proteins that are largely conserved across different domains of life and hypothesized to play a role in MLT's mechanism of action

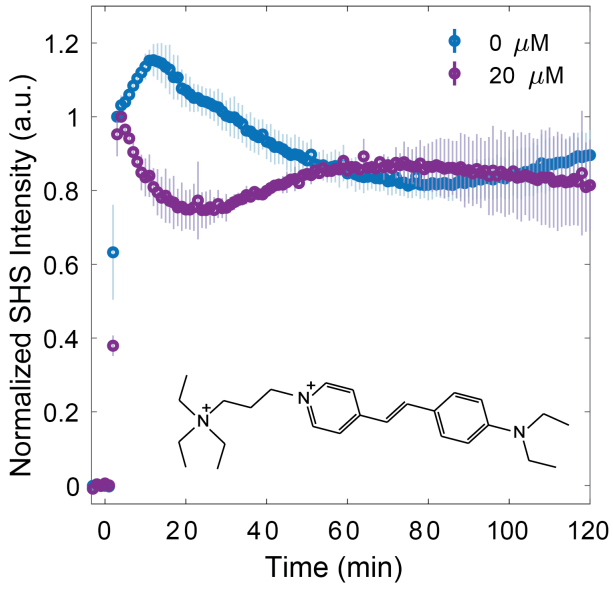


Figure 5.6: Normalized trSHS trials of *B. subtilis* with 16 μM FM 2-10 with 0 μM MLT (blue) and 20 μM MLT (purple). The structure of FM 2-10 is shown in the plot. For each condition, $n = 3$. Averaged data is shown as circles and the shaded error bars represent the standard deviation between the individual normalized trials.

for bacteria. [107, 158] Additionally, both membrane species are known to moderate their membrane fluidity via isoprenoid-derived minor lipid species. [246, 27, 151] For instance, *S. aureus* produces carotenoids, such as staphyloxanthin, and *B. subtilis* synthesizes hopanoids.[130, 229] Hopanoids in particular are structurally and functionally similar to that of ergosterol and cholesterol in eukaryotes. [188, 224, 223] Subsequently, both of these sterols in eukaryotes have been shown to be important constituents for MLT activity.[126, 251, 260, 134, 35, 88] Therefore, flotillin proteins and/or isoprenoid-derived molecules could be potential targets for MLT in the bacterial species studied here.

When attempting to understand how MLT does not affect laurdan and DPH behavior but does affect the behavior of MG, FM 2-10 and 4-Di-2-ASP, one may be quick to note the neutral forms of the former group of molecules vs. the ionic forms of the latter. This justification, however, is refuted by examining FM 1-43. Unlike the other three dyes measured with trSHS, FM 1-43 transport is unaffected by the presence of MLT. As can be seen in Fig. 5.7, after initial adsorption, the SHS signal from FM 1-43 decreases over 30 minutes before stabilizing. The signal from the MLT-affected cells exhibits the same behavior within the error of the measurement.

We propose two possible explanations for the differences in MLT's impact for these five different probe molecules. First, MLT may induce a more local effect to specific regions, *i. e.* domains, within the membrane that is limiting in its impact to only those molecules that are strongly associated with the same domains. This local impact is what has been proposed before for its behavior.[126, 107] The novelty of our measurements is then the suggestion that MG, FM 2-10 and 4-Di-2-ASP have a preferential association with such domains. Previous work has shown that both laurdan[230, 239] and DPH[128] can partition into multiple different lipid phases promoting a more homogeneous distribution within the membrane. In contrast, styryl dyes have been seen to heterogeneously localize within bacterial membranes[14] although this is not always the case.[99] The heterogeneous distribution has been attributed to the cationic charge on the styryl dyes interacting with the negatively charged phosphatidylglycerol (PG) lipid headgroup.[14] It is important to note, however, that such heterogeneous behavior was seen explicitly for FM 1-43 which we find to be unaffected by MLT.

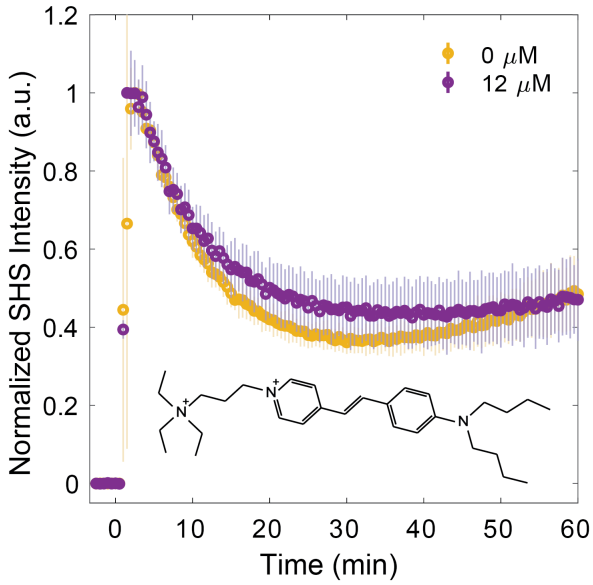


Figure 5.7: Normalized trSHS trials of *S. aureus* with 16 μM FM 1-43 with 0 μM MLT (yellow) and 12 μM MLT (purple). The structure of FM 1-43 is shown in the plot. For each condition, $n = 3$. Averaged data is shown as circles and the shaded error bars represent the standard deviation between the individual normalized trials.

As a second, not necessarily unrelated, explanation for the differing behavior, we consider the hydrophobic character of the probe molecules. As noted previously, both laurdan and DPH are neutral molecules predominantly interacting with lipids below the headgroup. Beyond those two molecules, the only other one not impacted by MLT was FM 1-43. In comparison to MG, FM 2-10 and 4-Di-2-ASP, FM 1-43 contains the largest hydrophilic moiety. As such it may be that those molecules with stronger interactions with the lipid tails and hydrophobic core of the membrane are less susceptible to MLT alterations.

5.5 Conclusions

The results of our trSHS experiments show that MLT does hold promise as an adjuvant species for small molecule antibiotics targeting Gram-positive bacteria. Our steady-state fluorescence measurements with laurdan and DPH show no evidence of a large-scale increase in the membranes of *S. aureus* cells induced by MLT. This result supports previous work by others[35, 134] but extends this finding to bacteria. In contrast, multiple small molecules exhibit altered interactions with the membranes after exposure to MLT. These alterations led to an overall higher propensity for the molecules to more efficiently traverse the lipid bilayer. While the lack of impact on FM 1-43 dynamics may seem limiting for MLT's use, it could alternatively be viewed as promising for future selectivity. Work remains, however, to better understand MLT's relationship with different small molecules and the mechanism by which MLT impacts bacterial membranes overall.

Chapter 6

Conclusions and Future Directions

6.1 Conclusions

Overall, my doctoral research sought to investigate how small molecules interact with living membranes of Gram-positive bacteria by employing the surface-specific technique: second harmonic scattering (SHS). Specifically, Chapter 3 focused on the structural parameters of both the molecules and the membranes that influenced the molecules' adsorption affinities to and transport behaviors within the membrane space. The results of which indicate that small hydrophobic molecules exhibit lower affinity to the membrane but more complex transport behaviors. Conversely, larger, more hydrophobic molecules have an increased affinity to bacterial membranes and a greater propensity to traverse to the inner leaflet of the lipid bilayer. The work presented in Chapter 3 also demonstrates the importance of the membrane identity as *Staphylococcus aureus* and *Bacillus subtilis* had disparate interactions with the same molecules. The results in this chapter establish the importance of monitoring small molecule transport in real-time with living bacteria.

The rise in SHS of small molecule FM 2-10 with *S. aureus* was further investigated by using polarization-resolved SHS (prSHS) in Chapter 4. This was the first application of this technique to living cells to the best of our knowledge. While a polarization-dependent response was observed, the experimental data did not match what was simulated from theory. In order to quantify the angular distribution, this discrepancy will need to be investigated further by either revisiting the model or implementing different experimental configurations.

Finally, SHS was used to examine how perturbing membrane organization through the use of miltefosine impacted molecule-membrane interactions in Chapter 5. By doing so, it was shown that although miltefosine has no apparent impact on the overall fluidity of the membrane, molecule transport through the cells' surface is significantly impacted - though not to the same degree for all molecules studied. In particular, molecules that were shown to remain in the outer leaflet of *S. aureus* in Chapter 3, were able to migrate to the inner leaflet in the presence of miltefosine in Chapter 5. However, for one molecule, the transport properties remained unaltered suggesting that miltefosine could be targeting the membrane heterogeneously. We further demonstrated that this drug alters membrane transport in both

S. aureus and *B. subtilis*. These results demonstrate the potential use of miltefosine as an adjuvant to assist in the delivery of drugs to their bacterial targets.

6.2 Future Directions

The results presented herein provide a basis for a number of avenues to explore to obtain a more complete picture as to how small molecules are interacting with bacterial membranes. Potential directions for future experiments that strike the most intrigue consist of evaluating the sources contributing to the rise in SHS seen in bacteria, considering other modes of transport, investigating the role of the cell wall, diving deeper into studies focused on domain disruption, and expanding the "toolbox" of membrane probes/systems.

6.2.1 Exploring the Rise

Although trSHS responses can be interpreted as the orientation of the molecules in the membrane space, the rise in SHS in bacteria is a more complicated result to disentangle, as we are the first to witness this transpiration.[147] As explained in Chapter 3, the SHS signals (E_{SHS}) seen can be explained by Equation 6.1,

$$E_{SHS} \propto N_s \langle \beta \rangle \tag{6.1}$$

where N_s is the population of molecules in the membrane and $\langle \beta \rangle$ is the orientational average of the hyperpolarizability. The latter term broadly describes how the individual dipoles are oriented in the membrane. However, the term β itself can be altered depending on the chemical environment of the molecules. [218, 12] An increase in either term, however, could result in an increase in SHS signal. For N_s, this is represented in Figure 6.1 (A) as either (i) an increase in the number of membrane bound probes in a constant cell population or (ii) an increase in the total number of binding sites through an increase in the cell population. Both of these hypotheses have been addressed previously [21, 147], however, and are shown to not be significant sources owing to the rise in SHS signal over time. Figure 6.1 (B) illustrates how a change in $\langle \beta \rangle$ could result in an increase in E_{SHS}. In panel B(i), the molecules are

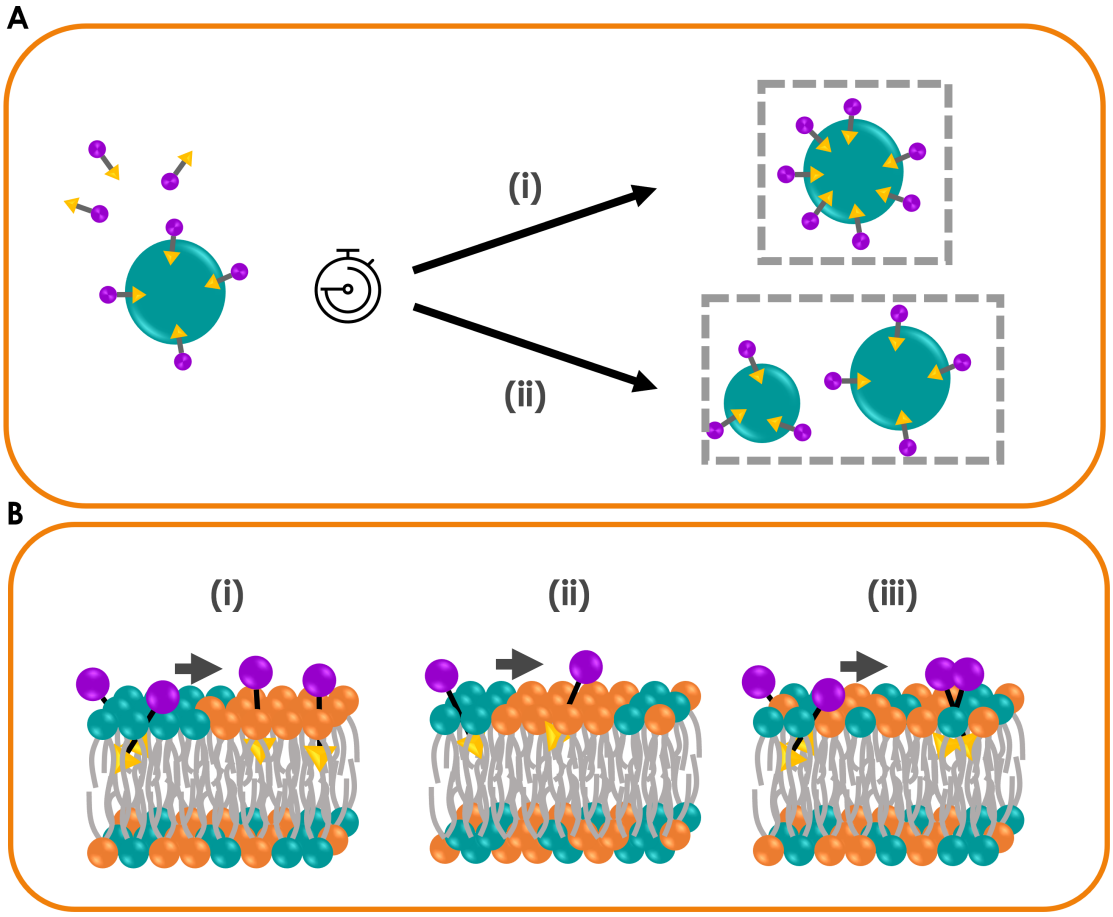


Figure 6.1: Cartoon schematic showing hypotheses for the sources of rising SHS signal. Panel A shows the potential origin of an increase in SHS based on N_s (Eq. 6.1) where (i) there could be an increase in binding sites in the cells present or (ii) an increase in the number of cells, and therefore, possible binding sites. Panel B illustrates three different hypotheses for an increase originating from $\langle\beta\rangle$ (Eq. 6.1) where (i) results from a change in orientation ($\langle\rangle$) and (ii) and (iii) results from a change in β itself.

moving to regions of the membrane where they are able to become better aligned with one another resulting in an increase in the overall orientation, and thus, $\langle\beta\rangle$. Another hypothesis, shown in Panel B(ii), is that the molecules could be moving to a different region of the membrane, and thus the molecules could be experiencing a different chemical environment leading to a potential increase in β. Lastly, panel B(iii) shows that an increase in β could arise from aggregation of the probe molecules. Monomers that have aggregated along a surface have been shown to increase this term by up to a factor of 6. [215, 137] Hereafter, the hypotheses presented in panels B(i) - B(iii) will be referred to as Hypothesis 1 - Hypothesis 3, respectively. Overall, a potential direction to continue this research is to probe these individual contributions to determine the source of the rise in SHS seen for small molecules FM 2-10 and 4-Di-2-ASP in Chapters 3 and 5.

Potential experiments to probe the first of these Hypotheses include improving experimental conditions of the pSHS experiments presented in Chapter 4. As mentioned above, the pSHS experiments with *S. aureus* in Chapter 4 resulted in inconclusive findings, however, we proposed possible directions to improve upon the technique. Nevertheless, quantifying angular orientations of small molecules adsorbed to living cells could be an invaluable tool in probing Hypothesis 1.

For Hypothesis 2, an exploration of the chemical environment over time would need to be carried out. One way to accomplish this is to employ time-resolved techniques with time-correlated single photon counting capabilities such as fluorescence lifetimes and ultrafast fluorescence anisotropy. By collecting the fluorescence lifetimes of the molecules while in the membrane space, changes in the immediate chemical environment, such as neighboring lipid species, can be deduced due to the inherent sensitivity of the lifetimes of fluorophores to their surroundings. [18] This technique could then easily be extended to time-resolved fluorescence anisotropy by integrating polarization optics. In doing so, anisotropy measurements could report on the orientation and rotational diffusion of the probe molecules, both of which could also be useful for considering Hypothesis 1 in addition to pSHS.

Finally, Hypothesis 3, or aggregation, could potentially be probed by evaluating changes in SHS signal due to changes in bulk concentration. If aggregation was a predominate mechanism at play, reducing the bulk concentration would reduce the amount of aggregates

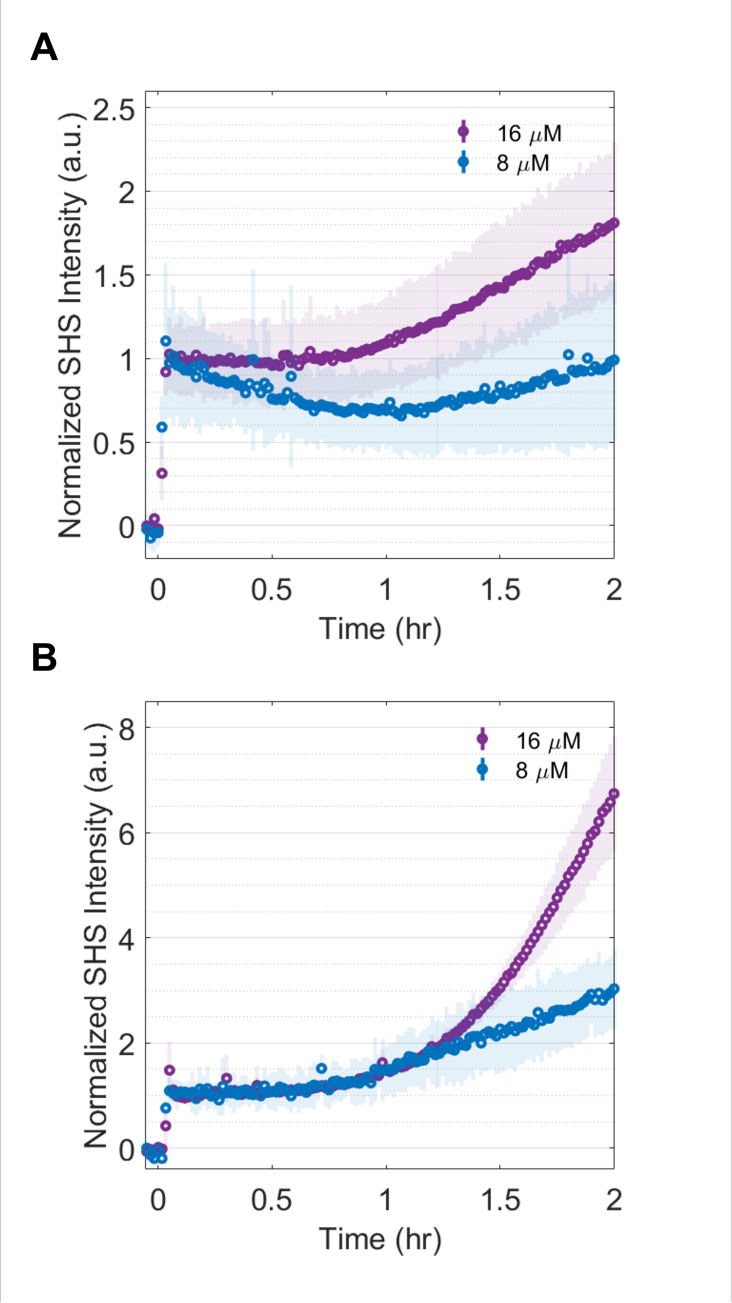


Figure 6.2: Concentration-dependent trSHS experiments of FM 2-10 and 4-Di-2-ASP with *S. aureus*. A) Normalized trSHS experiments of FM 2-10 at 16 (purple) and 8 (blue) μM. B) Normalized trSHS experiments of 4-Di-2-ASP at 16 (purple) and 8 (blue) μM concentrations. Circles represent the average normalized SHS intensity and shaded error bar regions represent the standard deviation between individual experiments.

capable of forming. As such, I have already carried out experiments in this area. Figure 6.2 shows that when the concentration of probe molecules FM 2-10 and 4-Di-2-ASP decreases from 16 to 8 μM with the same density of *S. aureus* cells, the rise diminishes, though not entirely. This suggests that aggregation may be a contributing factor to the total SHS signal seen. It should be noted, however, that by decreasing the concentration, other possibilities could arise. This observation illustrates that it may be difficult to isolate contributions to any one Hypothesis. Therefore, future works with a focus on additional complementary techniques would need to be employed to obtain a more complete picture of the behavior of these small molecules in the membrane.

6.2.2 Transport Mechanisms

The central hypothesis guiding the research here is that the probe molecules under investigation transport through the Gram-positive bacterial surfaces primarily by passive diffusion mediated by the lipid environment of the cytoplasmic membrane. Bacteria, however, are capable of transporting small molecules by many routes. For instance, aside from lipoidal passive diffusion, molecules can enter the cell through facilitated and active transport mechanisms.[220, 183, 222] Examples of the former consist of ion channels and carrier-mediated proteins that do not directly need an energy source to operate. Instead, these pathways are largely driven by ion and concentration gradients. [220] Active transport on the other hand requires an energy source in the form of sugars or adenosine triphosphate (ATP) in order to employ proteins spanning the membrane to transport molecular cargo into and out of the cell. [183, 222] Similar to how multiple hypotheses listed in Section 6.2.1 could be occurring simultaneously, it is possible that cells are utilizing multiple transport mechanisms mentioned here to mediate the transport of the molecules investigated in this dissertation. For instance, preliminary results in which ATP is depleted from the system via sodium arsenate dibasic heptahydrate (SADH) [43, 154] show that FM 2-10 might rely on the presence of energy in *S. aureus*, as seen in Figure 6.3. The extent at which each mechanism plays a role in this transport has yet to be investigated and remains a future direction.

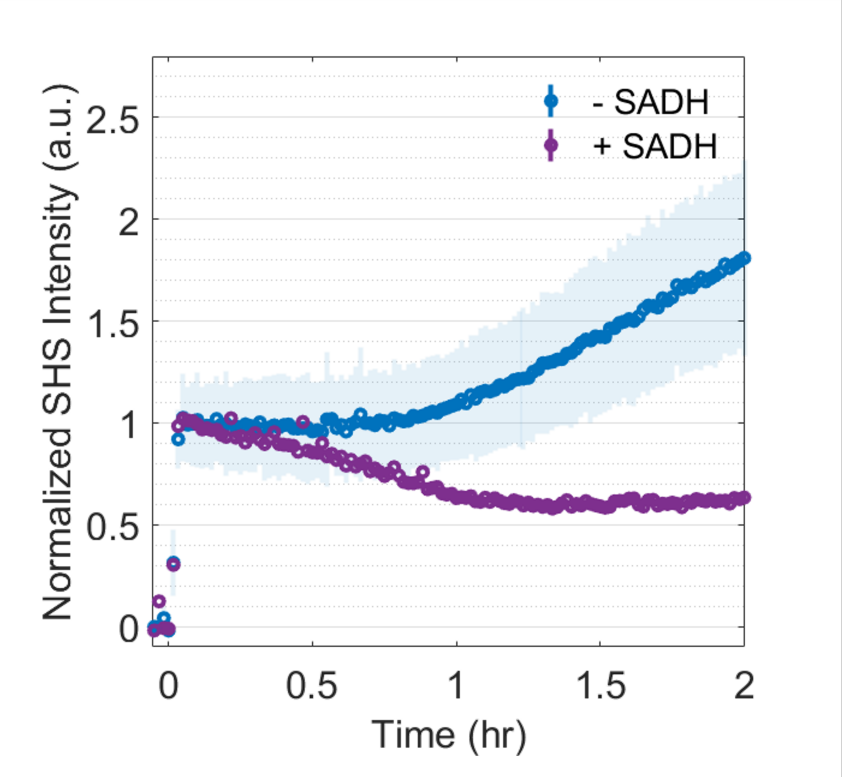


Figure 6.3: Impact of SADH on trSHS dynamics of 16 μM FM 2-10 with *S. aureus*.

6.2.3 More Mesh, More Problems

As depicted in Chapter 1, the Gram-positive bacterial surface is not solely composed of a cytoplasmic membrane, but instead is a lipid bilayer surrounded by a thick peptidoglycan mesh (PM), or cell wall, that acts as a physical barrier of protection. This PM layer is 30-100 nm thick and is equipped with intercalated sugar molecules, lipoteichoic acids and teichoic acids that carry negative charges. [187, 177] Without removing this structure, it is difficult to determine precisely which membrane structure the molecules studied here are interacting with. It is hypothesized that these anionic charges are more random than structured and that the dispersal of charges would result in a random orientation of probe molecules, thus rendering no significant SHS responses. Additionally, the PM for *S. aureus* and *B. subtilis*, specifically, has been shown to exhibit large pores [177] that potentially facilitate the movement of these molecules to the cytoplasmic membrane. Therefore, the cell wall is not expected to be the predominant membrane structure facilitating the SHS responses witnessed in this dissertation. Additionally, absence of the PM has been shown to disrupt the osmotic regulation and decrease the cell wall stiffness of *S. aureus*. [69] By removing the PM, its overall impact on these small molecule dynamics could assessed and mechanical impact on molecule transport can be elucidated.

6.2.4 Disrupting Domains

While the sole focus of Chapter 5 dealt with investigating the impact MLT has on the small molecule transport in the membranes of *S. aureus* and *B. subtilis*, MLT is only one potential disruptor of membrane domains. Additionally, while the structure of the molecule, as an alkylphosphocholine, dictates its primary mechanism of action begins by perturbing the membrane structural integrity directly, there are other disruptors that have been hypothesized to act by targeting cell machinery in the cytoplasm. One such disruptor is zaragozic acid (ZA). ZA is a squalene synthase inhibitor that has been shown to reduce the production of carotenoids in *S. aureus* and perturb flotillin protein localization in *B. subtilis*, with both carotenoids and flotillin proteins being potential membrane domain constituents.[129] Therefore, it would be interesting to explore other membrane disruptors

such as ZA and their potential impact on molecule transport to elucidate the roles domains play in small molecule-membrane dynamics.

6.2.5 Expanding the Toolbox

Lastly, the results presented in Chapter 3 were the start of a "molecular toolbox" to investigate how molecule and membrane structure influences a molecule's journey through the bacterial surface. Future works should expand the range of molecules to uncover how other tunable parameters, such as charge, aromaticity, and geometry, impact these dynamics. Further, this work focused on the membranes of *S. aureus* and *B. subtilis* illustrating that not all dynamics of these small molecules can be generalized for all membranes. Therefore, it is necessary to expand to other cell types to unveil the role of the membrane structure itself in small molecule-membrane interactions.

Bibliography

[1] (2006). Fluorescence Anisotropy. In Lakowicz, J. R., editor, *Principles of Fluorescence Spectroscopy*, pages 353–382. Springer US, Boston, MA. 29, 30

[2] Aghigh, A., Bancelin, S., Rivard, M., Pinsard, M., Ibrahim, H., and Légaré, F. (2023). Second harmonic generation microscopy: a powerful tool for bio-imaging. *Biophysical Reviews*, 15(1):43–70. 15

[3] Alger, J. R. and Prestegard, J. H. (1979). Nuclear magnetic resonance study of acetic acid permeation of large unilamellar vesicle membranes. *Biophysical Journal*, 28(1):1–13. 8

[4] Allhusen, J. S. and Conboy, J. C. (2017). The Ins and Outs of Lipid Flip-Flop. *Accounts of Chemical Research*, 50(1):58–65. Publisher: American Chemical Society. 36

[5] Aloia, R. C. and Boggs, J. M. (2013). *Membrane Fluidity in Biology: Cellular Aspects*. Academic Press. Google-Books-ID: GBvgBAAAQBAJ. 34

[6] Alonso, L., Mendanha, S. A., Marquezin, C. A., Berardi, M., Ito, A. S., Acuña, A. U., and Alonso, A. (2012). Interaction of miltefosine with intercellular membranes of stratum corneum and biomimetic lipid vesicles. *International Journal of Pharmaceutics*, 434(1):391–398. 73, 78

[7] Anglin, T. C. and Conboy, J. C. (2009). Kinetics and Thermodynamics of Flip-Flop in Binary Phospholipid Membranes Measured by Sum-Frequency Vibrational Spectroscopy. *Biochemistry*, 48(43):10220–10234. Publisher: American Chemical Society. 36

[8] Appala, K., Bimpeh, K., Freeman, C., and Hines, K. M. (2020). Recent applications of mass spectrometry in bacterial lipidomics. *Analytical and Bioanalytical Chemistry*, 412(24):5935–5943. 35

[9] Armstrong, V. T., Brzustowicz, M. R., Wassall, S. R., Jenski, L. J., and Stillwell, W. (2003). Rapid flip-flop in polyunsaturated (docosahexaenoate) phospholipid membranes. *Archives of Biochemistry and Biophysics*, 414(1):74–82. 36, 54

[10] Bach, J. N. and Bramkamp, M. (2013). Flotillins functionally organize the bacterial membrane. *Molecular Microbiology*, 88(6):1205–1217. _eprint: https://onlinelibrary.wiley.com/doi/pdf/10.1111/mmi.12252. 34, 35

[11] Baird, C. L., Courtenay, E. S., and Myszka, D. G. (2002). Surface plasmon resonance characterization of drug/liposome interactions. *Analytical Biochemistry*, 310(1):93–99. 8

[12] Bartkowiak, W., Zaleśny, R., Niewodniczański, W., and Leszczynski, J. (2001). Quantum Chemical Calculations of the First- and Second-Order Hyperpolarizabilities of Molecules in Solutions. *The Journal of Physical Chemistry A*, 105(47):10702–10710. Publisher: American Chemical Society. 74, 93

[13] Barák, I. and Muchová, K. (2013). The Role of Lipid Domains in Bacterial Cell Processes. *International Journal of Molecular Sciences*, 14(2):4050–4065. Number: 2 Publisher: Multidisciplinary Digital Publishing Institute. 34

[14] Barák, I., Muchová, K., Wilkinson, A. J., O'Toole, P. J., and Pavlendová, N. (2008). Lipid spirals in Bacillus subtilis and their role in cell division. *Molecular Microbiology*, 68(5):1315–1327. _eprint: https://onlinelibrary.wiley.com/doi/pdf/10.1111/j.1365-2958.2008.06236.x. 88

[15] Bassolino-Klimas, D., Alper, H. E., and Stouch, T. R. (1993). Solute diffusion in lipid bilayer membranes: An atomic level study by molecular dynamics simulation. *Biochemistry*, 32(47):12624–12637. Publisher: American Chemical Society. 8

[16] Bemporad, D., Essex, J. W., and Luttmann, C. (2004). Permeation of Small Molecules through a Lipid Bilayer: A Computer Simulation Study. *The Journal of Physical Chemistry B*, 108(15):4875–4884. Publisher: American Chemical Society. 8

[17] Berben, P., Bauer-Brandl, A., Brandl, M., Faller, B., Flaten, G. E., Jacobsen, A.-C., Brouwers, J., and Augustijns, P. (2018). Drug permeability profiling using cell-free permeation tools: Overview and applications. *European Journal of Pharmaceutical Sciences*, 119:219–233. 8

[18] Berezin, M. Y. and Achilefu, S. (2010). Fluorescence Lifetime Measurements and Biological Imaging. *Chemical Reviews*, 110(5):2641–2684. Publisher: American Chemical Society. 95

[19] Bessa, L. J., Ferreira, M., and Gameiro, P. (2018a). Data on Laurdan spectroscopic analyses to compare membrane fluidity between susceptible and multidrug-resistant bacteria. *Data in Brief*, 21:128–132. 78

[20] Bessa, L. J., Ferreira, M., and Gameiro, P. (2018b). Evaluation of membrane fluidity of multidrug-resistant isolates of *Escherichia coli* and *Staphylococcus aureus* in presence and absence of antibiotics. *Journal of Photochemistry and Photobiology B: Biology*, 181:150–156. 80

[21] Blake, M. J., Castillo, H. B., Curtis, A. E., and Calhoun, T. R. (2023). Facilitating flip-flop: Structural tuning of molecule-membrane interactions in living bacteria. *Biophysical Journal*, 122(10):1735–1747. 62, 66, 74, 75, 80, 86, 93

[22] Blake, M. J., Colon, B. A., and Calhoun, T. R. (2020). Leaving the Limits of Linearity for Light Microscopy. *The Journal of Physical Chemistry C*, 124(45):24555–24565. Publisher: American Chemical Society. 13, 35

[23] Bogdanov, M., Pyrshev, K., Yesylevskyy, S., Ryabichko, S., Boiko, V., Ivanchenko, P., Kiyamova, R., Guan, Z., Ramseyer, C., and Dowhan, W. (2020). Phospholipid distribution in the cytoplasmic membrane of Gram-negative bacteria is highly asymmetric, dynamic, and cell shape-dependent. *Science Advances*, 6(23):eaaz6333. Publisher: American Association for the Advancement of Science. 5

[24] Boudjema, L., Aarrass, H., Assaf, M., Morille, M., Martin-Gassin, G., and Gassin, P.-M. (2020). PySHS: Python Open Source Software for Second Harmonic Scattering. *Journal of Chemical Information and Modeling*, 60(12):5912–5917. Publisher: American Chemical Society. 25, 27, 63, 70

[25] Boxer, S. G., Kraft, M. L., and Weber, P. K. (2009). Advances in Imaging Secondary Ion Mass Spectrometry for Biological Samples. *Annual Review of Biophysics*, 38(1):53–74. _eprint: https://doi.org/10.1146/annurev.biophys.050708.133634. 35

[26] Boyd, R. W. (2008). *Nonlinear Optics*. Elsevier. Google-Books-ID: uoRUi1Yb7ooC. 11

[27] Bramkamp, M. (2022). Fluidity is the way to life: lipid phase separation in bacterial membranes. *The EMBO Journal*, 41(5):e110737. Publisher: John Wiley & Sons, Ltd. 88

[28] Brändén, M., Dahlin, S., and Höök, F. (2008). Label-Free Measurements of Molecular Transport across Liposome Membranes using Evanescent-Wave Sensing. *ChemPhysChem*, 9(17):2480–2485. _eprint: https://onlinelibrary.wiley.com/doi/pdf/10.1002/cphc.200800614. 8

[29] Brändén, M., Tabaei, S. R., Fischer, G., Neutze, R., and Höök, F. (2010). Refractive-Index-Based Screening of Membrane-Protein-Mediated Transfer across Biological Membranes. *Biophysical Journal*, 99(1):124–133. 8

[30] Bush, P. G., Wokosin, D. L., and Hall, A. C. (2007). Two-versus one photon excitation laser scanning microscopy: Critical importance of excitation wavelength. *Frontiers in bioscience : a journal and virtual library*, 12:2646–2657. 13

[31] Cama, J., Henney, A. M., and Winterhalter, M. (2019). Breaching the Barrier: Quantifying Antibiotic Permeability across Gram-negative Bacterial Membranes. *Journal of Molecular Biology*, 431(18):3531–3546. 34

[32] Campagnola, P. (2011). Second Harmonic Generation Imaging Microscopy: Applications to Diseases Diagnostics. *Analytical Chemistry*, 83(9):3224–3231. Publisher: American Chemical Society. 15

[33] Campagnola, P. J., Wei, M.-d., Lewis, A., and Loew, L. M. (1999). High-Resolution Nonlinear Optical Imaging of Live Cells by Second Harmonic Generation. *Biophysical Journal*, 77(6):3341–3349. 37, 74

[34] Carey, A. B., Ashenden, A., and Köper, I. (2022). Model architectures for bacterial membranes. *Biophysical Reviews*, 14(1):111–143. 34, 35

[35] Castro, B. M., Fedorov, A., Hornillos, V., Delgado, J., Acuña, A. U., Mollinedo, F., and Prieto, M. (2013). Edelfosine and Miltefosine Effects on Lipid Raft Properties: Membrane Biophysics in Cell Death by Antitumor Lipids. *The Journal of Physical Chemistry B*, 117(26):7929–7940. Publisher: American Chemical Society. 73, 78, 88, 90

[36] Centers for Disease Control and Prevention (U.S.) (2019). Antibiotic resistance threats in the United States, 2019. Technical report, Centers for Disease Control and Prevention (U.S.), Atlanta, GA. 2

[37] Centonze, V. E. and White, J. G. (1998). Multiphoton Excitation Provides Optical Sections from Deeper within Scattering Specimens than Confocal Imaging. *Biophysical Journal*, 75(4):2015–2024. Publisher: Elsevier. 13

[38] Chen, S. L., Liang, Y. Z., Hou, Y., Wang, H., Wu, X., Gan, W., and Yuan, Q. (2019). Simple physics in and easy manipulating of the interfacial behavior of charged molecules on drug delivery vesicles. *Materials Today Physics*, 9:100092. 37, 52, 62, 74

[39] Cheng, C.-Y., Goor, O. J., and Han, S. (2012). Quantitative Analysis of Molecular Transport across Liposomal Bilayer by J-Mediated 13C Overhauser Dynamic Nuclear Polarization. *Analytical Chemistry*, 84(21):8936–8940. Publisher: American Chemical Society. 8

[40] Cheng, C.-Y., Olijve, L. L. C., Kausik, R., and Han, S. (2014). Cholesterol enhances surface water diffusion of phospholipid bilayers. *The Journal of Chemical Physics*, 141(22):22D513. 8

[41] Cheng, J. T. J., Hale, J. D., Elliott, M., Hancock, R. E. W., and Straus, S. K. (2011). The importance of bacterial membrane composition in the structure and function of aurein 2.2 and selected variants. *Biochimica et Biophysica Acta (BBA) - Biomembranes*, 1808(3):622–633. 34

[42] Chopra, I. and Roberts, M. (2001). Tetracycline Antibiotics: Mode of Action, Applications, Molecular Biology, and Epidemiology of Bacterial Resistance. *Microbiology and Molecular Biology Reviews*, 65(2):232–260. Publisher: American Society for Microbiology. 37

[43] Conlon, B. P., Rowe, S. E., Gandt, A. B., Nuxoll, A. S., Donegan, N. P., Zalis, E. A., Clair, G., Adkins, J. N., Cheung, A. L., and Lewis, K. (2016). Persister formation in Staphylococcus aureus is associated with ATP depletion. *Nature Microbiology*, 1(5):1–7. Publisher: Nature Publishing Group. 97

[44] Corn, R. M. and Higgins, D. A. (1994). Optical second harmonic generation as a probe of surface chemistry. *Chemical Reviews*, 94(1):107–125. 15

[45] Costerton, J. W. (1979). The Role of Electron Microscopy in the Elucidation of Bacterial Structure and Function. *Annual Review of Microbiology*, 33(1):459–479. _eprint: https://doi.org/10.1146/annurev.mi.33.100179.002331. 35

[46] Danelian, E., Karlén, A., Karlsson, R., Winiwarter, S., Hansson, A., Löfås, S., Lennernäs, H., and Hämäläinen, M. D. (2000). SPR Biosensor Studies of the Direct Interaction between 27 Drugs and a Liposome Surface: Correlation with Fraction Absorbed in Humans. *Journal of Medicinal Chemistry*, 43(11):2083–2086. Publisher: American Chemical Society. 8

[47] Denev, S. A., Lummen, T. T. A., Barnes, E., Kumar, A., and Gopalan, V. (2011). Probing Ferroelectrics Using Optical Second Harmonic Generation. *Journal of the American Ceramic Society*, 94(9):2699–2727. _eprint: https://onlinelibrary.wiley.com/doi/pdf/10.1111/j.1551-2916.2011.04740.x. 15

[48] Denich, T. J., Beaudette, L. A., Lee, H., and Trevors, J. T. (2003). Effect of selected environmental and physico-chemical factors on bacterial cytoplasmic membranes. *Journal of Microbiological Methods*, 52(2):149–182. 34

[49] Denk, W., Strickler, J. H., and Webb, W. W. (1990). Two-Photon Laser Scanning Fluorescence Microscopy. *Science*, 248(4951):73–76. Publisher: American Association for the Advancement of Science. 13

[50] Diestra, E., Cayrol, B., Arluison, V., and Risco, C. (2009). Cellular Electron Microscopy Imaging Reveals the Localization of the Hfq Protein Close to the Bacterial Membrane. *PLoS ONE*, 4(12):e8301. 35

[51] Dikkumbura, A. S., Aucoin, A. V., Ali, R. O., Dalier, A., Gilbert, D. W., Schneider, G. J., and Haber, L. H. (2022). Influence of Acetaminophen on Molecular Adsorption and Transport Properties at Colloidal Liposome Surfaces Studied by Second Harmonic Generation Spectroscopy. *Langmuir*, 38(12):3852–3859. Publisher: American Chemical Society. 37, 62, 74

[52] Diomande, S., NGUYEN-THE, C., Guinebretière, M.-H., Broussolle, V., and Brillard, J. (2015). Role of fatty acids in Bacillus environmental adaptation. *Frontiers in Microbiology*, 6. 34

[53] Diver, J. M., Piddock, L. J. V., and Wise, R. (1990). The accumulation of five quinolone antibacterial agents by Escherichia coli. *Journal of Antimicrobial Chemotherapy*, 25(3):319–333. 8

[54] Dorlo, T. P. C., Balasegaram, M., Beijnen, J. H., and de Vries, P. J. (2012). Miltefosine: a review of its pharmacology and therapeutic efficacy in the treatment of leishmaniasis. *Journal of Antimicrobial Chemotherapy*, 67(11):2576–2597. 73

[55] Doughty, B., Rao, Y., Kazer, S. W., Kwok, S. J. J., Turro, N. J., and Eisenthal, K. B. (2013). Binding of the Anti-Cancer Drug Daunomycin to DNA Probed by Second Harmonic Generation. *The Journal of Physical Chemistry B*, 117(49):15285–15289. Publisher: American Chemical Society. 45

[56] Duboisset, J., Aït-Belkacem, D., Roche, M., Rigneault, H., and Brasselet, S. (2012). Generic model of the molecular orientational distribution probed by polarization-resolved second-harmonic generation. *Physical Review A*, 85(4):043829. 63

[57] Duboisset, J. and Brevet, P.-F. (2019). Second-Harmonic Scattering-Defined Topological Classes for Nano-Objects. *The Journal of Physical Chemistry C*, 123(41):25303–25308. Publisher: American Chemical Society. 63

[58] Eckenrode, H. M., Jen, S.-H., Han, J., Yeh, A.-G., and Dai, H.-L. (2005). Adsorption of a Cationic Dye Molecule on Polystyrene Microspheres in Colloids: Effect of Surface Charge and Composition Probed by Second Harmonic Generation. *The Journal of Physical Chemistry B*, 109(10):4646–4653. Publisher: American Chemical Society. 66, 70

[59] Eibl, H. and Unger, C. (1990). Hexadecylphosphocholine: a new and selective antitumor drug. *Cancer Treatment Reviews*, 17(2):233–242. 73

[60] Eisenthal, K. B. (1992). Equilibrium and Dynamic Processes at Interfaces by Second Harmonic and Sum Frequency Generation. *Annual Review of Physical Chemistry*, 43(1):627–661. _eprint: https://doi.org/10.1146/annurev.pc.43.100192.003211. 15, 47

[61] Ernst, R., Ejsing, C. S., and Antonny, B. (2016). Homeoviscous Adaptation and the Regulation of Membrane Lipids. *Journal of Molecular Biology*, 428(24, Part A):4776–4791. 5

[62] Evason, D. J., Claydon, M. A., and Gordon, D. B. (2001). Exploring the limits of bacterial identification by intact cell-mass spectrometry. *Journal of the American Society for Mass Spectrometry*, 12(1):49–54. 35

[63] Eyer, K., Paech, F., Schuler, F., Kuhn, P., Kissner, R., Belli, S., Dittrich, P. S., and Krämer, S. D. (2014). A liposomal fluorescence assay to study permeation kinetics of drug-like weak bases across the lipid bilayer. *Journal of Controlled Release*, 173:102–109. 8

[64] Feng, X., Hu, Y., Zheng, Y., Zhu, W., Li, K., Huang, C.-H., Ko, T.-P., Ren, F., Chan, H.-C., Nega, M., Bogue, S., López, D., Kolter, R., Götz, F., Guo, R.-T., and Oldfield, E. (2014). Structural and Functional Analysis of Bacillus subtilis YisP Reveals a Role of Its Product in Biofilm Production. *Chemistry & Biology*, 21(11):1557–1563. 56

[65] Fernandes, K. S., de Souza, P. E. N., Dorta, M. L., and Alonso, A. (2017). The cytotoxic activity of miltefosine against *Leishmania* and macrophages is associated with dynamic changes in plasma membrane proteins. *Biochimica et Biophysica Acta (BBA) - Biomembranes*, 1859(1):1–9. 73, 78

[66] Ferreira, R. J. and Kasson, P. M. (2019). Antibiotic Uptake Across Gram-Negative Outer Membranes: Better Predictions Towards Better Antibiotics. *ACS Infectious Diseases*, 5(12):2096–2104. Publisher: American Chemical Society. 34

[67] Fiebig, M., Pavlov, V. V., and Pisarev, R. V. (2005). Second-harmonic generation as a tool for studying electronic and magnetic structures of crystals: review. *JOSA B*, 22(1):96–118. Publisher: Optica Publishing Group. 15

[68] Frallicciardi, J., Melcr, J., Siginou, P., Marrink, S. J., and Poolman, B. (2022). Membrane thickness, lipid phase and sterol type are determining factors in the permeability of membranes to small solutes. *Nature Communications*, 13(1):1605. Number: 1 Publisher: Nature Publishing Group. 56

[69] Francius, G., Domenech, O., Mingeot-Leclercq, M. P., and Dufrêne, Y. F. (2008). Direct Observation of Staphylococcus aureus Cell Wall Digestion by Lysostaphin. *Journal of Bacteriology*, 190(24):7904–7909. Publisher: American Society for Microbiology. 99

[70] Franken, P. A., Hill, A. E., Peters, C. W., and Weinreich, G. (1961). Generation of Optical Harmonics. *Physical Review Letters*, 7(4):118–119. Publisher: American Physical Society. 15

[71] Furse, S. and Scott, D. J. (2016). Three-Dimensional Distribution of Phospholipids in Gram Negative Bacteria. *Biochemistry*, 55(34):4742–4747. Publisher: American Chemical Society. 5

[72] Gaffield, M. A. and Betz, W. J. (2006). Imaging synaptic vesicle exocytosis and endocytosis with FM dyes. *Nature Protocols*, 1(6):2916–2921. Number: 6 Publisher: Nature Publishing Group. 38

[73] García-Fernández, E., Koch, G., Wagner, R. M., Fekete, A., Stengel, S. T., Schneider, J., Mielich-Süss, B., Geibel, S., Markert, S. M., Stigloher, C., and Lopez, D. (2017). Membrane Microdomain Disassembly Inhibits MRSA Antibiotic Resistance. *Cell*, 171(6):1354–1367.e20. 34, 56

[74] Gayen, A., Kumar, D., Matheshwaran, S., and Chandra, M. (2019). Unveiling the Modulating Role of Extracellular pH in Permeation and Accumulation of Small Molecules in Subcellular Compartments of Gram-negative Escherichia coli using Nonlinear Spectroscopy. *Analytical Chemistry*, 91(12):7662–7671. Publisher: American Chemical Society. 75, 80

[75] Ghaemi, Z., Alberga, D., Carloni, P., Laio, A., and Lattanzi, G. (2016). Permeability Coefficients of Lipophilic Compounds Estimated by Computer Simulations. *Journal of Chemical Theory and Computation*, 12(8):4093–4099. Publisher: American Chemical Society. 8

[76] Ghaemi, Z., Minozzi, M., Carloni, P., and Laio, A. (2012). A Novel Approach to the Investigation of Passive Molecular Permeation through Lipid Bilayers from Atomistic Simulations. *The Journal of Physical Chemistry B*, 116(29):8714–8721. Publisher: American Chemical Society. 8

[77] Ghosh, C. and Haldar, J. (2015). Membrane-Active Small Molecules: Designs Inspired by Antimicrobial Peptides. *ChemMedChem*, 10(10):1606–1624. _eprint: https://onlinelibrary.wiley.com/doi/pdf/10.1002/cmdc.201500299. 2, 38

[78] Gibbs, K. A., Isaac, D. D., Xu, J., Hendrix, R. W., Silhavy, T. J., and Theriot, J. A. (2004). Complex spatial distribution and dynamics of an abundant Escherichia coli outer membrane protein, LamB. *Molecular Microbiology*, 53(6):1771–1783. _eprint: https://onlinelibrary.wiley.com/doi/pdf/10.1111/j.1365-2958.2004.04242.x. 35

[79] Gidden, J., Denson, J., Liyanage, R., Ivey, D. M., and Lay, J. O. (2009). Lipid compositions in Escherichia coli and Bacillus subtilis during growth as determined by MALDI-TOF and TOF/TOF mass spectrometry. *International Journal of Mass Spectrometry*, 283(1):178–184. 35

[80] Gonella, G. and Dai, H.-L. (2014). Second Harmonic Light Scattering from the Surface of Colloidal Objects: Theory and Applications. *Langmuir*, 30(10):2588–2599. Publisher: American Chemical Society. 17, 37, 62, 74

[81] Grigor'eva, A., Bardasheva, A., Tupitsyna, A., Amirkhanov, N., Tikunova, N., Pyshnyi, D., and Ryabchikova, E. (2020). Changes in the Ultrastructure of Staphylococcus aureus Treated with Cationic Peptides and Chlorhexidine. *Microorganisms*, 8(12):1991. 35

[82] Guilhelmelli, F., Vilela, N., Albuquerque, P., Derengowski, L., Silva-Pereira, I., and Kyaw, C. (2013). Antibiotic development challenges: the various mechanisms of action of antimicrobial peptides and of bacterial resistance. *Frontiers in Microbiology*, 4. 34

[83] Göppert-Mayer, M. (1931). Über Elementarakte mit zwei Quantensprüngen. *Annalen der Physik*, 401(3):273–294. _eprint: https://onlinelibrary.wiley.com/doi/pdf/10.1002/andp.19314010303. 15

[84] Halder, S., Yadav, K. K., Sarkar, R., Mukherjee, S., Saha, P., Haldar, S., Karmakar, S., and Sen, T. (2015). Alteration of Zeta potential and membrane permeability in bacteria: a study with cationic agents. *SpringerPlus*, 4(1):672. 34

[85] Hamal, P., Nguyenhuu, H., Subasinghege Don, V., Kumal, R. R., Kumar, R., McCarley, R. L., and Haber, L. H. (2019). Molecular Adsorption and Transport at Liposome Surfaces Studied by Molecular Dynamics Simulations and Second Harmonic Generation Spectroscopy. *The Journal of Physical Chemistry B*, 123(36):7722–7730. Publisher: American Chemical Society. 37, 62, 74

[86] Hamal, P., Subasinghege Don, V., Nguyenhuu, H., Ranasinghe, J. C., Nauman, J. A., McCarley, R. L., Kumar, R., and Haber, L. H. (2021). Influence of Temperature on Molecular Adsorption and Transport at Liposome Surfaces Studied by Molecular Dynamics Simulations and Second Harmonic Generation Spectroscopy. *The Journal of Physical Chemistry B*, 125(37):10506–10513. Publisher: American Chemical Society. 37, 62, 74

[87] Hartmann, M., Berditsch, M., Hawecker, J., Ardakani, M. F., Gerthsen, D., and Ulrich, A. S. (2010). Damage of the Bacterial Cell Envelope by Antimicrobial Peptides Gramicidin S and PGLa as Revealed by Transmission and Scanning Electron Microscopy. *Antimicrobial Agents and Chemotherapy*, 54(8):3132–3142. Publisher: American Society for Microbiology. 35

[88] Heczková, B. and Slotte, J. P. (2006). Effect of anti-tumor ether lipids on ordered domains in model membranes. *FEBS Letters*, 580(10):2471–2476. 73, 88

[89] Hines, K. M., Waalkes, A., Penewit, K., Holmes, E. A., Salipante, S. J., Werth, B. J., and Xu, L. (2017). Characterization of the Mechanisms of Daptomycin Resistance among Gram-Positive Bacterial Pathogens by Multidimensional Lipidomics. *mSphere*, 2(6):e00492–17. Publisher: American Society for Microbiology. 34

[90] Homan, R. and Pownall, H. J. (1988). Transbilayer diffusion of phospholipids: dependence on headgroup structure and acyl chain length. *Biochimica et Biophysica Acta (BBA) - Biomembranes*, 938(2):155–166. 36, 51

[91] Hou, Y., Chen, S.-L., Gan, W., Ma, X., and Yuan, Q. (2019). Understanding the Dynamic Behavior of an Anticancer Drug, Doxorubicin, on a Lipid Membrane Using Multiple Spectroscopic Techniques. *The Journal of Physical Chemistry B*, 123(17):3756–3762. Publisher: American Chemical Society. 37, 62

[92] Hou, Y., Li, J., Liu, X., Ruan, Y., Chen, S.-l., Yuan, Q., and Gan, W. (2021). The effect of side group on the dynamic behavior of anthracyclines on DOPG lipid membranes revealed by second harmonic generation and fluorescence. *Chemical Physics*, 541:111036. 74

[93] Hurdle, J. G., O'Neill, A. J., Chopra, I., and Lee, R. E. (2011). Targeting bacterial membrane function: an underexploited mechanism for treating persistent infections. *Nature Reviews Microbiology*, 9(1):62–75. Number: 1 Publisher: Nature Publishing Group. 2, 38

[94] Hyeon Park, J., Naw Sut, T., A. Jackman, J., Rahim Ferhan, A., Kyeong Yoon, B., and Cho, N.-J. (2017). Controlling adsorption and passivation properties of bovine serum albumin on silica surfaces by ionic strength modulation and cross-linking. *Physical Chemistry Chemical Physics*, 19(13):8854–8865. Publisher: Royal Society of Chemistry. 76

[95] Jay, A. G. and Hamilton, J. A. (2017). Disorder Amidst Membrane Order: Standardizing Laurdan Generalized Polarization and Membrane Fluidity Terms. *Journal of Fluorescence*, 27(1):243–249. 78

[96] Jen, S.-H., Dai, H.-L., and Gonella, G. (2010). The Effect of Particle Size in Second Harmonic Generation from the Surface of Spherical Colloidal Particles. II: The Nonlinear RayleighGansDebye Model. *The Journal of Physical Chemistry C*, 114(10):4302–4308. Publisher: American Chemical Society. 17

[97] Jespersen, H., Andersen, J. H., Ditzel, H. J., and Mouritsen, O. G. (2012). Lipids, curvature stress, and the action of lipid prodrugs: Free fatty acids and lysolipid enhancement of drug transport across liposomal membranes. *Biochimie*, 94(1):2–10. 8

[98] Jiang, Y., Dai, X., Qin, M., and Guo, Z. (2019). Identification of an amphipathic peptide sensor of the Bacillus subtilis fluid membrane microdomains. *Communications Biology*, 2(1):1–9. Number: 1 Publisher: Nature Publishing Group. 7

[99] Johnson, A. S., van Horck, S., and Lewis, P. J. (2004). Dynamic localization of membrane proteins in Bacillus subtilis. *Microbiology*, 150(9):2815–2824. Publisher: Microbiology Society,. 88

[100] Kamp, F., Zakim, D., Zhang, F., Noy, N., and Hamilton, J. A. (1995). Fatty Acid Flip-Flop in Phospholipid Bilayers Is Extremely Fast. *Biochemistry*, 34(37):11928–11937. Publisher: American Chemical Society. 36, 54

[101] Kaneda, T. (1977). Fatty acids of the genus Bacillus: an example of branched-chain preference. *Bacteriological Reviews*, 41(2):391–418. 56

[102] Kaneda, T. (1991). Iso- and anteiso-fatty acids in bacteria: biosynthesis, function, and taxonomic significance. *Microbiological Reviews*, 55(2):288–302. Publisher: American Society for Microbiology. 34

[103] Kawai, F., Shoda, M., Harashima, R., Sadaie, Y., Hara, H., and Matsumoto, K. (2004). Cardiolipin Domains in Bacillus subtilis Marburg Membranes. *Journal of Bacteriology*, 186(5):1475–1483. 5

[104] Kaščáková, S., Maigre, L., Chevalier, J., Réfrégiers, M., and Pagès, J.-M. (2012). Antibiotic Transport in Resistant Bacteria: Synchrotron UV Fluorescence Microscopy to Determine Antibiotic Accumulation with Single Cell Resolution. *PLOS ONE*, 7(6):e38624. Publisher: Public Library of Science. 8

[105] Kleinfeld, A. M., Chu, P., and Storch, J. (1997). Flip-Flop Is Slow and Rate Limiting for the Movement of Long Chain Anthroyloxy Fatty Acids across Lipid Vesicles. *Biochemistry*, 36(19):5702–5711. Publisher: American Chemical Society. 36

[106] Kleinzeller, A. (1997). Ernest Overton's Contribution to the Cell Membrane Concept: A Centennial Appreciation. *Physiology*, 12(1):49–53. Publisher: American Physiological Society. 8, 37

[107] Koch, G., Wermser, C., Acosta, I. C., Kricks, L., Stengel, S. T., Yepes, A., and Lopez, D. (2017). Attenuating *Staphylococcus aureus* Virulence by Targeting Flotillin Protein Scaffold Activity. *Cell Chemical Biology*, 24(7):845–857.e6. 73, 86, 88

[108] Kraft, M. L. and Klitzing, H. A. (2014). Imaging lipids with secondary ion mass spectrometry. *Biochimica et Biophysica Acta (BBA) - Molecular and Cell Biology of Lipids*, 1841(8):1108–1119. 35

[109] Krämer, A., Ghysels, A., Wang, E., Venable, R. M., Klauda, J. B., Brooks, B. R., and Pastor, R. W. (2020). Membrane permeability of small molecules from unbiased molecular dynamics simulations. *The Journal of Chemical Physics*, 153(12):124107. 8

[110] Kuhn, P., Eyer, K., Allner, S., Lombardi, D., and Dittrich, P. S. (2011). A Microfluidic Vesicle Screening Platform: Monitoring the Lipid Membrane Permeability

of Tetracyclines. *Analytical Chemistry*, 83(23):8877–8885. Publisher: American Chemical Society. 8

[111] Kumal, R. R., Nguyenhuu, H., Winter, J. E., McCarley, R. L., and Haber, L. H. (2017). Impacts of Salt, Buffer, and Lipid Nature on Molecular Adsorption and Transport in Liposomes As Observed by Second Harmonic Generation. *The Journal of Physical Chemistry C*, 121(29):15851–15860. Publisher: American Chemical Society. 37, 62, 74, 80

[112] Kumar, D., Gayen, A., and Chandra, M. (2023). Hypo-osmotic Stress Increases Permeability of Individual Barriers in Escherichia coli Cell Envelope, Enabling Rapid Drug Transport. *ACS Infectious Diseases*, 9(12):2471–2481. Publisher: American Chemical Society. 75, 80

[113] Lanni, E. J., Rubakhin, S. S., and Sweedler, J. V. (2012). Mass spectrometry imaging and profiling of single cells. *Journal of Proteomics*, 75(16):5036–5051. 35

[114] Lee, T.-H., Hofferek, V., Separovic, F., Reid, G. E., and Aguilar, M.-I. (2019). The role of bacterial lipid diversity and membrane properties in modulating antimicrobial peptide activity and drug resistance. *Current Opinion in Chemical Biology*, 52:85–92. 2, 34

[115] Lentz, B. R. (1989). Membrane "fluidity" as detected by diphenylhexatriene probes. *Chemistry and Physics of Lipids*, 50(3):171–190. 29, 30

[116] Lewis, K. (2013). Platforms for antibiotic discovery. *Nature Reviews Drug Discovery*, 12(5):371–387. Number: 5 Publisher: Nature Publishing Group. 33, 35

[117] Li, B., Li, J., Gan, W., Tan, Y., and Yuan, Q. (2021). Unveiling the Molecular Dynamics in a Living Cell to the Subcellular Organelle Level Using Second-Harmonic Generation Spectroscopy and Microscopy. *Analytical Chemistry*, 93(42):14146–14152. Publisher: American Chemical Society. 37, 74

[118] Li, S., Hu, P., and Malmstadt, N. (2010). Confocal Imaging to Quantify Passive Transport across Biomimetic Lipid Membranes. *Analytical Chemistry*, 82(18):7766–7771. Publisher: American Chemical Society. 8

[119] Lin, T.-Y. and Weibel, D. B. (2016). Organization and function of anionic phospholipids in bacteria. *Applied Microbiology and Biotechnology*, 100(10):4255–4267. 5

[120] Lipinski, C. A. (2004). Lead- and drug-like compounds: the rule-of-five revolution. *Drug Discovery Today: Technologies*, 1(4):337–341. 8

[121] Lipinski, C. A., Lombardo, F., Dominy, B. W., and Feeney, P. J. (2012). Experimental and computational approaches to estimate solubility and permeability in drug discovery and development settings. *Advanced Drug Delivery Reviews*, 64:4–17. 8, 35

[122] Liu, J. and Conboy, J. C. (2005). 1,2-Diacyl-Phosphatidylcholine Flip-Flop Measured Directly by Sum-Frequency Vibrational Spectroscopy. *Biophysical Journal*, 89(4):2522–2532. 36

[123] Llull, D., Rivas, L., and García, E. (2007). In Vitro Bactericidal Activity of the Antiprotozoal Drug Miltefosine against Streptococcus pneumoniae and Other Pathogenic Streptococci. *Antimicrobial Agents and Chemotherapy*, 51(5):1844–1848. Publisher: American Society for Microbiology. 73

[124] Lopez, D. and Koch, G. (2017). Exploring functional membrane microdomains in bacteria: an overview. *Current Opinion in Microbiology*, 36:76–84. 7, 56, 86

[125] Luchini, A., Cavasso, D., Radulescu, A., D'Errico, G., Paduano, L., and Vitiello, G. (2021). Structural Organization of Cardiolipin-Containing Vesicles as Models of the Bacterial Cytoplasmic Membrane. *Langmuir*, 37(28):8508–8516. Publisher: American Chemical Society. 34

[126] Luit, A. H. v. d., Budde, M., Ruurs, P., Verheij, M., and Blitterswijk, W. J. v. (2002). Alkyl-lysophospholipid Accumulates in Lipid Rafts and Induces Apoptosis via Raft-dependent Endocytosis and Inhibition of Phosphatidylcholine Synthesis *. *Journal of Biological Chemistry*, 277(42):39541–39547. Publisher: Elsevier. 73, 82, 88

[127] Luque-Ortega, J. R. and Rivas, L. (2007). Miltefosine (Hexadecylphosphocholine) Inhibits Cytochrome c Oxidase in Leishmania donovani Promastigotes. *Antimicrobial*

Agents and Chemotherapy, 51(4):1327–1332. Publisher: American Society for Microbiology. 73

[128] López, C. S., Garda, H. A., and Rivas, E. A. (2002). The effect of osmotic stress on the biophysical behavior of the *Bacillus subtilis* membrane studied by dynamic and steady-state fluorescence anisotropy. *Archives of Biochemistry and Biophysics*, 408(2):220–228. 78, 88

[129] López, D. and Kolter, R. (2010). Functional microdomains in bacterial membranes. *Genes & Development*, 24(17):1893–1902. Company: Cold Spring Harbor Laboratory Press Distributor: Cold Spring Harbor Laboratory Press Institution: Cold Spring Harbor Laboratory Press Label: Cold Spring Harbor Laboratory Press Publisher: Cold Spring Harbor Lab. 7, 73, 86, 99

[130] López, G.-D., Suesca, E., Álvarez Rivera, G., Rosato, A. E., Ibáñez, E., Cifuentes, A., Leidy, C., and Carazzone, C. (2021). Carotenogenesis of *Staphylococcus aureus*: New insights and impact on membrane biophysical properties. *Biochimica et Biophysica Acta (BBA) - Molecular and Cell Biology of Lipids*, 1866(8):158941. 88

[131] López-Lara, I. M. and Geiger, O. (2017). Bacterial lipid diversity. *Biochimica et Biophysica Acta (BBA) - Molecular and Cell Biology of Lipids*, 1862(11):1287–1299. 37, 58

[132] Maiman, T. H. (1960). Stimulated Optical Radiation in Ruby. *Nature*, 187(4736):493–494. Number: 4736 Publisher: Nature Publishing Group. 15

[133] Malanovic, N. and Lohner, K. (2016). Antimicrobial Peptides Targeting Gram-Positive Bacteria. *Pharmaceuticals*, 9(3):59. 86

[134] Malta de Sá, M., Sresht, V., Rangel-Yagui, C. O., and Blankschtein, D. (2015). Understanding Miltefosine–Membrane Interactions Using Molecular Dynamics Simulations. *Langmuir*, 31(15):4503–4512. Publisher: American Chemical Society. 73, 74, 78, 88, 90

[135] Mannhold, R., Poda, G. I., Ostermann, C., and Tetko, I. V. (2009). Calculation of Molecular Lipophilicity: State-of-the-Art and Comparison of LogP Methods on more than 96,000 Compounds. *Journal of Pharmaceutical Sciences*, 98(3):861–893. 35

[136] Margaritova Zaharieva, M., Dimitrov Kroumov, A., Dimitrova, L., Tsvetkova, I., Trochopoulos, A., Mihaylov Konstantinov, S., Reinhold Berger, M., Momchilova, M., Yoncheva, K., and Miladinov Najdenski, H. (2019). Micellar curcumin improves the antibacterial activity of the alkylphosphocholines erufosine and miltefosine against pathogenic Staphyloccocus aureus strains. *Biotechnology & Biotechnological Equipment*, 33(1):38–53. Publisher: Taylor & Francis _eprint: https://doi.org/10.1080/13102818.2018.1533792. 73

[137] Marowsky, G. and Steinhoff, R. (1988). Hemicyanine monolayer orientation studied by second-harmonic generation. *Optics Letters*, 13(9):707–709. Publisher: Optica Publishing Group. 74, 95

[138] Martin-Gassin, G., Paineau, E., Launois, P., and Gassin, P.-M. (2022). Water Organization around Inorganic Nanotubes in Suspension Probed by Polarization-Resolved Second Harmonic Scattering. *The Journal of Physical Chemistry Letters*, 13(30):6883–6888. Publisher: American Chemical Society. 27

[139] Matias, V. R. F. and Beveridge, T. J. (2005). Cryo-electron microscopy reveals native polymeric cell wall structure in Bacillus subtilis 168 and the existence of a periplasmic space. *Molecular Microbiology*, 56(1):240–251. _eprint: https://onlinelibrary.wiley.com/doi/pdf/10.1111/j.1365-2958.2005.04535.x. 56

[140] Matias, V. R. F. and Beveridge, T. J. (2006). Native Cell Wall Organization Shown by Cryo-Electron Microscopy Confirms the Existence of a Periplasmic Space in Staphylococcus aureus. *Journal of Bacteriology*, 188(3):1011–1021. 35, 56

[141] McConnell, H. M. and Kornberg, R. D. (1971). Inside-outside transitions of phospholipids in vesicle membranes. *Biochemistry*, 10(7):1111–1120. Publisher: American Chemical Society. 36, 51

[142] Menichetti, F. (2005). Current and emerging serious Gram-positive infections. *Clinical Microbiology and Infection*, 11(s3):22–28. _eprint: https://onlinelibrary.wiley.com/doi/pdf/10.1111/j.1469-0691.2005.01138.x. 34

[143] Meyer, P. and Dworkin, J. (2007). Applications of fluorescence microscopy to single bacterial cells. *Research in Microbiology*, 158(3):187–194. 35

[144] Mignot, T. and Shaevitz, J. W. (2008). Active and passive mechanisms of intracellular transport and localization in bacteria. *Current Opinion in Microbiology*, 11(6):580–585. 5

[145] Mileykovskaya, E. and Dowhan, W. (2005). Role of membrane lipids in bacterial division-site selection. *Current Opinion in Microbiology*, 8(2):135–142. 5

[146] Miller, L. N., Blake, M. J., Page, E. F., Castillo, H. B., and Calhoun, T. R. (2021). Phosphate Ions Alter the Binding of Daptomycin to Living Bacterial Cell Surfaces. *ACS Infectious Diseases*. Publisher: American Chemical Society. 37, 43, 45, 62, 74

[147] Miller, L. N., Brewer, W. T., Williams, J. D., Fozo, E. M., and Calhoun, T. R. (2019). Second Harmonic Generation Spectroscopy of Membrane Probe Dynamics in Gram-Positive Bacteria. *Biophysical Journal*, 117(8):1419–1428. 34, 37, 38, 42, 43, 45, 47, 49, 52, 62, 66, 74, 75, 76, 80, 82, 93

[148] Mingeot-Leclercq, M.-P. and Décout, J.-L. (2016). Bacterial lipid membranes as promising targets to fight antimicrobial resistance, molecular foundations and illustration through the renewal of aminoglycoside antibiotics and emergence of amphiphilic aminoglycosides. *MedChemComm*, 7(4):586–611. Publisher: The Royal Society of Chemistry. 38

[149] Mishra, N. N. and Bayer, A. S. (2013). Correlation of Cell Membrane Lipid Profiles with Daptomycin Resistance in Methicillin-Resistant Staphylococcus aureus. *Antimicrobial Agents and Chemotherapy*, 57(2):1082–1085. Publisher: American Society for Microbiology. 2, 34

[150] Missner, A. and Pohl, P. (2009). 110 Years of the Meyer–Overton Rule: Predicting Membrane Permeability of Gases and Other Small Compounds. *ChemPhysChem*, 10(9-10):1405–1414. _eprint: https://onlinelibrary.wiley.com/doi/pdf/10.1002/cphc.200900270. 8, 37

[151] Mitchison-Field, L. M. and Belin, B. J. (2023). Bacterial lipid biophysics and membrane organization. *Current Opinion in Microbiology*, 74:102315. 88

[152] Moen, E. K., Ibey, B. L., and Beier, H. T. (2014). Detecting Subtle Plasma Membrane Perturbation in Living Cells Using Second Harmonic Generation Imaging. *Biophysical Journal*, 106(10):L37–L40. 37

[153] Mohler, W., Millard, A. C., and Campagnola, P. J. (2003). Second harmonic generation imaging of endogenous structural proteins. *Methods*, 29(1):97–109. 15

[154] Moore, S. A., Moennich, D. M., and Gresser, M. J. (1983). Synthesis and hydrolysis of ADP-arsenate by beef heart submitochondrial particles. *Journal of Biological Chemistry*, 258(10):6266–6271. 97

[155] Moreaux, L., Sandre, O., and Mertz, J. (2000). Membrane imaging by second-harmonic generation microscopy. *JOSA B*, 17(10):1685–1694. Publisher: Optica Publishing Group. 37, 62, 74

[156] Moreira, R. A., Mendanha, S. A., Fernandes, K. S., Matos, G. G., Alonso, L., Dorta, M. L., and Alonso, A. (2014). Miltefosine Increases Lipid and Protein Dynamics in Leishmania amazonensis Membranes at Concentrations Similar to Those Needed for Cytotoxicity Activity. *Antimicrobial Agents and Chemotherapy*, 58(6):3021–3028. Publisher: American Society for Microbiology. 73, 74, 78

[157] Moreno, M. J., Estronca, L. M. B. B., and Vaz, W. L. C. (2006). Translocation of Phospholipids and Dithionite Permeability in Liquid-Ordered and Liquid-Disordered Membranes. *Biophysical Journal*, 91(3):873–881. Publisher: Elsevier. 36, 54

[158] Morrow, I. C. and Parton, R. G. (2005). Flotillins and the PHB Domain Protein Family: Rafts, Worms and Anaesthetics. *Traffic*, 6(9):725–740. _eprint: https://onlinelibrary.wiley.com/doi/pdf/10.1111/j.1600-0854.2005.00318.x. 88

[159] Mortimer, P. G. S. and Piddock, L. J. V. (1991). A comparison of methods used for measuring the accumulation of quinolones by Enterobacteriaceae, Pseudomonas aeruginosa and Staphylococcus aureus. *Journal of Antimicrobial Chemotherapy*, 28(5):639–653. 8

[160] Murray, C. J. L., Ikuta, K. S., Sharara, F., Swetschinski, L., Aguilar, G. R., Gray, A., Han, C., Bisignano, C., Rao, P., Wool, E., Johnson, S. C., Browne, A. J., Chipeta, M. G., Fell, F., Hackett, S., Haines-Woodhouse, G., Hamadani, B. H. K., Kumaran, E. A. P., McManigal, B., Achalapong, S., Agarwal, R., Akech, S., Albertson, S., Amuasi, J., Andrews, J., Aravkin, A., Ashley, E., Babin, F.-X., Bailey, F., Baker, S., Basnyat, B., Bekker, A., Bender, R., Berkley, J. A., Bethou, A., Bielicki, J., Boonkasidecha, S., Bukosia, J., Carvalheiro, C., Castañeda-Orjuela, C., Chansamouth, V., Chaurasia, S., Chiurchiù, S., Chowdhury, F., Donatien, R. C., Cook, A. J., Cooper, B., Cressey, T. R., Criollo-Mora, E., Cunningham, M., Darboe, S., Day, N. P. J., Luca, M. D., Dokova, K., Dramowski, A., Dunachie, S. J., Bich, T. D., Eckmanns, T., Eibach, D., Emami, A., Feasey, N., Fisher-Pearson, N., Forrest, K., Garcia, C., Garrett, D., Gastmeier, P., Giref, A. Z., Greer, R. C., Gupta, V., Haller, S., Haselbeck, A., Hay, S. I., Holm, M., Hopkins, S., Hsia, Y., Iregbu, K. C., Jacobs, J., Jarovsky, D., Javanmardi, F., Jenney, A. W. J., Khorana, M., Khusuwan, S., Kissoon, N., Kobeissi, E., Kostyanev, T., Krapp, F., Krumkamp, R., Kumar, A., Kyu, H. H., Lim, C., Lim, K., Limmathurotsakul, D., Loftus, M. J., Lunn, M., Ma, J., Manoharan, A., Marks, F., May, J., Mayxay, M., Mturi, N., Munera-Huertas, T., Musicha, P., Musila, L. A., Mussi-Pinhata, M. M., Naidu, R. N., Nakamura, T., Nanavati, R., Nangia, S., Newton, P., Ngoun, C., Novotney, A., Nwakanma, D., Obiero, C. W., Ochoa, T. J., Olivas-Martinez, A., Olliaro, P., Ooko, E., Ortiz-Brizuela, E., Ounchanum, P., Pak, G. D., Paredes, J. L., Peleg, A. Y., Perrone, C., Phe, T., Phommasone, K., Plakkal, N., Ponce-de Leon, A., Raad, M., Ramdin, T., Rattanavong, S., Riddell, A., Roberts, T., Robotham, J. V., Roca, A., Rosenthal, V. D., Rudd, K. E., Russell, N.,

Sader, H. S., Saengchan, W., Schnall, J., Scott, J. A. G., Seekaew, S., Sharland, M., Shivamallappa, M., Sifuentes-Osornio, J., Simpson, A. J., Steenkeste, N., Stewardson, A. J., Stoeva, T., Tasak, N., Thaiprakong, A., Thwaites, G., Tigoi, C., Turner, C., Turner, P., Doorn, H. R. v., Velaphi, S., Vongpradith, A., Vongsouvath, M., Vu, H., Walsh, T., Walson, J. L., Waner, S., Wangrangsimakul, T., Wannapinij, P., Wozniak, T., Sharma, T. E. M. W. Y., Yu, K. C., Zheng, P., Sartorius, B., Lopez, A. D., Stergachis, A., Moore, C., Dolecek, C., and Naghavi, M. (2022). Global burden of bacterial antimicrobial resistance in 2019: a systematic analysis. *The Lancet*, 399(10325):629–655. Publisher: Elsevier. 2

[161] Mykytczuk, N. C. S., Trevors, J. T., Leduc, L. G., and Ferroni, G. D. (2007). Fluorescence polarization in studies of bacterial cytoplasmic membrane fluidity under environmental stress. *Progress in Biophysics and Molecular Biology*, 95(1):60–82. 78

[162] Nagendra Prasad, H. S., Karthik, C. S., Manukumar, H. M., Mallesha, L., and Mallu, P. (2019). New approach to address antibiotic resistance: Miss loading of functional membrane microdomains (FMM) of methicillin-resistant *Staphylococcus aureus* (MRSA). *Microbial Pathogenesis*, 127:106–115. 7

[163] Needham, B. D. and Trent, M. S. (2013). Fortifying the barrier: the impact of lipid A remodelling on bacterial pathogenesis. *Nature Reviews Microbiology*, 11(7):467–481. Number: 7 Publisher: Nature Publishing Group. 34

[164] Nguyen, T. T. and Conboy, J. C. (2011). High-Throughput Screening of Drug–Lipid Membrane Interactions via Counter-Propagating Second Harmonic Generation Imaging. *Analytical Chemistry*, 83(15):5979–5988. 37, 62, 74

[165] Nguyen, T. T., Sly, K. L., and Conboy, J. C. (2012). Comparison of the Energetics of Avidin, Streptavidin, NeutrAvidin, and Anti-Biotin Antibody Binding to Biotinylated Lipid Bilayer Examined by Second-Harmonic Generation. *Analytical Chemistry*, 84(1):201–208. Publisher: American Chemical Society. 45

[166] Nickels, J. D., Chatterjee, S., Mostofian, B., Stanley, C. B., Ohl, M., Zolnierczuk, P., Schulz, R., Myles, D. A. A., Standaert, R. F., Elkins, J. G., Cheng, X., and

Katsaras, J. (2017). Bacillus subtilis Lipid Extract, A Branched-Chain Fatty Acid Model Membrane. *The Journal of Physical Chemistry Letters*, 8(17):4214–4217. Publisher: American Chemical Society. 34, 56

[167] Nishibori, A., Kusaka, J., Hara, H., Umeda, M., and Matsumoto, K. (2005). Phosphatidylethanolamine Domains and Localization of Phospholipid Synthases in Bacillus subtilis Membranes. *Journal of Bacteriology*, 187(6):2163–2174. 5

[168] Obando, D., Widmer, F., Wright, L. C., Sorrell, T. C., and Jolliffe, K. A. (2007). Synthesis, antifungal and antimicrobial activity of alkylphospholipids. *Bioorganic & Medicinal Chemistry*, 15(15):5158–5165. 73

[169] Oliver, P. M., Crooks, J. A., Leidl, M., Yoon, E. J., Saghatelian, A., and Weibel, D. B. (2014). Localization of Anionic Phospholipids in Escherichia coli Cells. *Journal of Bacteriology*, 196(19):3386–3398. Publisher: American Society for Microbiology. 5

[170] Omardien, S., Brul, S., and Zaat, S. A. J. (2016). Antimicrobial Activity of Cationic Antimicrobial Peptides against Gram-Positives: Current Progress Made in Understanding the Mode of Action and the Response of Bacteria. *Frontiers in Cell and Developmental Biology*, 4. 2

[171] Page, E. F., Blake, M. J., Foley, G. A., and Calhoun, T. R. (2022). Monitoring membranes: The exploration of biological bilayers with second harmonic generation. *Chemical Physics Reviews*, 3(4):041307. 74, 82

[172] Parasassi, T., De Stasio, G., d'Ubaldo, A., and Gratton, E. (1990). Phase fluctuation in phospholipid membranes revealed by Laurdan fluorescence. *Biophysical Journal*, 57(6):1179–1186. 29

[173] Parasassi, T., Ravagnan, G., Rusch, R. M., and Gratton, E. (1993). Modulation and Dynamics of Phase Properties in Phospholipid Mixtures Detected by Laurdan Fluorescence*. *Photochemistry and Photobiology*, 57(3):403–410. _eprint: https://onlinelibrary.wiley.com/doi/pdf/10.1111/j.1751-1097.1993.tb02309.x. 29

[174] Parisio, G., Sperotto, M. M., and Ferrarini, A. (2012). Flip-Flop of Steroids in Phospholipid Bilayers: Effects of the Chemical Structure on Transbilayer Diffusion. *Journal of the American Chemical Society*, 134(29):12198–12208. Publisher: American Chemical Society. 36, 51

[175] Park, J. H., Sut, T. N., Jackman, J. A., Ferhan, A. R., Yoon, B. K., and Cho, N.-J. (2017). Controlling adsorption and passivation properties of bovine serum albumin on silica surfaces by ionic strength modulation and cross-linking. *Physical Chemistry Chemical Physics*, 19(13):8854–8865. Publisher: The Royal Society of Chemistry. 44

[176] Park, N.-Y., Cho, Y. B., Kim, O. B., and Kim, K.-S. (2020). Cyclo(Phe-Pro) produced by Vibrio species passes through biological membranes by simple diffusion. *Applied Microbiology and Biotechnology*, 104(15):6791–6798. 8

[177] Pasquina-Lemonche, L., Burns, J., Turner, R. D., Kumar, S., Tank, R., Mullin, N., Wilson, J. S., Chakrabarti, B., Bullough, P. A., Foster, S. J., and Hobbs, J. K. (2020). The architecture of the Gram-positive bacterial cell wall. *Nature*, 582(7811):294–297. Publisher: Nature Publishing Group. 61, 99

[178] Peetla, C., Stine, A., and Labhasetwar, V. (2009). Biophysical Interactions with Model Lipid Membranes: Applications in Drug Discovery and Drug Delivery. *Molecular Pharmaceutics*, 6(5):1264–1276. Publisher: American Chemical Society. 8

[179] Perez-Lopez, M. I., Mendez-Reina, R., Trier, S., Herrfurth, C., Feussner, I., Bernal, A., Forero-Shelton, M., and Leidy, C. (2019). Variations in carotenoid content and acyl chain composition in exponential, stationary and biofilm states of *Staphylococcus aureus*, and their influence on membrane biophysical properties. *Biochimica et Biophysica Acta (BBA) - Biomembranes*, 1861(5):978–987. 78

[180] Peter, S., Alven, S., Maseko, R. B., and Aderibigbe, B. A. (2022). Doxorubicin-Based Hybrid Compounds as Potential Anticancer Agents: A Review. *Molecules*, 27(14):4478. Number: 14 Publisher: Multidisciplinary Digital Publishing Institute. 37

[181] Petit, K., Suwalsky, M., Colina, J. R., Aguilar, L. F., Jemiola-Rzeminska, M., and Strzalka, K. (2019). *In vitro* effects of the antitumor drug miltefosine on human erythrocytes and molecular models of its membrane. *Biochimica et Biophysica Acta (BBA) - Biomembranes*, 1861(1):17–25. 73, 78

[182] Pogliano, J., Osborne, N., Sharp, M. D., Abanes-De Mello, A., Perez, A., Sun, Y.-L., and Pogliano, K. (1999). A vital stain for studying membrane dynamics in bacteria: a novel mechanism controlling septation during Bacillus subtilis sporulation. *Molecular Microbiology*, 31(4):1149–1159. _eprint: https://onlinelibrary.wiley.com/doi/pdf/10.1046/j.1365-2958.1999.01255.x. 35

[183] Putman, M., van Veen, H. W., and Konings, W. N. (2000). Molecular Properties of Bacterial Multidrug Transporters. *Microbiology and Molecular Biology Reviews*, 64(4):672–693. Publisher: American Society for Microbiology. 97

[184] Rakotomanga, M., Blanc, S., Gaudin, K., Chaminade, P., and Loiseau, P. M. (2007). Miltefosine Affects Lipid Metabolism in Leishmania donovani Promastigotes. *Antimicrobial Agents and Chemotherapy*, 51(4):1425–1430. Publisher: American Society for Microbiology. 73

[185] Regev, R., Yeheskely-Hayon, D., Katzir, H., and Eytan, G. D. (2005). Transport of anthracyclines and mitoxantrone across membranes by a flip-flop mechanism. *Biochemical Pharmacology*, 70(1):161–169. 36

[186] Reynolds, P. E. (1989). Structure, biochemistry and mechanism of action of glycopeptide antibiotics. *European Journal of Clinical Microbiology and Infectious Diseases*, 8(11):943–950. 34

[187] Rohde, M. (2019). The Gram-Positive Bacterial Cell Wall. *Microbiology Spectrum*, 7(3):10.1128/microbiolspec.gpp3–0044–2018. Publisher: American Society for Microbiology. 99

[188] Rohmer, M., Bouvier, P., and Ourisson, G. (1979). Molecular evolution of biomembranes: structural equivalents and phylogenetic precursors of sterols. *Proceedings*

of the National Academy of Sciences, 76(2):847–851. Publisher: Proceedings of the National Academy of Sciences. 88

[189] Roke, S. and Gonella, G. (2012). Nonlinear Light Scattering and Spectroscopy of Particles and Droplets in Liquids. *Annual Review of Physical Chemistry*, 63(1):353–378. _eprint: https://doi.org/10.1146/annurev-physchem-032511-143748. 17, 62

[190] Rokitskaya, T. I., Aleksandrova, E. V., Korshunova, G. A., Khailova, L. S., Tashlitsky, V. N., Luzhkov, V. B., and Antonenko, Y. N. (2022). Membrane Permeability of Modified Butyltriphenylphosphonium Cations. *The Journal of Physical Chemistry B*, 126(2):412–422. Publisher: American Chemical Society. 36, 52

[191] Rokitskaya, T. I., B. Luzhkov, V., A. Korshunova, G., N. Tashlitsky, V., and N. Antonenko, Y. (2019). Effect of methyl and halogen substituents on the transmembrane movement of lipophilic ions. *Physical Chemistry Chemical Physics*, 21(42):23355–23363. Publisher: Royal Society of Chemistry. 36, 52, 56

[192] Rokitskaya, T. I., Korshunova, G. A., and Antonenko, Y. N. (2018). Effect of Alkyl Chain Length on Translocation of Rhodamine B n-Alkyl Esters across Lipid Membranes. *Biophysical Journal*, 115(3):514–521. 36

[193] Romantsov, T., Battle, A. R., Hendel, J. L., Martinac, B., and Wood, J. M. (2010). Protein Localization in Escherichia coli Cells: Comparison of the Cytoplasmic Membrane Proteins ProP, LacY, ProW, AqpZ, MscS, and MscL. *Journal of Bacteriology*, 192(4):912–924. Publisher: American Society for Microbiology. 5

[194] Romantsov, T., Stalker, L., Culham, D. E., and Wood, J. M. (2008). Cardiolipin Controls the Osmotic Stress Response and the Subcellular Location of Transporter ProP in Escherichia coli*. *Journal of Biological Chemistry*, 283(18):12314–12323. Publisher: Elsevier. 5

[195] Rothman, J. E. and Kennedy, E. P. (1977). Symmetrical distribution of phospholipids in the membrane of *Bacillus megaterium*. *Journal of Molecular Biology*, 110(3):603–618. 5

[196] Rowlett, V. W., Mallampalli, V. K. P. S., Karlstaedt, A., Dowhan, W., Taegtmeyer, H., Margolin, W., and Vitrac, H. (2017). Impact of Membrane Phospholipid Alterations in Escherichia coli on Cellular Function and Bacterial Stress Adaptation. *Journal of Bacteriology*, 199(13):10.1128/jb.00849–16. Publisher: American Society for Microbiology. 4

[197] Ruan, Y., Guha, P., Chen, S.-L., Yuan, Q., and Gan, W. (2021). Observing the structural variations on binary complex vesicle surfaces and the influence on molecular transportation. *Chemical Physics*, 548:111250. 37, 62, 74

[198] Róg, T., Stimson, L. M., Pasenkiewicz-Gierula, M., Vattulainen, I., and Karttunen, M. (2008). Replacing the Cholesterol Hydroxyl Group with the Ketone Group Facilitates Sterol Flip-Flop and Promotes Membrane Fluidity. *The Journal of Physical Chemistry B*, 112(7):1946–1952. Publisher: American Chemical Society. 36, 51

[199] Schildkraut, J. S., Penner, T. L., Willand, C. S., and Ulman, A. (1988). Absorption and second-harmonic generation of monomer and aggregate hemicyanine dye in Langmuir–Blodgett films. *Optics Letters*, 13(2):134–136. Publisher: Optica Publishing Group. 40, 52

[200] Schneider, J., Klein, T., Mielich-Süss, B., Koch, G., Franke, C., Kuipers, O. P., Kovács, T., Sauer, M., and Lopez, D. (2015). Spatio-temporal Remodeling of Functional Membrane Microdomains Organizes the Signaling Networks of a Bacterium. *PLOS Genetics*, 11(4):e1005140. Publisher: Public Library of Science. 4, 7, 56

[201] Sen, S., Sirobhushanam, S., Johnson, S. R., Song, Y., Tefft, R., Gatto, C., and Wilkinson, B. J. (2016). Growth-Environment Dependent Modulation of Staphylococcus aureus Branched-Chain to Straight-Chain Fatty Acid Ratio and Incorporation of Unsaturated Fatty Acids. *PLOS ONE*, 11(10):e0165300. Publisher: Public Library of Science. 56

[202] Shah, P., Jogani, V., Bagchi, T., and Misra, A. (2006). Role of Caco-2 Cell Monolayers in Prediction of Intestinal Drug Absorption. *Biotechnology Progress*, 22(1):186–198. _eprint: https://onlinelibrary.wiley.com/doi/pdf/10.1021/bp050208u. 8

[203] Shai, Y. (2002). Mode of action of membrane active antimicrobial peptides. *Peptide Science*, 66(4):236–248. _eprint: https://onlinelibrary.wiley.com/doi/pdf/10.1002/bip.10260. 34

[204] Sharifian Gh., M. (2021). Recent Experimental Developments in Studying Passive Membrane Transport of Drug Molecules. *Molecular Pharmaceutics*, 18(6):2122–2141. Publisher: American Chemical Society. 8

[205] Sharifian Gh., M., Wilhelm, M. J., and Dai, H.-L. (2016). Label-Free Optical Method for Quantifying Molecular Transport Across Cellular Membranes In Vitro. *The Journal of Physical Chemistry Letters*, 7(17):3406–3411. Publisher: American Chemical Society. 37, 62, 74

[206] Sharifian Gh., M., Wilhelm, M. J., and Dai, H.-L. (2018). Azithromycin-Induced Changes to Bacterial Membrane Properties Monitored in Vitro by Second-Harmonic Light Scattering. *ACS Medicinal Chemistry Letters*, 9(6):569–574. 37, 62, 74

[207] Sharifian Gh., M., Wilhelm, M. J., and Dai, H.-L. (2024). Observing mechanosensitive channels in action in living bacteria. *Biophysical Reports*, 4(1). Publisher: Elsevier. 75, 80

[208] Sharifian Gh., M., Wilhelm, M. J., Moore, M., and Dai, H.-L. (2019). Spatially Resolved Membrane Transport in a Single Cell Imaged by Second Harmonic Light Scattering. *Biochemistry*, 58(14):1841–1844. Publisher: American Chemical Society. 37, 74, 80

[209] Shen, Y. R. (1986). Surface Second Harmonic Generation: A New Technique for Surface Studies. *Annual Review of Materials Science*, 16(1):69–86. _eprint: https://doi.org/10.1146/annurev.ms.16.080186.000441. 15

[210] Shen, Y. R. (1989). Surface properties probed by second-harmonic and sum-frequency generation. *Nature*, 337(6207):519–525. Number: 6207 Publisher: Nature Publishing Group. 15, 37

[211] Shimanouchi, T., Ishii, H., Yoshimoto, N., Umakoshi, H., and Kuboi, R. (2009). Calcein permeation across phosphatidylcholine bilayer membrane: Effects of membrane fluidity, liposome size, and immobilization. *Colloids and Surfaces B: Biointerfaces*, 73(1):156–160. 8

[212] Simon, F., Clevers, S., Dupray, V., and Coquerel, G. (2015). Relevance of the Second Harmonic Generation to Characterize Crystalline Samples. *Chemical Engineering & Technology*, 38(6):971–983. _eprint: https://onlinelibrary.wiley.com/doi/pdf/10.1002/ceat.201400756. 15

[213] Smith, D., Artursson, P., Avdeef, A., Di, L., Ecker, G. F., Faller, B., Houston, J. B., Kansy, M., Kerns, E. H., Krämer, S. D., Lennernäs, H., van de Waterbeemd, H., Sugano, K., and Testa, B. (2014). Passive Lipoidal Diffusion and Carrier-Mediated Cell Uptake Are Both Important Mechanisms of Membrane Permeation in Drug Disposition. *Molecular Pharmaceutics*, 11(6):1727–1738. 34

[214] Srivastava, A. and Eisenthal, K. B. (1998). Kinetics of molecular transport across a liposome bilayer. *Chemical Physics Letters*, 292(3):345–351. 37, 62, 74, 80

[215] Steinhoff, R., Chi, L. F., Marowsky, G., and Möbius, D. (1989). Protonation and monolayer aggregation studied by second-harmonic generation. *JOSA B*, 6(4):843–847. Publisher: Optica Publishing Group. 40, 52, 74, 95

[216] Strahl, H., Bürmann, F., and Hamoen, L. W. (2014). The actin homologue MreB organizes the bacterial cell membrane. *Nature Communications*, 5(1):3442. Number: 1 Publisher: Nature Publishing Group. 7, 56

[217] Strahl, H. and Errington, J. (2017). Bacterial Membranes: Structure, Domains, and Function. *Annual Review of Microbiology*, 71(1):519–538. _eprint: https://doi.org/10.1146/annurev-micro-102215-095630. 4, 5, 33, 34, 73

[218] Stähelin, M., Burland, D. M., and Rice, J. E. (1992). Solvent dependence of the second order hyperpolarizability in p-nitroaniline. *Chemical Physics Letters*, 191(3):245–250. 40, 74, 93

[219] Subramani, S., Perdreau-Dahl, H., and Morth, J. P. (2016). The magnesium transporter A is activated by cardiolipin and is highly sensitive to free magnesium in vitro. *eLife*, 5:e11407. Publisher: eLife Sciences Publications, Ltd. 5

[220] Sugano, K., Kansy, M., Artursson, P., Avdeef, A., Bendels, S., Di, L., Ecker, G. F., Faller, B., Fischer, H., Gerebtzoff, G., Lennernaes, H., and Senner, F. (2010). Coexistence of passive and carrier-mediated processes in drug transport. *Nature Reviews Drug Discovery*, 9(8):597–614. Number: 8 Publisher: Nature Publishing Group. 4, 97

[221] Suhonen, M., Li, S. K., Higuchi, W. I., and Herron, J. N. (2008). A Liposome Permeability Model for Stratum Corneum Lipid Bilayers Based on Commercial Lipids. *Journal of Pharmaceutical Sciences*, 97(10):4278–4293. Publisher: Elsevier. 8

[222] Sun, J., Deng, Z., and Yan, A. (2014). Bacterial multidrug efflux pumps: Mechanisms, physiology and pharmacological exploitations. *Biochemical and Biophysical Research Communications*, 453(2):254–267. 97

[223] Sáenz, J. P., Grosser, D., Bradley, A. S., Lagny, T. J., Lavrynenko, O., Broda, M., and Simons, K. (2015). Hopanoids as functional analogues of cholesterol in bacterial membranes. *Proceedings of the National Academy of Sciences of the United States of America*, 112(38):11971–11976. 88

[224] Sáenz, J. P., Sezgin, E., Schwille, P., and Simons, K. (2012). Functional convergence of hopanoids and sterols in membrane ordering. *Proceedings of the National Academy of Sciences*, 109(35):14236–14240. Publisher: Proceedings of the National Academy of Sciences. 88

[225] Tague, E. D., Woodall, B. M., Harp, J. R., Farmer, A. T., Fozo, E. M., and Campagna, S. R. (2019). Expanding lipidomics coverage: effective ultra performance liquid chromatography-high resolution mass spectrometer methods for detection and quantitation of cardiolipin, phosphatidylglycerol, and lysyl-phosphatidylglycerol. *Metabolomics*, 15(4):53. 34

[226] Thomae, A. V., Koch, T., Panse, C., Wunderli-Allenspach, H., and Krämer, S. D. (2007). Comparing the Lipid Membrane Affinity and Permeation of Drug-like Acids: The Intriguing Effects of Cholesterol and Charged Lipids. *Pharmaceutical Research*, 24(8):1457–1472. 8

[227] Torcato, I. M., Huang, Y.-H., Franquelim, H. G., Gaspar, D. D., Craik, D. J., Castanho, M. A. R. B., and Henriques, S. T. (2013). The Antimicrobial Activity of Sub3 is Dependent on Membrane Binding and Cell-Penetrating Ability. *ChemBioChem*, 14(15):2013–2022. _eprint: https://onlinelibrary.wiley.com/doi/pdf/10.1002/cbic.201300274. 34

[228] van Blitterswijk, W. J. and Verheij, M. (2008). Anticancer Alkylphospholipids: Mechanisms of Action, Cellular Sensitivity and Resistance, and Clinical Prospects. *Current Pharmaceutical Design*, 14(21):2061–2074. 73

[229] van Tilburg, A. Y., Warmer, P., van Heel, A. J., Sauer, U., and Kuipers, O. P. (2022). Membrane composition and organization of Bacillus subtilis 168 and its genome-reduced derivative miniBacillus PG10. *Microbial Biotechnology*, 15(5):1633–1651. _eprint: https://onlinelibrary.wiley.com/doi/pdf/10.1111/1751-7915.13978. 88

[230] Vanounou, S., Pines, D., Pines, E., Parola, A. H., and Fishov, I. (2002). Coexistence of Domains with Distinct Order and Polarity in Fluid Bacterial Membranes¶. *Photochemistry and Photobiology*, 76(1):1–11. _eprint: https://onlinelibrary.wiley.com/doi/pdf/10.1562/0031-8655%282002%290760001CODWDO2.0.CO2. 78, 88

[231] Vazquez-Muñoz, R., Meza-Villezcas, A., Fournier, P. G. J., Soria-Castro, E., Juarez-Moreno, K., Gallego-Hernández, A. L., Bogdanchikova, N., Vazquez-Duhalt, R., and Huerta-Saquero, A. (2019). Enhancement of antibiotics antimicrobial activity due to the silver nanoparticles impact on the cell membrane. *PLOS ONE*, 14(11):e0224904. Publisher: Public Library of Science. 35

[232] Venable, R. M., Krämer, A., and Pastor, R. W. (2019). Molecular Dynamics Simulations of Membrane Permeability. *Chemical Reviews*, 119(9):5954–5997. Publisher: American Chemical Society. 8

[233] Vijaya Kumar, S., Abraham, P. E., Hurst, G. B., Chourey, K., Bible, A. N., Hettich, R. L., Doktycz, M. J., and Morrell-Falvey, J. L. (2020). A carotenoid-deficient mutant of the plant-associated microbe Pantoea sp. YR343 displays an altered membrane proteome. *Scientific reports*, 10(1):14985. Publisher: Nature Publishing Group tex.copyright: 2020 This is a U.S. Government work and not under copyright protection in the US; foreign copyright protection may apply. 56

[234] Wang, H., Troxler, T., Yeh, A.-G., and Dai, H.-L. (2000). In Situ, Nonlinear Optical Probe of Surfactant Adsorption on the Surface of Microparticles in Colloids. *Langmuir*, 16(6):2475–2481. Publisher: American Chemical Society. 23

[235] Wang, H., Yan, E. C. Y., Borguet, E., and Eisenthal, K. B. (1996). Second harmonic generation from the surface of centrosymmetric particles in bulk solution. *Chemical Physics Letters*, 259(1):15–20. 15, 44, 62

[236] Weber, G. and Farris, F. J. (1979). Synthesis and spectral properties of a hydrophobic fluorescent probe: 6-propionyl-2-(dimethylamino)naphthalene. *Biochemistry*, 18(14):3075–3078. Publisher: American Chemical Society. 28

[237] Weihs, F., Wacnik, K., Turner, R. D., Culley, S., Henriques, R., and Foster, S. J. (2018). Heterogeneous localisation of membrane proteins in Staphylococcus aureus. *Scientific Reports*, 8(1):3657. Number: 1 Publisher: Nature Publishing Group. 34

[238] Wenzel, M., Dekker, M. P., Wang, B., Burggraaf, M. J., Bitter, W., van Weering, J. R. T., and Hamoen, L. W. (2021). A flat embedding method for transmission electron microscopy reveals an unknown mechanism of tetracycline. *Communications Biology*, 4(1):1–13. Number: 1 Publisher: Nature Publishing Group. 35

[239] Wenzel, M., Vischer, N. O. E., Strahl, H., and Hamoen, L. W. (2018). Assessing Membrane Fluidity and Visualizing Fluid Membrane Domains in Bacteria Using Fluorescent Membrane Dyes. *Bio-protocol*, 8(20):e3063. 88

[240] Wilhelm, M. J. and Dai, H.-L. (2020). Molecule-Membrane Interactions in Biological Cells Studied with Second Harmonic Light Scattering. *Chemistry – An Asian Journal*,

15(2):200–213. _eprint: https://onlinelibrary.wiley.com/doi/pdf/10.1002/asia.201901406. 37, 62, 74, 75, 80, 82

[241] Wilhelm, M. J., Sharifian Gh., M., and Dai, H.-L. (2015a). Chemically Induced Changes to Membrane Permeability in Living Cells Probed with Nonlinear Light Scattering. *Biochemistry*, 54(29):4427–4430. Publisher: American Chemical Society. 37, 62, 74

[242] Wilhelm, M. J., Sharifian Gh., M., and Dai, H.-L. (2019). Influence of molecular structure on passive membrane transport: A case study by second harmonic light scattering. *The Journal of Chemical Physics*, 150(10):104705. Publisher: American Institute of Physics. 37, 62, 74

[243] Wilhelm, M. J., Sharifian Gh., M., Wu, T., Li, Y., Chang, C.-M., Ma, J., and Dai, H.-L. (2021). Determination of bacterial surface charge density via saturation of adsorbed ions. *Biophysical Journal*, 120(12):2461–2470. 37, 62, 74

[244] Wilhelm, M. J., Sheffield, J. B., Gonella, G., Wu, Y., Spahr, C., Zeng, J., Xu, B., and Dai, H.-L. (2014). Real-time molecular uptake and membrane-specific transport in living cells by optical microscopy and nonlinear light scattering. *Chemical Physics Letters*, 605-606:158–163. 37, 62, 74

[245] Wilhelm, M. J., Sheffield, J. B., Sharifian Gh., M., Wu, Y., Spahr, C., Gonella, G., Xu, B., and Dai, H.-L. (2015b). Gram's Stain Does Not Cross the Bacterial Cytoplasmic Membrane. *ACS Chemical Biology*, 10(7):1711–1717. Publisher: American Chemical Society. 37, 62, 74

[246] Willdigg, J. R. and Helmann, J. D. (2021). Mini Review: Bacterial Membrane Composition and Its Modulation in Response to Stress. *Frontiers in Molecular Biosciences*, 8. Publisher: Frontiers. 33, 88

[247] Woodford, N. and Livermore, D. M. (2009). Infections caused by Gram-positive bacteria: a review of the global challenge. *Journal of Infection*, 59:S4–S16. 34

[248] Wu, T., Wilhelm, M. J., Li, Y., Ma, J., and Dai, H.-L. (2022a). Indole Facilitates Antimicrobial Uptake in Bacteria. *ACS Infectious Diseases*. Publisher: American Chemical Society. 37, 62, 74, 75

[249] Wu, T., Wilhelm, M. J., Ma, J., Li, Y., Wu, Y., and Dai, H.-L. (2022b). Influence of Phase Transitions on Diffusive Molecular Transport Across Biological Membranes. *Angewandte Chemie International Edition*, 61(42):e202205608. _eprint: https://onlinelibrary.wiley.com/doi/pdf/10.1002/anie.202205608. 80, 82

[250] Wu, X., Busschaert, N., Wells, N. J., Jiang, Y.-B., and Gale, P. A. (2015). Dynamic Covalent Transport of Amino Acids across Lipid Bilayers. *Journal of the American Chemical Society*, 137(4):1476–1484. Publisher: American Chemical Society. 8

[251] Wu, Y., Wu, M., Gao, J., and Ying, C. (2020). Antifungal Activity and Mode of Action of Miltefosine Against Clinical Isolates of Candida krusei. *Frontiers in Microbiology*, 11:854. 73, 88

[252] Wu, Y., Yeh, F. L., Mao, F., and Chapman, E. R. (2009). Biophysical Characterization of Styryl Dye-Membrane Interactions. *Biophysical Journal*, 97(1):101–109. 38, 47

[253] Wydro, P. and Witkowska, K. (2009). The interactions between phosphatidylglycerol and phosphatidylethanolamines in model bacterial membranes: The effect of the acyl chain length and saturation. *Colloids and Surfaces B: Biointerfaces*, 72(1):32–39. 34

[254] Yan, E. C. Y. and Eisenthal, K. B. (2000). Effect of Cholesterol on Molecular Transport of Organic Cations across Liposome Bilayers Probed by Second Harmonic Generation. *Biophysical Journal*, 79(2):898–903. 37, 62, 74, 80

[255] Yusook, K., Weeranantanapan, O., Hua, Y., Kumkrai, P., and Chudapongse, N. (2017). Lupinifolin from Derris reticulata possesses bactericidal activity on Staphylococcus aureus by disrupting bacterial cell membrane. *Journal of Natural Medicines*, 71(2):357–366. 35

[256] Zeng, J., Eckenrode, H. M., Dai, H.-L., and Wilhelm, M. J. (2015). Adsorption and transport of charged vs. neutral hydrophobic molecules at the membrane of murine erythroleukemia (MEL) cells. *Colloids and Surfaces B: Biointerfaces*, 127:122–129. 37, 74

[257] Zeng, J., Eckenrode, H. M., Dounce, S. M., and Dai, H.-L. (2013). Time-Resolved Molecular Transport across Living Cell Membranes. *Biophysical Journal*, 104(1):139–145. 37, 62, 74, 75, 80, 82

[258] Zhang, Y.-M. and Rock, C. O. (2008). Membrane lipid homeostasis in bacteria. *Nature Reviews Microbiology*, 6(3):222–233. Number: 3 Publisher: Nature Publishing Group. 34

[259] Zhu, C., Jiang, L., Chen, T.-M., and Hwang, K.-K. (2002). A comparative study of artificial membrane permeability assay for high throughput profiling of drug absorption potential. *European Journal of Medicinal Chemistry*, 37(5):399–407. 8

[260] Zulueta Díaz, Y. d. l. M. and Fanani, M. L. (2017). Crossregulation between the insertion of Hexadecylphosphocholine (miltefosine) into lipid membranes and their rheology and lateral structure. *Biochimica et Biophysica Acta (BBA) - Biomembranes*, 1859(10):1891–1899. 73, 88

[261] Zuo, X., Djordjevic, J. T., Oei, J. B., Desmarini, D., Schibeci, S. D., Jolliffe, K. A., and Sorrell, T. C. (2011). Miltefosine Induces Apoptosis-Like Cell Death in Yeast via Cox9p in Cytochrome c Oxidase. *Molecular Pharmacology*, 80(3):476–485. Publisher: American Society for Pharmacology and Experimental Therapeutics Section: Article. 73

Vita

Marea Blake was born in Cullman, Alabama but grew up in Ashland City, Tennessee where she graduated from Cheatham County Central High School in 2015. She went on to receive a Bachelor of Science in Biology and Chemistry in 2019 from Austin Peay State University. While at APSU she participated in undergraduate research with Dr. Leslie Hiatt who was the catalyst for her wanting to further her education in analytical chemistry. She pursued her Doctorate of Philosophy degree with Prof. Tessa Calhoun at the University of Tennessee, Knoxville where her passion now lies in pursuing highly interdisciplinary research bridging ideas from physical chemistry to cellular biology.